Lattice instabilities in metallic elements

Göran Grimvall

Department of Theoretical Physics, KTH Royal Institute of Technology, AlbaNova University Center, SE-10691 Stockholm, Sweden

Blanka Magyari-Köpe

Department of Electrical Engineering, Stanford University, Stanford, California 94305, USA

Vidvuds Ozoliņš

Department of Materials Science and Engineering, University of California, Los Angeles, California 90095-1595, USA

Kristin A. Persson

Advanced Energy Technology, Lawrence Berkeley National Laboratory, Berkeley, California 94720, USA

(published 4 June 2012)

Most metallic elements have a crystal structure that is either body-centered cubic (bcc), face-centered close packed, or hexagonal close packed. If the bcc lattice is the thermodynamically most stable structure, the close-packed structures usually are dynamically unstable, i.e., have elastic constants violating the Born stability conditions or, more generally, have phonons with imaginary frequencies. Conversely, the bcc lattice tends to be dynamically unstable if the equilibrium structure is close packed. This striking regularity essentially went unnoticed until *ab initio* total-energy calculations in the 1990s became accurate enough to model dynamical properties of solids in hypothetical lattice structures. After a review of stability criteria, thermodynamic functions in the vicinity of an instability, Bain paths, and how instabilities may arise or disappear when pressure, temperature, and/or chemical composition is varied are discussed. The role of dynamical instabilities in the ideal strength of solids and in metallurgical phase diagrams is then considered, and comments are made on amorphization, melting, and low-dimensional systems. The review concludes with extensive references to theoretical work on the stability properties of metallic elements.

DOI: 10.1103/RevModPhys.84.945 PACS numbers: 63.20.dk, 64.10.+h, 62.20.D−

CONTENTS

I. INTRODUCTION

A crystalline material in thermal equilibrium at ambient conditions has the lattice structure that minimizes the Gibbs free energy. For instance, the elements copper, silver, and gold all have the face-centered cubic (fcc) structure, and chromium, molybdenum, and tungsten have the body-centered cubic (bcc) structure, from 0 K to their melting points. It has often been assumed that if the atoms of Cu, Ag, or Au were instead arranged in a bcc lattice, it would represent a metastable state, i.e., a state that can be in local mechanical equilibrium but is not that of the lowest Gibbs free energy. Similarly, the fcc lattice structure has been assumed to be a metastable state of Cr, Mo, and W. Because pure Cu, Ag, and Au have not been found in bulk form in the bcc structure at ambient conditions, and pure Cr, Mo, and W have not been found in the fcc structure, it has not been possible to obtain the properties of such phases experimentally.

Ab initio electronic structure calculations offer a way to study phases of any assumed lattice structure and greatly extend the knowledge gained from experiments. An early example is the work by Yin and Cohen (1982), in which the total energy of silicon and germanium at 0 K is calculated for the diamond-type, fcc, bcc, and four other structures. The volume per atom is varied and the energy minimum is found. Such calculations can give the cohesive energy, the atomic volume, and the bulk modulus of each considered phase. Yin and Cohen (1982) correctly found that the energy minima of Si in the fcc and bcc structures lie at higher energies than that of the experimentally observed diamond-type lattice structure (see Fig. 1). However, later *ab initio* calculations (Ekman, Persson, and Grimvall, 2000) showed that the fcc and bcc phases at their energy minima do not represent metastable states, because these structures of Si are dynamically unstable. It means that there exist infinitesimal deformations of the lattice, for which the atoms do not return to their assumed equilibrium positions. In the literature, dynamical instability is sometimes called mechanical instability.

The Pt-W system illustrates another aspect of dynamical instabilities. Pure platinum has the fcc lattice structure, and pure tungsten has the bcc structure. At low concentrations of

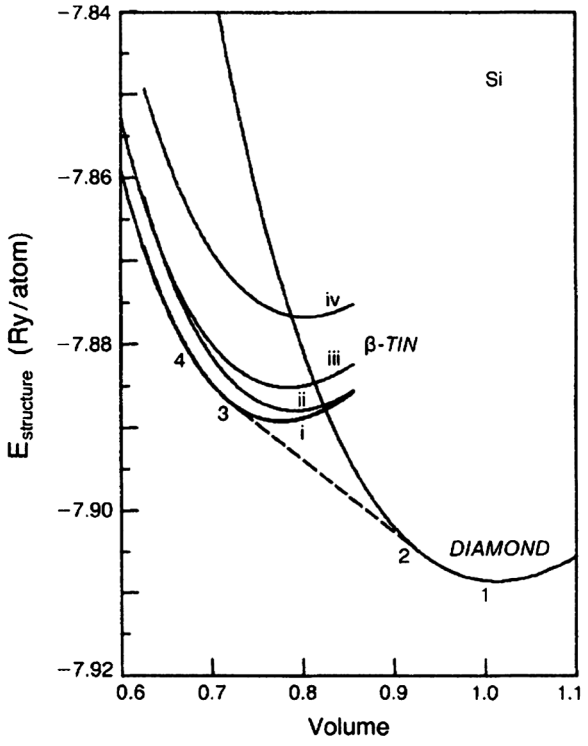

FIG. 1. The total energy of Si at 0 K and ambient pressure calculated *ab initio* for various lattice structures by Yin and Cohen (1982).

tungsten, the fcc solid solution structure of the Pt-W alloy is the thermodynamically most stable state, according to the experimentally determined phase diagram (see Fig. 2). However, pure fcc W is dynamically unstable, at least at low temperatures, as will be discussed later in more detail (see Fig. 3). A hypothetical Pt-W fcc solid solution therefore cannot represent a metastable phase at high W concentrations. There must be a critical concentration $c_{\rm crit}$ beyond which fcc $Pt_{1-c}W_c$ is dynamically unstable. Similarly, magnesium has the hexagonal close-packed (hcp) structure in thermal equilibrium at ambient temperature and pressure. Under those conditions, the bcc structure of Mg turns out to be dynamically unstable, but at high pressure the bcc lattice of Mg not is only dynamically stabilized but also becomes the thermodynamically most stable phase. There is a critical pressure $P_{\rm crit}$ below which bcc Mg is dynamically unstable.

The lattice stability can also depend on the temperature T. For instance, in thermodynamic equilibrium at ambient pressure, the elements Ti, Zr, and Hf all have the hcp structure at low temperatures and the bcc structure at high temperatures. However, the bcc lattice is dynamically unstable below certain critical temperatures $T_{\rm crit}$. Therefore, bcc Ti, Zr, and Hf cannot be regarded as metastable phases at 0 K.

The critical concentration $c_{\rm crit}$, critical pressure $P_{\rm crit}$, and critical temperature $T_{\rm crit}$ that separate dynamically stable and unstable regions should not be confused with the actual concentration, pressure, and temperature where there is a phase change governed by the Gibbs free energy of thermodynamic equilibrium. For example, the thermodynamic stability range of the fcc structure in the Pt-W phase diagram terminates before one reaches $c = c_{\rm crit}$. Similarly the hcp-to-bcc transition in Mg takes place at a pressure higher than $P_{\rm crit}$, and the hcp-to-bcc transitions in Ti, Zr, and Hf occur at temperatures above $T_{\rm crit}$.

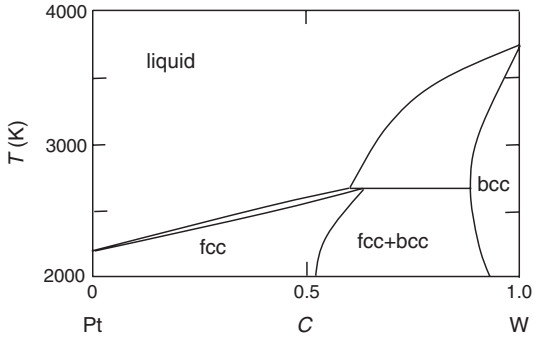

FIG. 2. The essential parts of the Pt-W phase diagram. From Guillermet *et al.*, 1995.

Ca Sr Ba	Sc Y La	Ti Zr Hf	V Nb Ta	Cr Mo W	Mn Tc Re	Fe Ru Os	Co Rh Ir	Ni Pd Pt	Cu Ag Au
fcc	hcp	hcp	bcc	bcc	"bcc"	bcc	hcp	fcc	fcc
fcc	hcp	hcp	bcc	bcc	hcp	hcp	fcc	fcc	fcc
bcc	hcp	hcp	bcc	bcc	hcp	hcp	fcc	fcc	fcc

FIG. 3. Elements from the third, fourth, and fifth rows in the periodic table. The ambient-condition ground-state structure is shown in each box, for the sequence of elements in the top row (Donohue, 1974; Young, 1991). Generally, the bcc structure is dynamically unstable if the equilibrium structure is close packed (fcc or hcp), or the fcc structure is dynamically unstable if the equilibrium structure is bcc. For Pt and the noble metals this trend is uncertain or less pronounced. Manganese has a complex bcc-related ground-state structure with 58 atoms per unit cell and is unstable in the conventional bcc structure.

Figure 3 gives an overview of the stability and instability of the fcc and bcc structures for elements from the third, fourth, and fifth rows in the periodic table. There is a tendency for the bcc phase to be dynamically unstable when the fcc structure is the equilibrium phase, and vice versa. This feature will get a natural explanation in terms of Bain paths, which represent how a certain structure is continuously deformed into another structure, e.g., the bcc-to-fcc transformation through distortion of a tetragonal lattice.

It must be stressed that not all structural changes are associated with a dynamical instability. For example, iron has the bcc structure at low temperatures and ambient pressure. At $T = 1173$ K, fcc Fe becomes the thermodynamically most stable phase, but at 1660 K it returns to the bcc structure. Iron melts at 1811 K. At room temperature, the bcc Fe lattice transforms to the hcp structure when the pressure exceeds about 13 GPa. The phases of Fe that are not the thermodynamically most stable ones nevertheless remain dynamically stable, and thus represent metastable states in wide ranges of temperature and pressure. Such transformations, which are not related to dynamical lattice instabilities, lie outside the scope of this review. Further, we will not consider internal-coordinate instabilities such as ferroelectric phenomena and Jahn-Teller distortions, or isostructural transitions such as between the two fcc phases of Ce that have different atomic volumes. The hcp structure is in many respects similar to the fcc structure and will also be dealt with here, although the emphasis is on bcc and fcc lattices.

II. LATTICE INSTABILITIES

A. Phonon dispersion curves

A lattice wave (phonon) in a periodic lattice is characterized by its frequency $\omega(\mathbf{q}, s)$, where $\mathbf{q}$ is the wave vector and s is a label denoting the polarization (one longitudinal and two transverse modes) and the phonon branches (acoustic and optical). The time dependence of the amplitude is given by a factor $\exp(-i\omega t)$. An imaginary $\omega(\mathbf{q}, s) = i\Gamma$ leads to an exponentially increasing factor $\exp(\Gamma t)$. A general stability criterion, in the harmonic approximation and at zero external load, therefore is

$$\omega^2(\mathbf{q}, s) > 0 \tag{1}$$

for all $\mathbf{q}$ and s.

Often an instability is present only for small $\mathbf{q}$, i.e., for long-wavelength phonons. We call it an elastic instability. In fact, it has been suggested (Born, 1940; Born and Fürth, 1940; Power, 1942) that if a lattice is stable at long wavelengths, it is very likely stable also at short wavelengths. However, a counterexample was given by Wallace and Patrick (1965) in the diamond structure. Many examples

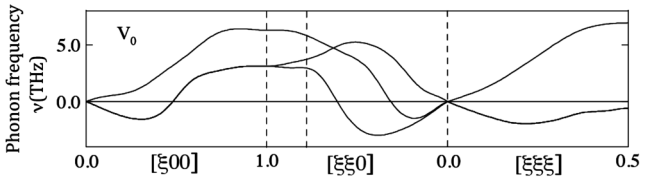

FIG. 4. At ambient pressure, fcc tungsten is dynamically unstable for all long-wavelength transverse modes and for some Brillouin zone boundary modes, but there are also regions of **q** where all modes are stable. From Einarsdotter *et al.*, 1997.

were later found of lattices that are dynamically stable in the elastic limit of the phonon dispersion curves but are unstable when **q** is close to the Brillouin zone boundary, or are unstable only at intermediate **q** values. The fcc structure of tungsten exemplifies dynamical instabilities in large regions of **q** in the first Brillouin zone (see Fig. 4).

In Eq. (1) we labeled the eigenfrequencies by a wave vector **q**, which refers to eigenstates that are plane waves. In a disordered alloy with N atoms, and in the harmonic approximation, there are still $3N$ (or, rather, $3N-6$) eigenfrequencies but the corresponding wave functions may not all be well represented by plane waves. However, also in a nonperiodic lattice all the eigenfrequencies must be real and positive, as expressed by Eq. (1). This stability condition holds for systems of any size and structural disorder. The dynamical matrix in nonperiodic systems may conveniently be expressed in real-space coordinates (instead of reciprocal space); cf. Umeno, Kitamura, and Tagawa (2007) in a study of amorphous metals, and Pacheco and Batra (2008) on finite-size gold crystals. It is often referred to as the Hessian, or Hessian matrix. Further comments on stability criteria in nonuniform systems are given in Sec. VIII.C on defect formation. In this review we keep the descriptions $(\mathbf{q}, s)$ and $\omega(\mathbf{q}, s)$ of perfect lattices in alloys and in thermally disordered systems also, even though the vibrations may be heavily damped.

B. Elastic constants

1. Born stability criteria

The elastic properties of a lattice are described by the elastic constants C_{ij}. The elastic energy change associated with an arbitrary deformation given by small strains e_i is (Born, 1940)

$$U_{\text{elast}} = \frac{1}{2} V_0 \sum_{i,j=1}^{6} C_{ij} e_i e_j + O(e^3). \tag{2}$$

We used the standard Voigt contraction scheme for the indices i and j. V_0 is the volume of the unstrained sample and $O(e^3)$ denotes terms of order e^3 or higher. In a lattice of cubic symmetry (e.g., fcc, bcc, diamond type, NaCl type, or CsCl type) there are three independent elastic constants: C_{11}, C_{12}, and C_{44}. Then Eq. (2) reduces to

$$U_{\text{elast}} = \tfrac{1}{2} V_0 [(C_{11}-C_{12})(e_1^2+e_2^2+e_3^2) + C_{12}(e_1+e_2+e_3)^2 + C_{44}(e_4^2+e_5^2+e_6^2)] + O(e^3). \tag{3}$$

A lattice is dynamically stable only if U_{elast} is positive for any small deformation. This implies restrictions on C_{ij}, which are mathematically expressed by the condition that the principal minors of the determinant with elements C_{ij} are all positive (Born, 1940; Born and Huang, 1954). In cubic lattice symmetry, dynamical stability requires that

$$C_{11} + 2C_{12} > 0, \qquad C_{11} > |C_{12}|, \qquad C_{44} > 0. \tag{4}$$

Usually $C_{12} > 0$, with intermediate-valent compounds such as Tm_xSe (Boppart *et al.*, 1980) and $Sm_xLa_{1-x}S$ (Schärer and Wachter, 1995) being exceptions. Further, it is convenient to work with the bulk modulus

$$B = \frac{C_{11} + 2C_{12}}{3} \tag{5}$$

and the shear modulus

$$C' = \frac{C_{11} - C_{12}}{2}. \tag{6}$$

A common formulation of the stability conditions therefore is

$$B > 0, \qquad C' > 0, \qquad C_{44} > 0. \tag{7}$$

The case $B < 0$ is referred to as spinodal instability (Appendix A). The vanishing bulk modulus leads to decohesion without lattice symmetry change. Failure through $C' < 0$, called the Born instability, is characterized by symmetry breaking with coupling of shear modes under volume conservation. $C_{44} < 0$ is a pure shear instability. The three relations in Eq. (4) or Eq. (7) are often called the Born stability criteria.

The analogous stability criteria for tetragonal and hexagonal lattice structures follow from relations given in Eqs. (13) and (14), when the external load is set to zero.

2. The stability triangle

An illuminating description of elastic properties in cubic lattices is obtained with the parameters s_1, s_2, and s_3, where

$$s_1 = C_{11} + 2C_{44} \tag{8}$$

is a characteristic measure of the magnitude of the elastic constants, and

$$s_2 = \frac{C_{11} - C_{44}}{C_{11} + 2C_{44}}, \qquad s_3 = \frac{C_{11} - C_{12} - 2C_{44}}{C_{11} + 2C_{44}} \tag{9}$$

are dimensionless parameters. The Born stability criteria are fulfilled for all points inside a prism in the (s_1, s_2, and s_3) space with $s_1 > 0$ and a triangular base, as shown in Fig. 5 (Paszkiewicz, Pruchnik, and Zieliński, 2001; Paszkiewicz and Wolski, 2008). That base is called the stability triangle. Elastically isotropic systems (e.g., bcc W) are located on the s_2 axis. The two shorter sides of the triangle represent symmetry-breaking soft shear modes ($C' = 0$ or $C_{44} = 0$) while the longest side represents cubic isostructural phase transitions ($B = 0$). When $C_{44} \to 0$ ($s_2 \to 1$, i.e., anywhere on the vertical side of the stability triangle in Fig. 5) all elastic shear modes with $\mathbf{q} = (q_1, q_2, 0)$ and polarization vector (0, 0, 1) simultaneously have $\omega \to 0$. Special cases are the modes in the [100] and [110] directions. When $C' \to 0$ (anywhere on the lower side in the stability triangle) only

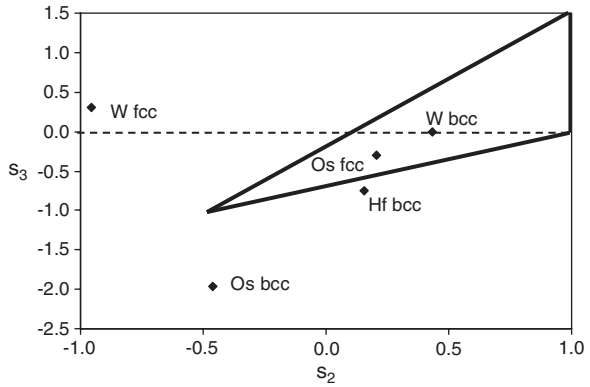

FIG. 5. Cubic crystal structures are dynamically stable when the values of C_{11}, C_{12}, and C_{44} are such that (s_2, s_3) falls inside the stability triangle bounded by the thick lines, corresponding to $s_3 = (5/3)s_2 - 1/6$, $s_3 = (2/3)s_2 - 2/3$, and $s_2 = 1$, respectively. Data points are shown for two very stable structures (bcc W, fcc Os), two very unstable structures (fcc W, bcc Os), and one structure that is weakly unstable (bcc Hf); cf. Table II.

the mode in the [110] direction with polarization in the (110) plane has a vanishing frequency. In this respect, one can say that $C_{44} \to 0$ leads to a more severe lattice instability than is the case for $C' \to 0$. Instabilities in cubic lattices are usually associated with $C' < 0$, while still $C_{44} > 0$; cf. Tables II and III and Appendixes D and I.

Phonon dispersion curves $\omega(\mathbf{q})$ in cubic structures are often presented for the three high-symmetry directions [100], [110], and [111]. It follows from what has just been said that if they show dynamical stability in the [100] and [110] directions, all elastic shear modes will be dynamically stable. This result holds only in the small-$\mathbf{q}$ limit. For instance, we note in Fig. 4 for tungsten that the transverse phonons at the Brillouin zone boundary in the [100] and [110] directions are stable, but the transverse zone boundary mode in the [111] direction is unstable.

Paszkiewicz and Wolski (2007) used the concept of the stability triangle to discuss Young's modulus E, the shear modulus G, and Poisson's number ν for cubic lattices.

3. Elastic stability under external load

The Born stability criteria in Eq. (4) must be modified when the solid is subject to an external load, specified by the stress tensor σ (Hill, 1975; Hill and Milstein, 1977). We introduce an elastic stiffness matrix $\mathbf{B}$ (Wallace, 1967, 1972) with elements

$$B_{ijkl} = C_{ijkl} + \tfrac{1}{2}(\delta_{ik}\sigma_{jl} + \delta_{jk}\sigma_{il} + \delta_{il}\sigma_{jk} + \delta_{jl}\sigma_{ik} - 2\delta_{kl}\sigma_{ij}). \tag{10}$$

Here C_{ijkl} are elements in the elastic constant tensor $\mathbf{C}$ evaluated at the current stressed state (which may not have cubic symmetry), σ_{ij} specify the external stresses, and δ_{ij} is the Kronecker delta (1 if $i = j$; 0 if $i \neq j$). The Born criteria, which followed from the determinant condition $|\mathbf{C}| = 0$, are now replaced by criteria derived from $|\mathbf{A}| = 0$, where $\mathbf{A} = (\mathbf{B}^T + \mathbf{B})/2$ and superscript T denotes transposition (Wang *et al.*, 1995). In the special case of hydrostatic pressure, $\sigma_{11} = \sigma_{22} = \sigma_{33} = -P$, the new conditions for elastic stability are (Wallace, 1967; Milstein and Hill, 1979a, 1979b; Wang *et al.*, 1993, 1995; Mizushima, Yip, and Kaxiras, 1994; Milstein and Rasky, 1996; Zhou and Joós, 1996; Morris, Jr. and Krenn, 2000; Yip *et al.*, 2001)

$$\begin{aligned} &C_{11} + 2C_{12} + P > 0, \qquad C_{44} - P > 0, \\ &C_{11} - C_{12} - 2P > 0, \end{aligned} \tag{11}$$

or equivalently

$$B + P/3 > 0, \qquad C_{44} - P > 0, \qquad C' - P > 0. \tag{12}$$

The spinodal instability with $P < 0$, i.e., under a uniform tension, might be achieved indirectly as a result of lattice expansion through the insertion of large atoms in the lattice.

In a tetragonal crystal structure one has six independent elastic constants: $C_{11} = C_{22}$, C_{33}, C_{12}, $C_{13} = C_{23}$, $C_{44} = C_{55}$, and C_{66}; all other $C_{ij} = 0$. Under hydrostatic pressure the stability conditions are (Cleri, Wang, and Yip, 1995; Sin'ko and Smirnov, 2002)

$$\begin{aligned} &C_{44} - P > 0, \qquad C_{66} - P > 0, \\ &C_{11} - C_{12} - 2P > 0, \end{aligned} \tag{13}$$

and

$$(C_{33} - P)(C_{11} + C_{12}) - 2(C_{13} + P)^2 > 0. \tag{14}$$

A special case is the hexagonal lattice symmetry, where $C_{66} = (C_{11} - C_{12})/2$. For cubic symmetry, where $C_{33} = C_{11}$ and $C_{13} = C_{12}$, Eq. (14) can be factorized as $(C_{11} - C_{12} - 2P)(C_{11} + 2C_{12} + P) > 0$, in agreement with Eq. (11).

If a tetragonal crystal structure is subject to uniaxial tension σ in the [001] direction, the stability criteria are $C_{11} - C_{12} > 0$, $C_{44} + \sigma/2 > 0$, $C_{66} > 0$, and $(C_{33} + \sigma)(C_{11} + C_{12}) - 2(C_{13} - \sigma/2)^2 > 0$ (Wang *et al.*, 1993, 1995; Li and Wang, 1998; Pokluda *et al.*, 2004).

In this context we note that the elastic constants in a specimen subject to an external load can be defined in different ways, leading to different stability criteria (Milstein and Rasky, 1996; Pokluda *et al.*, 2004); see also Steinle-Neumann and Cohen (2004) and Marcus and Qiu (2009a, 2009b). The stability conditions (11)–(14) correspond to the definition of elastic constants from the energy expansion of Green's variables (Hill and Milstein, 1977).

4. Phonon stability under hydrostatic pressure

How should the stability criterion $\omega^2(\mathbf{q}, s) > 0$ be generalized under external hydrostatic pressure? In the case of short-wavelength phonons, the lattice modulation varies over a length scale given by the size of atoms. The medium that provides the external pressure is also discrete on a similar length scale. Therefore the meaning of constant pressure as a boundary condition is troublesome. In practice, theoretical calculations of phonon spectra are instead performed at constant volume, corresponding to a certain pressure. Before we treat that case, it is instructive to look at a specific example in which constant pressure is nevertheless assumed to be well defined.

Consider a transverse phonon mode in the [001] direction, where $\omega^2(\mathbf{q}) = q^2 C_{44}/\rho$ for small q. Then $C_{44} - P > 0$ can be rewritten as

$$\omega(q) - q\sqrt{\frac{P}{\rho}} > 0. \tag{15}$$

The relation $C_{44} - P > 0$ expresses the stability condition that the enthalpy $H = U + PV$ increases when a specimen is subject to a small shear under an external hydrostatic pressure P. The shear leads to volume decrease ΔV (cf. the volume change due to shear alone, as discussed in Sec. IV.B). Thus, $\Delta U_{\text{elast}} - P\Delta V$ must be positive.

The potential energy of a single harmonic oscillator of frequency ω and instantaneous displacement u is $M\omega^2u^2/2$. The analogous result for a transverse wave of frequency ω propagating in the z direction with displacement $x = a\sin(qz)$ and wavelength $\lambda = 2\pi/q$, averaged over a specimen of volume V_0, is $\Delta U_{\text{internal}} = V_0a^2\omega^2\rho/4$. Further, this shear deformation of the crystal unit cells shortens the specimen in the z direction, leading to a total volume decrease $\Delta V = V_0a^2q^2/4$. The stability condition $\Delta U_{\text{internal}} - P\Delta V = V_0(a^2\omega^2\rho/4 - a^2q^2P/4) > 0$ has the same q and P dependence as in the small-q limit in Eq. (15), which therefore holds for all wavelengths in this example.

We next turn to calculations of the phonon dispersion relations $\omega(\mathbf{q}, s)$ referring to a certain pressure but actually performed at constant volume. One starts with a specimen having the equilibrium volume V' when the atoms are at their equilibrium positions and there is an external hydrostatic pressure P. The lattice then is modulated according to the phonon mode $(\mathbf{q}, s)$, which increases the energy but also changes the specimen volume. Through an additional deformation, the specimen volume is brought back to V'. The resulting energy change ΔE after the two kinds of deformations is calculated by *ab initio* techniques and yields the corresponding frequency $\omega(\mathbf{q}, s)$. The energy change in the volume-conserving step just mentioned is the equivalent of the enthalpy gain $P\Delta V$ in the case of a calculation at constant pressure. Therefore the calculated $\omega(\mathbf{q}, s)$ already includes the effect of external pressure on the stability condition, and no explicit correction such as in Eq. (15) should be added. There seems to be no rigorous discussion of this point in papers that have presented *ab initio* calculations of phonon dispersion curves under pressure, but it has been clarified in the case of elastic constants, equivalent to the long-wavelength limit of $\omega(\mathbf{q}, s)$. Consider the strain-energy density expressed in the elastic constants (the stress-strain coefficients) C_{ijkl} (Barron and Klein, 1965; Steinle-Neumann and Cohen, 2004):

$$\frac{\Delta E}{V} = -Pe_{ii} + \frac{1}{2}\left[C_{ijkl} - \frac{1}{2}P(2\delta_{ij}\delta_{kl} - \delta_{il}\delta_{jk} - \delta_{jl}\delta_{ik})\right] \times e_{ij}e_{kl}. \tag{16}$$

The convention of summation over repeated indices is applied. If the strains e are chosen such as exemplified in Sec. IV.B, all terms proportional to P vanish in Eq. (16), to the order of e^2; cf. Steinle-Neumann and Cohen (2004). Therefore, no further pressure correction should be added to the elastic constants calculated from ΔE, contrary to what was argued by Marcus, Ma, and Qiu (2002), but also see later clarifications (Marcus and Qiu, 2004, 2009a, 2009b; Sin'ko and Smirnov, 2004).

III. THERMODYNAMIC FUNCTIONS

A. Harmonic approximation

The Helmholtz free energy $F(T)$ per atom for a harmonic phonon spectrum can be written

$$F = k_BT\int_0^{\omega_{\max}} \ln\left[2\sinh\left(\frac{\hbar\omega}{2k_BT}\right)\right]D(\omega)d\omega. \tag{17}$$

$D(\omega)$ is the density of phonon states, normalized to 3 per atom. The high-temperature expansion of F, in a system with N atoms, is

$$F = -Nk_BT\int_0^{\omega_{\max}}\left[\ln\left(\frac{k_BT}{\hbar\omega}\right) - \frac{1}{24}\left(\frac{\hbar\omega}{k_BT}\right)^2 + \cdots\right]D(\omega)d\omega. \tag{18}$$

Thus the leading term in the Helmholtz free energy at high temperatures,

$$F(T) = -3Nk_BT\ln\left(\frac{k_BT}{\hbar\omega_{\log}}\right), \tag{19}$$

and the corresponding entropy

$$S(T) = -\left(\frac{\partial F}{\partial T}\right)_V \approx 3Nk_B\left[1 + \ln\left(\frac{k_BT}{\hbar\omega_{\log}}\right)\right], \tag{20}$$

depend on only a single parameter, i.e., on the logarithmic average $\omega_{\log}$ of the phonon frequencies, defined as

$$\ln(\omega_{\log}) = \frac{1}{3}\int_0^{\omega_{\max}} \ln(\omega)D(\omega)d\omega. \tag{21}$$

B. Vibrational properties near instabilities

1. Entropy

Consider a solid that is dynamically unstable when the composition or the pressure has passed a certain critical value. Let $\mathbf{q}_0$ be the wave vector of that phonon whose frequency first becomes zero when the critical condition is approached. Thus $\omega^2(\mathbf{q}_0, s_{\text{crit}}) = 0$ but all other $\omega^2(\mathbf{q}, s) > 0$ when $\mathbf{q} \to \mathbf{q}_0$. An expansion of $\omega(\mathbf{q}, s_{\text{crit}})$ in small $\mathbf{q} - \mathbf{q}_0$ around $\mathbf{q}_0$, for the unstable mode $s = s_{\text{crit}}$, can be written in the form

$$\omega(\mathbf{q}, s_{\text{crit}}) = \omega(\mathbf{q}_0, s_{\text{crit}}) + \alpha(q_x - q_{0,x})^2 + \beta(q_y - q_{0,y})^2 + \gamma(q_z - q_{0,z})^2. \tag{22}$$

To get the contribution to $\omega_{\log}$ from phonons close to the unstable mode, we integrate over d^3q in the region $|\mathbf{q} - \mathbf{q}_0| < q_r$, where q_r is a suitable cutoff parameter, and use the fact that the density of states for phonons in $\mathbf{q}$ space (reciprocal space) is a constant. When $\omega(\mathbf{q}_0, s_{\text{crit}}) \to 0$, and for the special case $\alpha = \beta = \gamma$, we have $\ln\omega(\mathbf{q}, s_{\text{crit}}) = \ln[\alpha(\mathbf{q} - \mathbf{q}_0)^2]$. Then, with integration variable $q = |\mathbf{q} - \mathbf{q}_0|$,

$$\frac{\int_0^{q_r}\ln[\alpha(\mathbf{q} - \mathbf{q}_0)^2]d^3q}{\int_0^{q_r} d^3q} = \frac{3}{q_r^3}\int_0^{q_r}\ln(\alpha q^2)q^2dq = \ln(\alpha q_r^2) - \frac{2}{3}. \tag{23}$$

Thus we obtain the important result that the logarithmic average $\omega_{\log}$ does not diverge, but has a finite limit when $\omega(\mathbf{q}_0, s_{\rm crit}) \to 0$. It now follows from Eq. (20) that the entropy has a well-defined limit (Guillermet *et al.*, 1995). This qualitative result is obtained also when the isotropy condition $\alpha = \beta = \gamma$ does not hold. If the critical condition first arises at the Brillouin zone center, i.e., for $\mathbf{q}_0 = 0$, then $\omega(\mathbf{q}, s_{\rm crit})$ is linear in q for small $\mathbf{q}$. The entropy still has a finite limit when the instability condition is approached, but only when one takes into account that $\omega(\mathbf{q}, s_{\rm crit})$ is not strictly isotropic for small $\mathbf{q}$; see Sec. III.B.3.

2. Atomic displacement

The conventional expression for the average of the squared thermal atomic displacement at high temperature T in a monatomic lattice of cubic symmetry and with atomic mass M is (Grimvall, 1999)

$$\langle u^2 \rangle = \frac{k_{\rm B}T}{NM} \sum_{\mathbf{q}s} \frac{1}{\omega^2(\mathbf{q}, s)}. \tag{24}$$

Following the approach above, with $\omega(\mathbf{q}, s_{\rm crit}) = \omega(\mathbf{q}_0, s_{\rm crit}) + \alpha(\mathbf{q} - \mathbf{q}_0)^2$ inserted into Eq. (24), and after a summation over $\mathbf{q}$ vectors with $|\mathbf{q} - \mathbf{q}_0| < q_r$, one finds that $\langle u^2 \rangle$ diverges as $1/[\omega(\mathbf{q}_0, s_{\rm crit})]^{1/2}$ when $\omega(\mathbf{q}_0, s_{\rm crit}) \to 0$. A similar consideration shows that $\langle u^2 \rangle$ diverges also in the elastic-limit instabilities that arise when $C_{44} \to 0$ or $C' \to 0$. This seems inconsistent with the fact that the entropy does not diverge, since in classical physics (high T), the entropy is a measure of the occupied part of phase space. However, $\langle u^2 \rangle$ in Eq. (24) refers to the displacement of a specified atom relative to its equilibrium position. Because of the correlated motion of the atoms, one cannot take $\langle u^2 \rangle$ as a measure of the total occupied phase space. Let $\langle u^2(\mathbf{R}) \rangle$ be the average of the squared thermal displacement of the distance $\mathbf{R} = \mathbf{R}_j - \mathbf{R}_0$ between atoms labeled j and 0. The high-temperature expression corresponding to Eq. (24) is (Grüneisen and Goens, 1924; Warren, 1969; Grimvall, 1998)

$$\langle u^2(\mathbf{R}) \rangle = \frac{2k_{\rm B}T}{NM} \sum_{\mathbf{q}s} \frac{[\boldsymbol{\epsilon}(\mathbf{q}, s) \cdot \hat{e}]^2}{\omega^2(\mathbf{q}, s)} \times \{1 - \cos[\mathbf{q} \cdot (\mathbf{R}_j^0 - \mathbf{R}_0^0)]\}. \tag{25}$$

Here $\boldsymbol{\epsilon}(\mathbf{q}, s)$ is a phonon polarization vector and $\hat{e}$ is a unit vector along $\mathbf{R}_j^0 - \mathbf{R}_0^0$, where the superscript 0 denotes the equilibrium position. In the elastic limit (small $\mathbf{q}$), and to lowest order, $1 - \cos[\mathbf{q} \cdot (\mathbf{R}_j^0 - \mathbf{R}_0^0)] \approx [\mathbf{q} \cdot (\mathbf{R}_j^0 - \mathbf{R}_0^0)]^2/2$, which cancels the singularity from $\omega^2(\mathbf{q}, s) \sim q^2$ in the denominator. On the other hand, ignoring the cosine term yields $\langle u^2(\mathbf{R}) \rangle = 2\langle u^2 \rangle/3$ with $\langle u^2 \rangle$ as in Eq. (24), i.e., the result of noncorrelated vibrations. Another simple case is when $\mathbf{q}$ lies at the boundary of the first Brillouin zone. Then every second atom moves in phase. We let these examples illustrate how the finite vibrational entropy close to the lattice instability can be reconciled only with correlated vibrational displacements.

3. Generalized Debye models

The conventional Debye model has a density of states $D(\omega) \sim \omega^2$, with a cutoff frequency $\omega_{\rm D}$ related to the sound velocity $C_{\rm sound} = \omega_{\rm D}/q_{\rm D}$, where $q_{\rm D}$ is the Debye cutoff wave number. Thus the longitudinal and transverse lattice vibrations are described by a common parameter $\omega_{\rm D}$. Such a model is unrealistic in a treatment of dynamical instabilities, because of the crucial role of shear vibrations; the vibrational entropy would diverge when $\omega_{\rm D} \to 0$. In Appendix D it is shown that this divergence remains even if the longitudinal and shear modes are treated separately, but are still isotropic. However, in a real system where the elastic waves are described by the three independent constants C_{11}, C_{12}, and C_{44}, the vibrational entropy is finite when either $C' \to 0$ or $C_{44} \to 0$. As an example, we show in Fig. 6 how the entropy increase ΔS varies in a model alloy when a shear instability is approached with $C_{44} \to 0$ (C' fixed) and with $C' \to 0$ (C_{44} fixed), respectively. *Ab initio* calculations by Rousseau *et al.* (2011) show a related behavior for $\omega_{\log}$ in fcc Li under pressure, where phonons close to the K point in the Brillouin zone become unstable but elastic stability is retained.

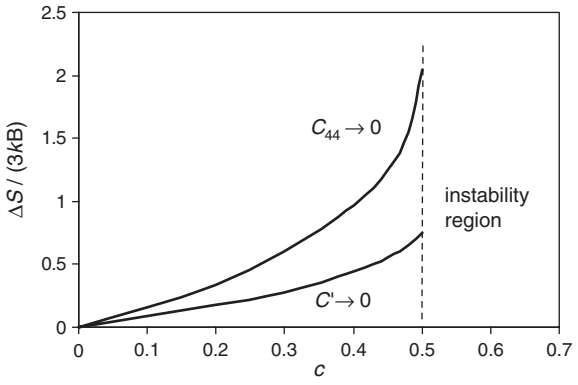

FIG. 6. The entropy increase per atom in a Debye model of a monatomic solid, plotted as $\Delta S/(3k_{\rm B})$, when either C_{44} or C' varies linearly with the concentration c and becomes zero at $c_{\rm crit} = 0.5$, while the other shear constant is kept constant. At concentration $c = 0$, our model system is assumed to be isotropic with $C' = C_{44} = C_{11}/3$. Note that ΔS does not diverge at $c = c_{\rm crit}$.

4. Effect of anharmonicity

The results obtained above for the entropy and the atomic displacement were derived within the harmonic approximation for lattice vibrations. As one approaches an instability, anharmonic effects will be important. However, it is known that the harmonic expression for the entropy (but not for, e.g., the energy) remains valid, within low-order perturbation theory, if one lets the frequencies $\omega(\mathbf{q}, s)$ be shifted due to the anharmonicity (Barron, 1965; Cowley and Cowley, 1966; Grimvall, 1999). Therefore the entropy is well described also in the case of moderate anharmonic effects. This is sufficent to account for phase diagrams, as done in Sec. IX, since then the thermodynamic functions in the immediate vicinity of the lattice instability are not important. After the onset of an instability, the vibrational entropy is of course not a thermodynamically defined quantity. A much more intricate aspect of strong anharmonicity is considered in Sec. VI, dealing with temperature-dependent effects in the combined vibrational and electronic systems.

IV. STRUCTURAL TRANSFORMATIONS

A. Transformation paths

1. Classical (uniaxial) Bain path

Bain (1924) pointed out that an fcc lattice can be transformed into a bcc lattice by stretching the three sides in the cubic unit cell by factors of 1, $\sqrt{2}$, and $\sqrt{2}$, respectively. Conversely, if the axes of a bcc lattice are stretched by factors of $\sqrt{2}$, 1, and 1, respectively, the lattice transforms into an fcc structure (see Fig. 7). The intermediate lattice has tetragonal structure, with the crystallographic unit cell axes a and c. Going from the bcc to the fcc lattice in this case corresponds to c/a varying from 1 to $\sqrt{2}$ in a body-centered tetragonal (bct) structure (see Fig. 8). Alternatively, we define a lattice parameter $a' = a/\sqrt{2}$. Going from the fcc to the bcc lattice then corresponds to c/a' varying in a face-centered tetragonal (fct) lattice from 1 to $1/\sqrt{2} \approx 0.71$. We use the first description in this review, but both of them occur in the literature.

There are several similar deformation modes of a lattice, which all pass through the special cases of fcc and bcc lattices. They are called Bain paths; see, for example, reviews by Milstein, Fang, and Marschall, (1994) and Marcus, Jona, and Qiu (2002). The simplest of them, which we call the classical Bain path, has an intermediate tetragonal lattice structure and is subject to the additional condition that the volume per atom $\Omega_a = a^2c/2$ is kept constant. To distinguish it from other Bain paths, it can be referred to as the volume-conserving tetragonal Bain path. [In the original paper by Bain (1924) no such volume constraint is mentioned, but it has been used in numerous later works; see Milstein, Fang, and Marschall (1994).]

Let the total energy of the static tetragonal lattice be $U(a, c)$. At the special points of bcc ($c/a = 1$) and fcc ($c/a = \sqrt{2}$) lattices, symmetry arguments imply that U has either a minimum corresponding to a stable or metastable state or a maximum corresponding to a dynamically unstable state (Craievich *et al.*, 1994; Marcus, Jona, and Qiu, 2002). In the limits of very large and very small c/a, the atoms strongly overlap and the energy $U(a, c)$ goes to infinity. It follows that there must be at least three points of energy extrema along the tetragonal Bain path; two of them for cubic and one for tetragonal lattice symmetry (Marcus, Jona, and Qiu, 2002). The extremum in $U(a, c)$ that represents a noncubic structure is not located at a particular c/a dictated by symmetry. In rare cases, for example, zinc (Marcus, Jona, and Qiu, 2002), there is more than one energy extremum for a tetragonal (noncubic) lattice structure. Figure 9 shows Bain paths in Ir and W at zero temperature and constant volume, and Fig. 10 shows three qualitatively different shapes of $U(a, c)$ for tungsten at different volumes. If $U(a, c)$ has a maximum at zero strain, a distortion can lower the total lattice energy, i.e., the structure is dynamically (mechanically) unstable. In Fig. 9, the bcc Ir and the fcc W lattices are unstable.

Magnetism can play an important role, and one must take into account how the magnetic state varies along a deformation path. We leave that discussion to Sec. VII.D and to the treatment of magnetic elements in Appendix J.

As argued above, the existence of a minimum and a local maximum in the classical Bain path implies the existence of another (secondary) local minimum. Mehl *et al.* (2004) investigated this extended tetragonal Bain path in some detail for elements that are thermodynamically stable in fcc or bcc structures. For Sr the secondary minimum coincides with the bcc lattice, and for Ba with the fcc lattice. Figures 11 and 12 exemplify their results for Pt and W, showing minima to the left of the bcc structure and to the right of the fcc structure, respectively. These minima, which represent saddle points in graphs of energy versus displacement, are unstable against shear. The question now arises if the structure at the secondary minimum is dynamically stable. Mehl *et al.* (2004) found that in all cases (except Sr and Ba) it is unstable, with $C' < 0$ for those elements that have the equilibrium fcc structure, and

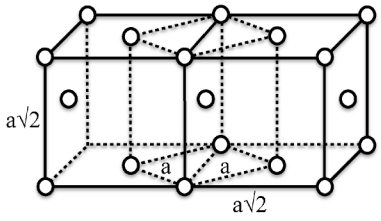

FIG. 7. The fcc lattice structure results when a bcc lattice (central part with short-dashed sides in the figure) is stretched in one direction by a factor $c/a = \sqrt{2}$.

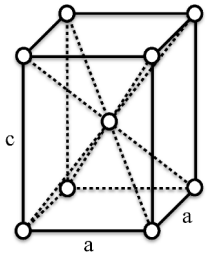

FIG. 8. The body-centered tetragonal structure.

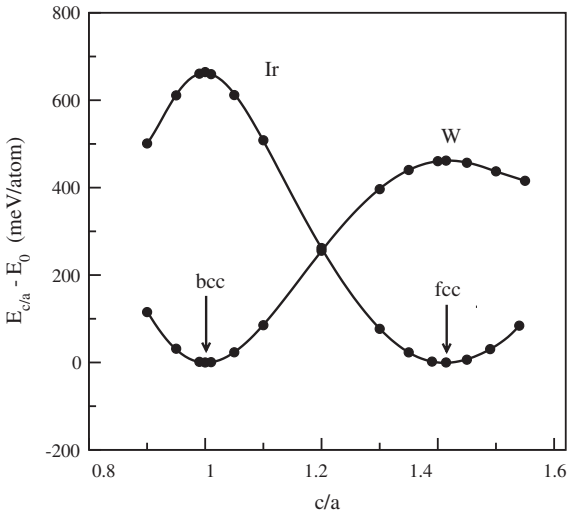

FIG. 9. Bain paths illustrating cases where either the fcc or the bcc structure is stable. From Šob, Wang, and Vitek, 1997a.

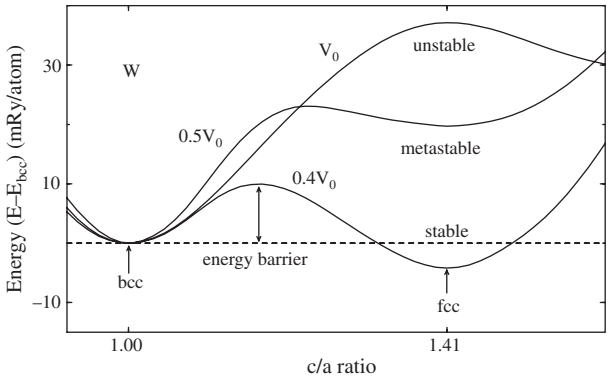

FIG. 10. The bcc-fcc volume-conserving tetragonal Bain path for tungsten at different volumes, where V_0 is the volume at pressure $P = 0$. The fcc structure gradually goes from being dynamically unstable to metastable and finally to the thermodynamical equilibrium structure. From Einarsdotter *et al.*, 1997.

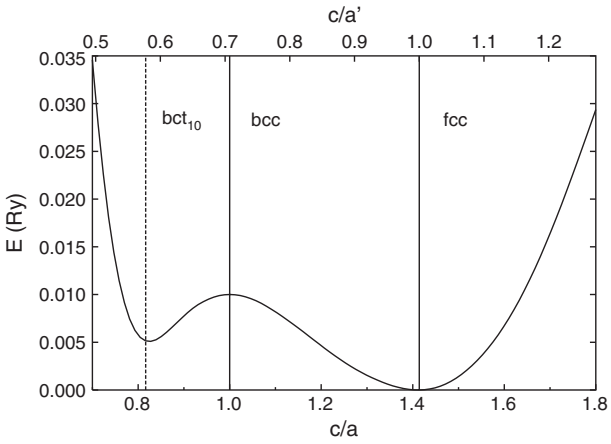

FIG. 11. Extended Bain path for Pt. From Mehl *et al.*, 2004.

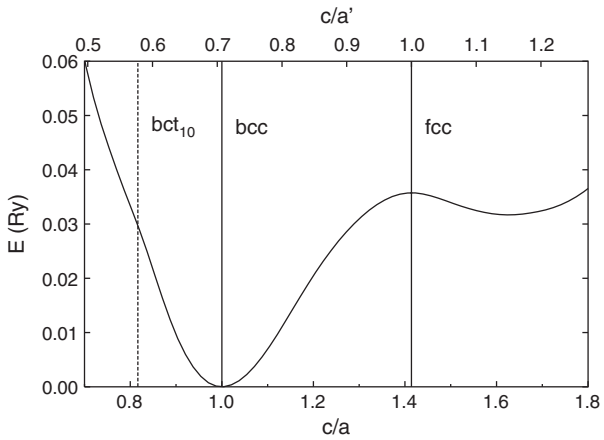

FIG. 12. Extended Bain path for W. From Mehl *et al.*, 2004.

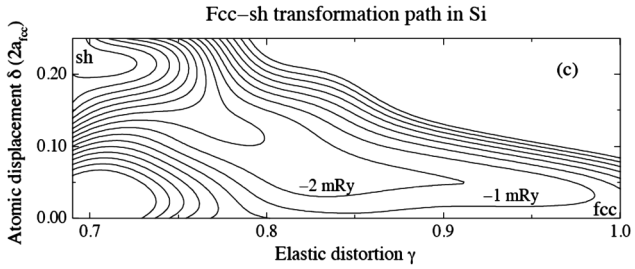

FIG. 13. The two-parameter fcc → sh transformation in Si. The shear parameter $\gamma = (c/a)^{3/2}$. From Persson, 2001.

with $C_{66} < 0$ for those that have the equilibrium bcc structure.

The three possible positions of an energy extremum for the bct structure relative to the energy extrema of the bcc and fcc structures in the sequence (minimum, maximum, minimum) along the tetrgonal Bain path are in the order (bct, bcc, fcc), (bcc, fct, fcc), and (bcc, fcc, bct), as illustrated in Fig. 11, Fig. 10 (at reduced volumes), and Fig. 12, respectively.

We can abandon the condition of the conserved volume and consider, e.g., a relaxed uniaxial Bain path where the dimensions of the lattice in the directions perpendicular to the direction of the uniaxial stress are relaxed (Alippi, Marcus, and Scheffler, 1997). This path corresponds to a simulation of a uniaxial tensile test (see Sec. VIII).

Usually the energy is plotted in one dimension, i.e., along the coordinate representing the transition path. A more general description is to plot the "energy landscape" in which the special structures are located at peaks, troughs, or saddle points, as exemplified by Černý *et al.* (2005) for Cu and Al, and in Fig. 13 for Si.

In our plots of Bain path energies, a certain path has been prescribed. However, there can be instabilities along that primary path, such that the deformation branches off along a secondary path with another lattice structure. For instance, if one follows a primary [100] loading path with tetragonal lattice symmetry and reaches a point where $C_{22} = C_{23}$, there can be a transition to a secondary equilibrium path with orthorhombic lattice structure, while the specimen is still subject to a uniaxial load (Hill and Milstein, 1977; Milstein and Huang, 1978; Milstein, 1980). Bifurcation along a loading path was discussed in detail by Milstein and Huang (1978) for an fcc crystal subject to [110] loading. We return to other examples of bifurcation in Sec. VIII.B on the theoretical strength.

2. Epitaxial tetragonal Bain path

For each set of lattice parameter values a and c there is a quantity $U(a, c)$ that gives the total quantum-mechanical energy per atom of the corresponding rigid lattice. The stress in the crystallographic c direction is

$$\sigma_c = \frac{\partial U(a, c)}{\partial c}. \tag{26}$$

The expitaxial tetragonal Bain path is defined as that curve in the two-dimensional ac plane where $\sigma_c = 0$ (Alippi, Marcus, and Scheffler, 1997; Marcus, Jona, and Qiu, 2002). It always passes through the points of cubic symmetry, $c/a = 1$ and $c/a = \sqrt{2}$, of the relaxed uniaxial Bain path where the energy $U(a, c)$ has an extremum, exactly at the same volume per atom Ω_a at these energy extrema (Alippi,

Marcus, and Scheffler, 1997). Note that the epitaxial tetragonal path with biaxial compression corresponds to uniaxial tension; cf. Sec. VIII.B.1.

Of course, the atomic volume along the epitaxial Bain path is not conserved. Also in many other cases, as, e.g., when simulating tensile tests (see Sec. VIII) or analyzing shear, the corresponding dimensions of the lattice or atomic volume should be relaxed. One case is illustrated in Fig. 14, which shows the variation of the energy with the engineering shear strain along ⟨112⟩ in the (111) plane for fcc Cu (Roundy *et al.*, 1999). We also note the possibility of bifurcation, as discussed in Sec. VIII.B.

The name expitaxial derives from the close connection to the stress and strain conditions for an epitaxial surface layer. Of particular interest in this review is the case in which the structure of the epitaxial layer is dynamically unstable in bulk form. As an example, fcc Co is thermodynamically stable up to its melting temperature, and bcc Co is dynamically unstable. However, the bcc structure was reported in ultrathin layers of Co when grown epitaxially on GaAs(110) (Prinz, 1985) and on Cr(100) (Metoki, Donner, and Zabel, 1994). Similarly, the equilibrium structures of Ni and Pd are fcc, and their bcc lattices are dynamically unstable, but a bcc Ni film was formed epitaxially on Fe(100) (Heinrich *et al.*, 1987). Further examples are given in Appendix I.

A theoretical account of the stabilization of an epitaxial layer must include the interfacial energy as well as the strain energy caused by lattice parameter mismatch between film and substrate. When the film thickness becomes too large, the dynamical instability of the equilibrium bulk phase cannot be suppressed. For instance, there is a critical thickness of about ten atomic monolayers when bcc Cu is grown on Ag(100) (Li *et al.*, 1991; Pfeifer *et al.*, 2005). One can also grow more complicated structures with alternating layers of two substances, e.g., bcc Ti/bcc Nb and bcc Zr/bcc Nb (Thompson *et al.*, 2004), and Ag/V multilayers with continuous and reversible bcc-fcc transformation (Wei, Liu, and Misra, 2011).

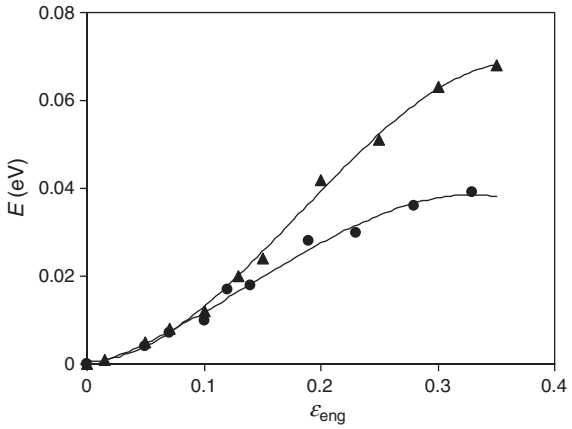

FIG. 14. The variation of the unrelaxed (triangles) and relaxed (circles) energy E when fcc Cu is sheared along ⟨112⟩ in the {111} plane. The engineering strain is defined as $\epsilon_{eng} = (c/a)^{2/3} - 1$. Adapted from Roundy *et al.*, 1999.

3. Trigonal Bain path

There are several paths that can take a lattice continuously between bcc and fcc structures. The tetragonal Bain path involved strains but no shear. In the trigonal Bain path (or trigonal deformation path) the lattice is both strained and sheared. It goes from the bcc to the fcc structure through an intermediate simple cubic (sc) structure. Figure 15 shows how a bcc lattice structure can be seen as the special case when the angle α in the rhombohedral (trigonal) unit cell is 109.47°. The sc structure has $\alpha = 90°$ and the fcc structure has $\alpha = 60°$. Figure 16 shows the energy along the bcc-fcc trigonal Bain path in tungsten. Analogous results have been obtained by Šob, Wang, and Vitek (1997a) and Mehl and Finkenstadt (2008). Zelený, Friák, and Šob (2011) compared the energetics of nonmagnetic (NM), ferromagnetic (FM), and antiferromagnetic (AFM) states in Fe, Co, and Ni along the trigonal deformation path.

It should be remarked that tellurium transforms at high pressure from a rhombohedral (trigonal) to a bcc structure. Further, the phonons near [0.2, 0, 0] in the Te bcc structure become dynamically unstable at low pressure. However, since both the rhombohedral and the bcc structures have one atom per unit cell, they cannot be linked by a transition path described by a nonzero phonon **q** vector. The fact that the bcc Te phonon mode becomes dynamically unstable near

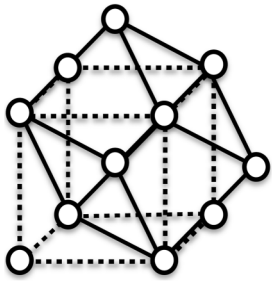

FIG. 15. The bcc lattice structure (dashed lines) can be represented by rhombohedral primitive cells (solid lines) with rhombohedral angle $\alpha = 109.47°$.

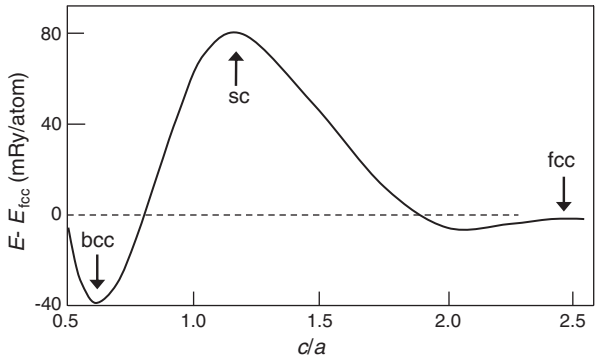

FIG. 16. The energy $E - E_{fcc}$ along the bcc-fcc trigonal Bain path for W. The c and a lengths refer to the [111] direction and a perpendicular direction, respectively [cf. Kraft *et al.* (1993)]. Adapted from Einarsdotter *et al.*, 1997.

the rhombohedral-to-bcc transition pressure thus is coincidental (Mauri *et al.*, 1996).

We conclude the discussion of trigonal Bain paths by contrasting the three cases exemplified by W, Ir, and Po. In W there is an absolute energy minimum at the bcc structure (see Fig. 16), in Ir the absolute energy minimum is at the fcc structure (Šob, Wang, and Vitek, 1997a), and in Po it is at the sc structure [see Legut, Friák, and Šob (2007, 2010)].

4. Burgers path and other bcc or fcc to hcp transformations

Burgers (1934) suggested a continuous deformation path from bcc to hcp through a shear followed by a shuffling of atomic planes. However, later research showed that the transformation can be very complicated, and we give only a few references here. Johnson and Carter (2008) found paths in the pressure-induced bcc-to-hcp Fe transformation with a lower enthalpy barrier than that of the Burgers path. The bcc-hcp transformation was also treated by Zhao, Maroudas, and Milstein (2000) for Morse-type interactions, Chen, Ho, and Harmon (1988) for Ba, Wentzcovitch and Cohen (1995) for Mg, Craievich *et al.* (1997) for Mo and Nb, and Ekman *et al.* (1998), Friák and Šob (2008), and Friák (2011) for Fe. Djohari, Milstein, and Maroudas (2009) investigated the bcc-hcp Burgers transition through molecular-dynamics simulations in a model alkali metal subject to a uniaxial compressive load. Kolluri, Gungor, and Maroudas (2008) studied the fcc-hcp transformation in thin films, and Folkins and Walker (1990) discussed another fcc-hcp structural transition mode. The temperature-induced hcp-to-bcc transitions in Ti, Zr, and Hf are discussed in Sec. VI.

B. Calculation of elastic constants

Ab initio electronic structure calculations can give the change in total energy for any combination of small strains e_i, and in this way provide theoretical results for the elastic constants. The strains e_i are related to the components of the strain tensor ϵ as $e_i = \epsilon_i$ for $i = 1$, 2, or 3, and $e_i = 2\epsilon_i$ for $i = 4$, 5, or 6, with indices expressed through Voigt's contraction scheme. The volume change is given by the determinant $|\mathbf{I} + \epsilon|$, where $\mathbf{I}$ is the unit tensor.

In a tetragonal deformation of a cubic lattice, two sides of the cubic unit cell are strained by small and equal amounts $\epsilon_1 = \epsilon_2 = \delta$. Conservation of the volume per atom Ω_a requires that the third side is simultaneously strained by $\epsilon_3 = (1+\delta)^{-2} - 1$. Further, there is no shear, $\epsilon_4 = \epsilon_5 = \epsilon_6 = 0$. Then the elastic energy per atom, relative to the unstrained lattice, takes the form (to order δ^3)

$$U_{\mathrm{a,elast}} = 6\Omega_a \frac{C_{11} - C_{12}}{2}\delta^2 = 6\Omega_a C'\delta^2 + O(\delta^3). \tag{27}$$

$U_{\mathrm{a,elast}}$ refers to macroscopic deformations. Therefore Eq. (27) is independent of the precise atomic configuration (e.g., bcc or fcc) in the cubic lattice structure.

Since we are also interested in energy variations along the tetragonal Bain path, it is useful to rewrite Eq. (27) in a form that explicitly refers to the energy $U(a, c)$ of the tetragonal structure. With new lattice parameters $a(1+\delta)$ and $c[1 + (1+\delta)^{-2} - 1] \approx c(1-2\delta)$, the ratio c/a changes to $(c/a)(1-3\delta)$, and we get

$$U_{\mathrm{a,elast}} = \frac{1}{2}\frac{\partial^2 U(a,c)}{\partial (c/a)^2}\delta^2, \tag{28}$$

i.e.,

$$\frac{C_{11} - C_{12}}{2} = \frac{1}{12\Omega_a}\frac{\partial^2 U(a,c)}{\partial (c/a)^2}. \tag{29}$$

$U(a, c)$ is the energy along the Bain path, relative to some reference level (e.g., the bcc or the fcc structure). The derivative is taken at constant a^2c, and where $c/a = 1$ (for bcc structure) or $c/a = \sqrt{2}$ (for fcc structure). The stability criterion that $U(a, c)$ has a minimum is equivalent to $C' > 0$.

A volume-conserving monoclinic deformation of the cubic lattice is obtained through $\epsilon_1 = \epsilon_2 = 0$, $\epsilon_3 = \delta^2/(1-\delta^2)$, and a shear distortion with $\epsilon_4 = \epsilon_5 = 0$, $\epsilon_6 = \delta$ (i.e., $e_6 = 2\delta$). Then

$$U_{\mathrm{a,elast}} = 2\Omega_a C_{44}\delta^2 + O(\delta^4). \tag{30}$$

A volume-conserving orthorhombic deformation of a cubic lattice is obtained with the strains $\epsilon_1 = \delta$, $\epsilon_2 = -\delta$, $\epsilon_3 = \delta^2/(1-\delta^2)$, and $\epsilon_4 = \epsilon_5 = \epsilon_6 = 0$. Then

$$U_{\mathrm{a,elast}} = \Omega_a(C_{11} - C_{12})\delta^2 + O(\delta^4). \tag{31}$$

We note that there is no term of order δ^3 in Eqs. (30) and (31), unlike Eq. (27).

There are many other types of deformations that lead to energies expressed in the elastic constants of the cubic structure and therefore can be used in *ab initio* calculations of C_{ij}. Deformations that yield the elastic constants in the hcp lattice are found in, e.g., Fast *et al.* (1995), Cohen, Stixrude, and Wasserman (1997), Steinle-Neumann, Stixrude, and Cohen (1999), and Guo and Wang (2000a, 2000b).

In all the methods to calculate the elastic constants described above, one obtains the energy as a function of the imposed strain [Eq. (2)]. An alternative (Le Page and Saxe, 2002; Le Page, Saxe, and Rogers, 2002) is to calculate the stress resulting from a given strain and find the elastic constants from the well-known relation

$$\sigma_i = \sum_{j=1}^{6} C_{ij} e_j. \tag{32}$$

Here the stress change is a first-order function of the applied strain, while the energy change in Eq. (2) is a second-order function. Therefore, the stress-based approach can allow smaller strains than the energy approach and still yield reasonable accuracy (Karki, Karato, and Silva, 1998; Le Page and Saxe, 2002). The approach is particularly suitable to treat complex structures, for instance, as in the calculation of the elastic constants of the triclinic polymorph of Al_2SiO_5 (kyanite), and Ti_4As_3 under uniaxial strain (Le Page and Saxe, 2002). In spite of such advantages, the stress-strain approach has not been used as much as the energy-strain approach. One reason is that common calculational packages give the energy, and not the stress, as output.

C. Soft modes as precursors to structural changes

The tetragonal and trigonal transformation paths described above are one-parameter transformations taking the bcc to the

TABLE I. Some displacive structural transformation paths.

Parent phase	Distortion modes: Phonon	Distortion modes: Strain	Product phase
bcc		C'	bct, fcc
		C_{44}	sc, fcc
	LA$[\frac{2}{3},\frac{2}{3},\frac{2}{3}]$		ω
	TA$_1(N)$	C'	hcp
	TA$_1[\frac{1}{4},\frac{1}{4},0]$	C'	dhcp
	TA$_1[\frac{1}{3},\frac{1}{3},0]$	C' + tilting$[110]_{bcc}$	$9R$
	TA$_2(N)$	C'	sh
	LA(N)	C'	sc
fcc	TA(X)	C'	sh

fcc structure, or vice versa. In the tetragonal path, a small C' implies a low energy barrier for such a structural change. Similarly, a small C_{44} implies a low energy barrier in the trigonal transformation path. A softening of C' or C_{44}, arising from changes in pressure, temperature, or composition, can therefore be viewed as a precursor to a displacive structural change. Further, phonon softening and instabilities are not limited to the long-wavelength shear modes described by C' or C_{44} but can occur for Brillouin zone boundary modes or for modes with wave vectors in the interior of the Brillouin zone; cf. Fig. 4. The best known example in the bcc lattice is the LA$[2/3, 2/3, 2/3]$ phonon mode, which provides a path between the bcc and the hexagonally structured ω phase; see Table I. The atoms in the $\{111\}$ planes of the bcc structure are hexagonally distributed. Allowing two of these planes to collapse into each other, while the third plane is kept fixed, yields the ω phase. Thus the bcc-ω transformation is also a one-parameter path, which takes place without diffusion of atoms. Often it is referred to as a martensitic transformation, a name borrowed from a diffusionless structural change in carbon steel. It is of particular interest in Ti, Zr, and Hf alloys; see Figs. 17 and 18, phonon dispersion curve measurements in bcc Zr by Heiming *et al.* (1991), and a molecular-dynamics simulation for Ti by Hennig *et al.* (2008). A broad investigation of the role of elastic and shear stabilities in the martensitic transformation path in NiTi is given by Hatcher, Kontsevoi, and Freeman (2009).

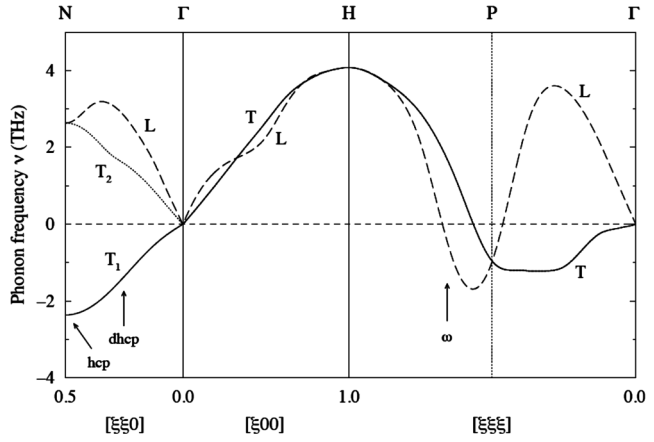

FIG. 17. Calculated phonon dispersion curves for bcc Hf, with arrows marking modes relevant for displacive transformation paths. From Persson, Ekman, and Ozoliņš, 2000.

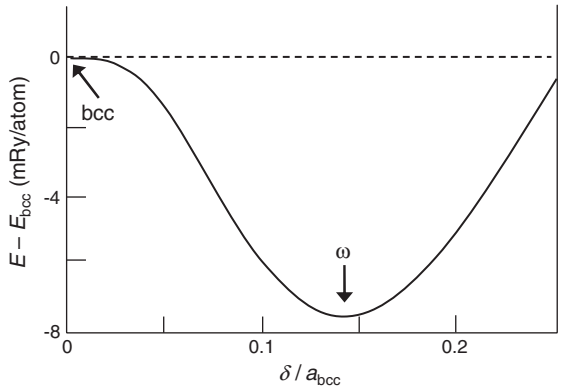

FIG. 18. The energy $E - E_{bcc}$ along the bcc $\rightarrow \omega$ transformation path in Ti. δ is the displacement associated with the LA$[2/3, 2/3, 2/3]$ phonon mode; cf. Ho, Fu, and Harmon (1983). From Persson, Ekman, and Ozoliņš, 2000.

Transformation paths between the bcc and fcc phases and other hexagonal phases, such as the sh (simple hexagonal), hcp (hexagonal close-packed), dhcp (double hexagonal close-packed), and $9R$ structures, are connected with special phonon modes in the transverse acoustic $[\xi\xi 0]$ branch, together with a shearing of the lattice corresponding to the C' elastic constant; see Table I and Fig. 17. As a result, the crystal can be relaxed according to two independent parameters.

Body-centered cubic structures of Ti, La, and Hf are unstable through the TA$_1$ N-point phonon, with an atomic displacement $\delta = 1/12$, which yields an hcp stacking in the $[110]_{bcc}$ direction. Further, the tetragonal Bain path in these materials exhibits a minimum for $c/a \approx 0.82$, which corresponds to the ideal hexagonal angle of 120° in the $(110)_{bcc}$ planes (Persson, Ekman, and Ozoliņš, 2000). Thus, the energy surface spanned by the two distortion parameters allows for several possible paths in which the energy is continuously lowered. However, often a detailed crosswise relaxation of the two parameters is required for the transformation to proceed. Silicon is then a good illustration (Ekman, Persson, and Grimvall, 2000). Both the bcc and fcc phases are dynamically unstable for displacements toward the sh phase, through the N-point phonons and the elastic constant C'. Figure 13 shows the energy landscape for the fcc-sh transformation in Si.

Note that although small values of C' or C_{44}, or of the frequency of other phonon modes, can be associated with transformation paths along certain crystallographic directions, the thermal displacement amplitude $\langle u^2 \rangle$ relative to the equilibrium lattice position for harmonic vibrations in a lattice of cubic symmetry is isotropic, i.e., we have the counterintuitive result that the thermal displacements are not exceptionally large in the special directions of the transformation paths, as long as anharmonic effects can be ignored; cf. Eq. (24).

Finally, it must be stressed that although a soft mode may indicate a possible path to another structure, the actual transition is usually of first order and occurs before a phonon mode in the parent phase has become unstable.

V. PRESSURE EFFECTS

A. General aspects

For later reference we first recapitulate three concepts related to pressure effects: the Grüneisen parameter, the Clausius-Clapeyron equation, and the common-tangent construction.

The pressure dependence of the elastic constants $(\partial C_{ij}/\partial P)$ is known from experiments for many substances (Every and McCurdy, 1992). Converting that information into the volume dependence of C' and C_{44} we get

$$\frac{\partial \ln C'}{\partial \ln V} = \frac{V}{2C'}\left[\left(\frac{\partial C_{11}}{\partial P}\right) - \left(\frac{\partial C_{12}}{\partial P}\right)\right]\left(\frac{\partial P}{\partial V}\right) = -\frac{B}{2C'}\left[\left(\frac{\partial C_{11}}{\partial P}\right) - \left(\frac{\partial C_{12}}{\partial P}\right)\right] = -\gamma', \tag{33}$$

$$\frac{\partial \ln C_{44}}{\partial \ln V} = \frac{V}{C_{44}}\left(\frac{\partial C_{44}}{\partial P}\right)\left(\frac{\partial P}{\partial V}\right) = -\frac{B}{C_{44}}\left(\frac{\partial C_{44}}{\partial P}\right) = -\gamma_{44}. \tag{34}$$

The dimensionless quantities γ' and γ_{44} introduced here are similar to the Grüneisen parameters $\gamma_G(\mathbf{q}, s) = -\partial \ln\omega(\mathbf{q}, s)/\partial \ln V$ of individual phonon modes $(\mathbf{q}, s)$. Equations (33) and (34) give $\gamma' = 3.9$, $\gamma_{44} = 3.8$ in bcc Fe, and $\gamma' = 4.4$, $\gamma_{44} = 5.2$ in fcc Al (Grimvall, 1999).

The Clausius-Clapeyron equation expresses the pressure dependence of the temperature $T_{\rm eq}$ at which two phases α and β are in thermal equilibrium:

$$\frac{dT_{\rm eq}}{dP} = \frac{V_\alpha - V_\beta}{S_\alpha - S_\beta}. \tag{35}$$

The common-tangent construction is illustrated in Fig. 1 (between points 2 and 3). The slope of the tangent gives the (sign-reversed) pressure $P_{\rm tr}$ at which a transformation from one phase to another becomes energetically favorable. That pressure should not be confused with the critical pressure $P_{\rm crit}$ at which a lattice becomes dynamically unstable.

The equation of state $V(P, T)$ for stable structures of several metallic elements has been discussed by, e.g., Karbasi, Saxena, and Hrubiak (2011).

B. Pressure-induced instabilities at $T = 0$ K

The Grüneisen parameters are usually positive. Thus we expect that $\omega(\mathbf{q}, s)$, C', and C_{44} increase with pressure. However, this can be interpreted as a change in the energy scale for atomic vibrations, while instabilities depend on the relative energies in different atomic configurations. In Fig. 19 the phonon dispersion curves have therefore been normalized to enhance the emerging instability.

There are many examples where a structure that is dynamically unstable at low pressures becomes stabilized at high pressures. There are also examples where certain phonon modes soften so much with increasing pressure that the initially stable lattice becomes dynamically unstable. Since an unstable lattice is not accessible to experiment, one must rely on theoretical calculations. They are most easily carried out at constant volume, rather than at constant pressure (see Sec. II.B.4). The bcc and fcc phases of W give an illustrating example. At $T = 0$ K some phonon modes in the bcc phase soften under compression (see Figs. 19 and 20). On the other hand, the unstable fcc phase is gradually stabilized, with all phonon frequencies being positive at very high compression (see Fig. 21).

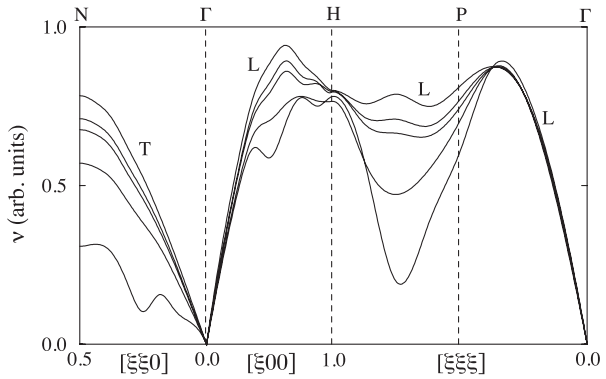

FIG. 19. Calculated phonon dispersion curves for selected branches of bcc W at the ground-state volume V_0 (top curves) and four compressed volumes $(0.91V_0, 0.85V_0, 0.66V_0, 0.44V_0)$, scaled to a common maximum frequency; 18.9 THz for longitudinal and 15.7 THz for transverse modes, respectively. For each Brillouin zone direction, the polarization (L or T) with the strongest pressure-induced softening is plotted. The lowest curve corresponds to the lowest volume, and so forth. From Einarsdotter *et al.*, 1997.

Figure 22 shows that a pressure-induced instability may be localized to a certain pressure range, with stability on either side of that interval (Qiu and Marcus, 2008a); see also Suzuki and Otani (2002), Landa *et al.* (2006a, 2006b), Lee *et al.* (2007), and Verma and Modak (2008). Closely related to the pressure-induced lattice instabilities are instabilities under

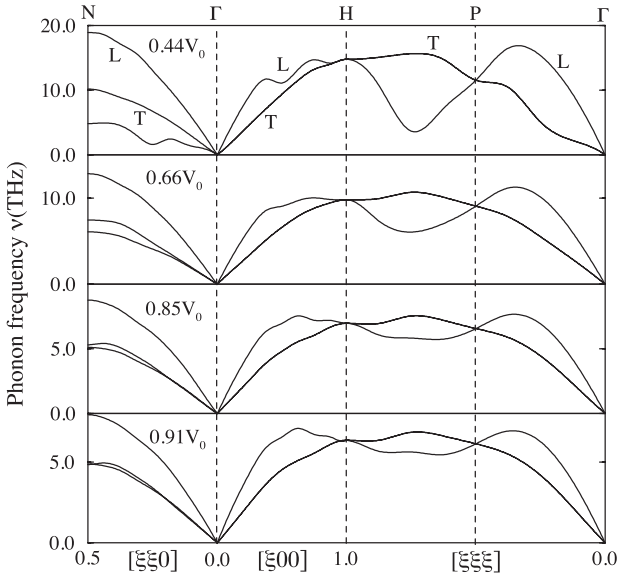

FIG. 20. Calculated phonon frequencies in bcc W at different volumes, corresponding to the pressures 1200, 300, 60, and 30 GPa, respectively. V_0 is the equilibrium volume of bcc W at zero pressure. From Einarsdotter *et al.*, 1997.

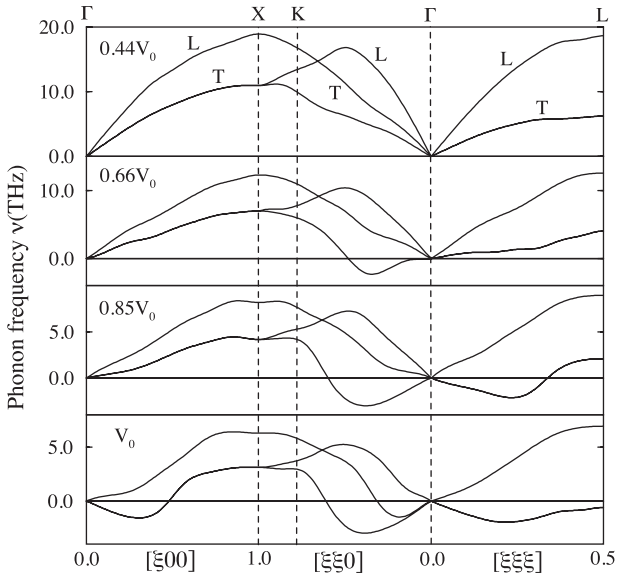

FIG. 21. Calculated phonon frequencies in fcc W at four different volumes. V_0 is the equilibrium volume of fcc W at zero pressure. From Einarsdotter *et al.*, 1997.

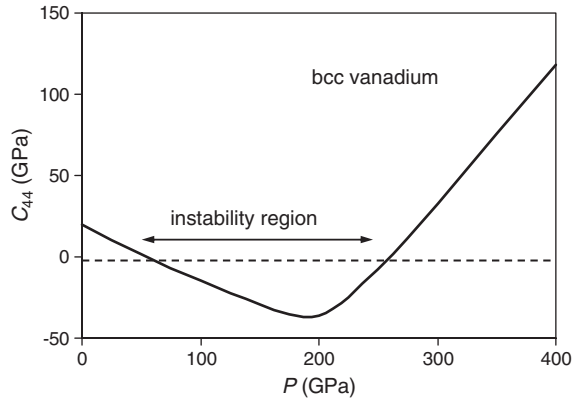

FIG. 22. An elastic instability may be localized to a certain pressure range, with stability at lower and higher pressures. The figure, based on data from Qiu and Marcus (2008a), shows smoothed C_{44} in bcc vanadium, as a function of pressure P. This system has the less common feature that $C_{44} < 0$ while $C' > 0$.

other load conditions. They are discussed in Sec. VIII on the theoretical strength.

C. *P-T* phase diagram with a lattice instability

Magnesium has the hcp structure in thermal equilibrium at ambient temperature and pressure, where its bcc structure is dynamically unstable. At high pressures, however, bcc Mg is the thermodynamically most stable phase. Thus there is a critical pressure P_{crit} below which bcc Mg is dynamically unstable. Figure 23 shows a suggested *P-T* phase diagram. A characteristic feature is the maximum in the phase boundary at $(P_{\max}, T_{\max})$, where the two crystalline phases are dynamically stable and in thermal equilibrium with each other. However, experiments have cast doubts on this shape (Errandonea *et al.*, 2003). In Appendix E we therefore

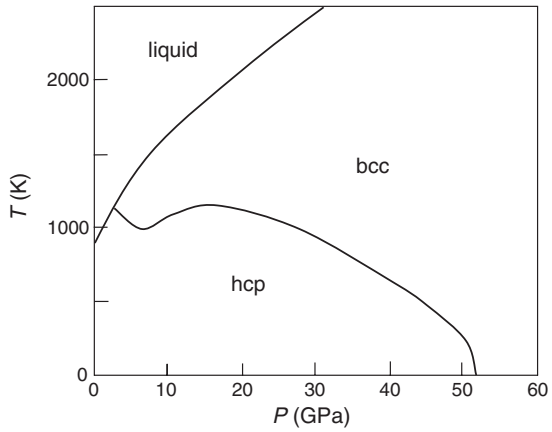

FIG. 23. A tentative *P-T* phase diagram for Mg, from Grimvall (1999) and based on calculations by Moriarty and Althoff (1995).

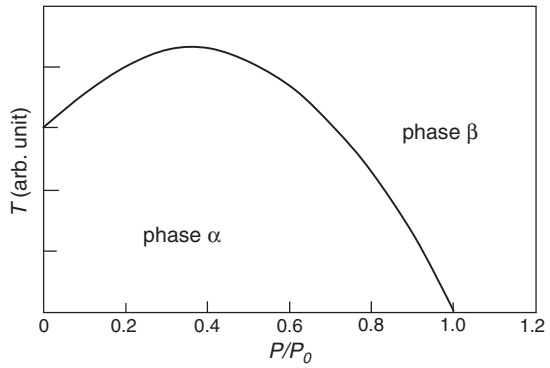

FIG. 24. *P-T* phase diagram obtained in a simple model for $G(P, T)$; see Appendix E.

construct a simple model for the Gibbs free energy $G(P, T)$ that gives a shape similar to that in Fig. 23.

The phase α in the model is thermodynamically stable at low temperatures and pressures and has no unusual features. Phase β is dynamically unstable at pressures $P < P_{\mathrm{crit}}$, but has no other irregularities. With data chosen as in Appendix E we get the phase diagram in Fig. 24, which gives a schematic illustration of how the presence of a dynamical lattice instability can give rise to a maximum in T_{eq}. (The phase boundary should be modified at low T, since the third law of thermodynamics requires that $\partial T_{\mathrm{eq}}/\partial P \to -\infty$ when $T \to 0$, but that is not important for the point we want to make here.) According to the Clausius-Clapeyron equation, $dT_{\mathrm{eq}}/dP = 0$ implies that $V_\alpha = V_\beta$ at $T_{\mathrm{eq}} = T_{\max}$. It is the excess entropy related to the vibrational instability that leads to a variation in the sign of $V_\alpha - V_\beta$ and hence to a maximum in the *P-T* phase diagram; see Appendix E and also the discussion of bcc and hcp Be of Sin'ko and Smirnov (2005).

VI. TEMPERATURE EFFECTS

A. General aspects

We write the temperature-dependent phonon frequencies in the form (Barron, 1965; Cowley and Cowley, 1966; Grimvall, 1999)

$$\omega(\mathbf{q}, s) = \omega_0(\mathbf{q}, s) + \Delta_{\mathrm{qh}}(\mathbf{q}, s; T) + \Delta_{\mathrm{anh}}(\mathbf{q}, s; T), \quad (36)$$

where $\omega_0(\mathbf{q}, s)$ is the frequency in the strictly harmonic approximation, $\Delta_{\mathrm{qh}}(\mathbf{q}, s; T)$ is the quasiharmonic shift that is caused by thermal expansion, and $\Delta_{\mathrm{anh}}(\mathbf{q}, s; T)$ is the explicitly anharmonic shift that is caused by the change in vibrational displacement with varying T. The last term is present also at fixed crystal volume. In phases that are far from being unstable, such as the ground states of the simple metallic elements, $\Delta_{\mathrm{qh}}(\mathbf{q}, s; T)$ usually dominates over $\Delta_{\mathrm{anh}}(\mathbf{q}, s; T)$ and leads to a gradual softening of the phonons, typically by 10%–15% from low T to the melting point (Rosén and Grimvall, 1983). Then $C_V(T)$ is close to the classical value $3k_B$/atom also at high T, which is often taken as a sign that the explicit anharmonicity is small. However, that argument can be misleading, as shown in Al where anharmonic effects are significant but tend to cancel in $C_V(T)$ (Forsblom, Sandberg, and Grimvall, 2004).

Equation (36) implies that it is meaningful to talk about an effective and temperature-dependent phonon frequency (or corresponding Debye temperatures and elastic constant) even in the presence of anharmonicity. As we noted in Sec. III.B.4 this is true within low-order perturbation theory, but in the spirit of a variational approach we use such a description in this review also when the vibrations are far from harmonic. It is also the assumption made when a thermodynamic function is divided into vibrational, electronic, defect formation, and magnetic contributions (Forsblom, Sandberg, and Grimvall, 2004; Grabowski, Hickel, and Neugebauer, 2007; Körmann *et al.*, 2008, 2010; Grabowski *et al.*, 2009).

The thermal expansion alone may be sufficient to make a metastable phase dynamically unstable at high T, as found in the metallic body-centered tetragonal structure of Si (Ekman, Persson, and Grimvall, 2000). More important, and of main concern here, is the stabilization of a structure that has dynamically unstable phonon modes at low T. Striking examples are bcc Ti, Zr, Hf, and Pu that not only become metastable but also the thermodynamically most stable phase at high temperatures.

B. Double-well potential

The stabilization of phonon modes which are unstable at low T has often been discussed with reference to a double-well potential in the form (in one dimension) $V(x) = Ax^4 - Bx^2$. At low temperatures the system is unstable for $x = 0$, while at high temperatures (large thermal energies and atomic displacements) $V(x)$ is dominated by the x^4 term. The potential is reminiscent of the Landau model of phase transformations, which has led to confusion regarding soft phonon modes. The Landau model *per se* will not be further discussed here, since Landau-type mode softening usually plays a secondary role in structural phase transformations (Krumhansl and Gooding, 1989; Krumhansl, 1992).

Much work has been done on bcc Zr. Figure 25 shows a double well used to model the low-lying transverse mode at the N point in the Brillouin zone; $\mathbf{q} = [0.5, 0.5, 0]$ (Willaime and Massobrio, 1991). Similar results were obtained by Chen *et al.* (1985) and Wang *et al.* (2002). An alternative shape of the double well was suggested by Drummond and Ackland (2002). Sanati *et al.* (2001) applied a Landau-type free energy expression. Ye *et al.* (1987) and Nishitani, Kawabe, and Aoki (2001) found anharmonic stabilization of bcc Zr. Trubitsin (2006a, 2006b) invoked electronic entropy effects that change the double-well character. Porta and Castán (2001) modeled bcc Zr with a tight-binding potential in a Monte Carlo simulation and found that C' was stabilized above about 1500 K.

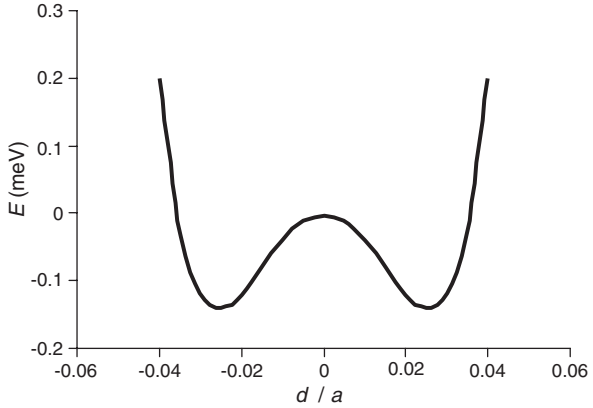

FIG. 25. A double well used by Willaime and Massobrio (1991) to model the instability of the T_1 N-point phonon in bcc Zr. The displacement d is in units of the lattice parameter a.

C. Self-consistent phonon calculations

Although analytic potentials such as those in the preceding section can be used to model the stabilization of phonons at high temperatures, they do not provide much additional insight for a real system. Instead we turn to a combination of molecular dynamics and electronic structure calculations.

Souvatzis *et al.* (2008, 2009) developed the so-called self-consistent *ab initio* lattice dynamical (SCAILD) calculations, which is a quantum-mechanical realization of the self-consistent phonon method (Born, 1951; Hooton, 1958; Koehler, 1968). The self-consistent phonon method was developed to treat strongly anharmonic systems where the harmonic phonon frequencies may even be unstable, such as crystals of noble gases. It is particularly well suited to study the dynamical properties of the high-temperature bcc phases of early transition metals (Sc, Ti, Zr, La, Hf) where the harmonic approximation gives unstable phonons. SCAILD determines phonon frequencies using Hellmann-Feynman forces in a periodic bulk supercell where atoms have been displaced from their equilibrium positions according to the phonon amplitudes determined by the temperature and phonon mode frequencies. Since the phonon amplitudes themselves depend on the temperature and phonon mode frequencies, the approach requires a self-consistency loop where one iterates until the phonon frequencies used to generate the displacement coincide with those calculated from the Hellmann-Feynman forces. Since all phonons that are commensurate with the size and shape of the supercell contribute to the displacements, anharmonic interactions between different phonon modes are included in the calculated frequencies. The SCAILD method gives a set of harmonic phonon frequencies in which anharmonic effects are

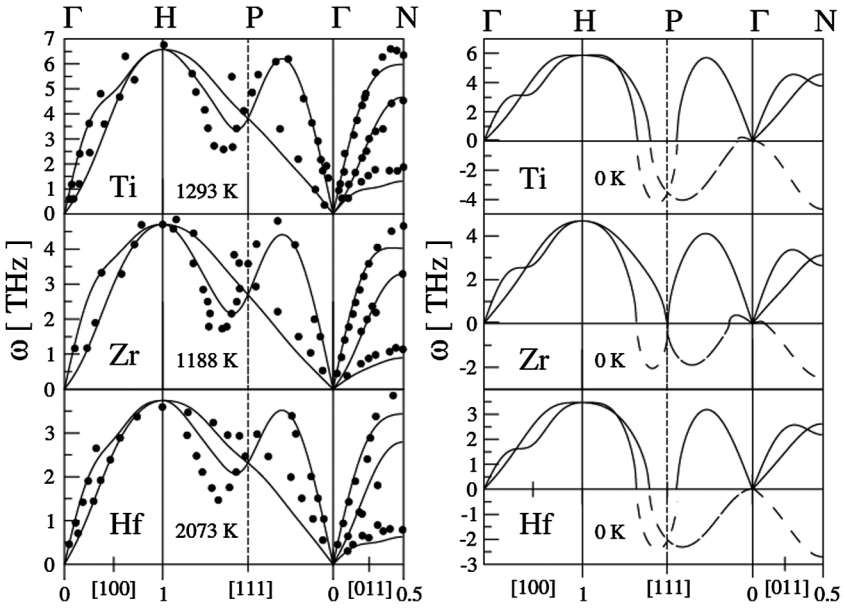

FIG. 26. Calculated phonon dispersion curves for bcc Ti, Zr, and Hf at $T = 0$ K and at high temperatures. Filled circles are experimental data (Heiming *et al.*, 1991; Petry *et al.*, 1991; Trampenau *et al.*, 1991). From Souvatzis *et al.*, 2008.

approximately accounted for in a self-consistent way. Even though higher-order anharmonicity can be treated, effects associated with phonon-phonon scattering and finite phonon lifetimes remain unaccounted for. Previous SCAILD calculations based on the density-functional theory (DFT) showed that phonons in the bcc phases of Ti, Zr, and Hf can be stabilized at high temperatures, and that phonon anomalies in these phases can be reproduced (see Fig. 26). This approach can also yield anharmonic contributions to the free energies if the self-consistent phonon frequencies are used in the formula for the harmonic entropy. In fact, it can be shown that the self-consistent phonon approach represents a variational upper bound on the exact anharmonic free energy and can be derived from the Bogoliubov inequality in statistical mechanics (Feynman, 1972).

Another class of approaches is based on using *ab initio* molecular-dynamics (AIMD) simulations at high temperatures with the forces calculated from the DFT using the Hellmann-Feynman theorem. These methods are firmly established and will not be reviewed here. Even though AIMD usually involves significantly greater computational expense than SCAILD, these simulations give access to a wealth of information about the true anharmonic dynamics at high temperatures. For instance, MD trajectories can be used to analyze the average atomic positions and mean-square displacements, offering information about the crystal structure and correlation functions. Phonon densities of states can be obtained via the Fourier transform of the velocity autocorrelation function, and the calculated dynamical structure factors can be used to extract anharmonic frequency shifts and phonon lifetimes (Zhang *et al.*, 1995). AIMD can also be used to obtain anharmonic free energies; see below.

Recently, Asker *et al.* (2008) studied the effect of vibrational disorder in fcc Mo that is well known to be dynamically unstable in $T = 0$ K calculations. It should then be noted that for Mo (unlike Ti, Zr, and Hf) the ground-state structure (bcc) remains the thermodynamically stable phase up to the melting temperature. Asker *et al.* (2008) found that within the constraint of a fixed supercell, fcc Mo was dynamically stabilized at high temperatures.

Ozoliņš (2009) used another approach to study the possible stabilization of fcc W at high temperatures. We recall that this phase is strongly unstable at 0 K, both elastically ($C' < 0$ and $C_{44} < 0$) and for short-wavelength phonons (see Fig. 4). However, if the atoms are confined to a simulation supercell of fixed shape and size Λ, the instabilities corresponding to modes with wave vectors shorter than $2\pi/\Lambda$ can be suppressed. Under these constraints, *ab initio* free energy and entropy differences between the fcc and bcc phases of W were obtained by using thermodynamic integration of average stresses along the Bain path. The validity of this approach is based on the fact that high-temperature anharmonic effects can stabilize harmonically unstable short-wavelength phonons. In agreement with the results of Asker *et al.* (2008) for Mo, Ozoliņš (2009) found that the tungsten atoms could maintain the fcc structure inside the simulation cell above 2500 K, showing that all the short-wavelength phonons had then been stabilized. Figure 27 shows the changes in the internal energy, total entropy (including vibrational and electronic contributions), and the free energy as functions of the Bain distortion in W. The calculated fcc-bcc enthalpy and entropy differences at $T = 3500$ K (308 meV and $0.74k_B$ per atom, respectively) agree well with the range of values derived from comprehensive analysis of experimental data (Guillermet *et al.*, 1995).

The calculations of Ozoliņš (2009) also showed that the instability $C' < 0$ remained up to 3500 K. Thus, as illustrated in Fig. 28, the transverse acoustic $[\xi\xi 0]$ phonon branch with the $[\bar{1}10]$ polarization is unstable in the long-wavelength limit for wave vectors below some critical value ξ_c, setting an upper limit on the possible system size. Supercells with linear dimensions above $\Lambda_c = 2\pi/\xi_c$ transform into martensitic

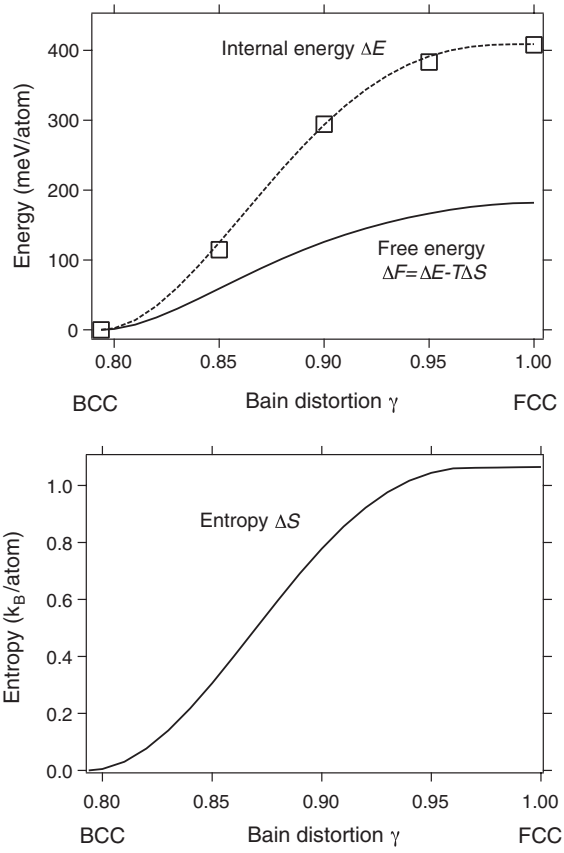

FIG. 27. The changes in the free energy and the entropy as calculated by Ozoliņš (2009) at $T = 2500$ K, as a function of the Bain distortion in W.

configurations, which are characterized by bcc-like regions separated by domain walls or twin boundaries (Pinsook and Ackland, 1998, 2000; Morris and Ho, 2001).

It is worth pointing out a shortcoming of supercell-based approaches, which can give information only about phonons at a discrete set of wave vectors that are commensurate with the size and shape of the chosen supercell. In contrast, the DFT perturbation theory (Baroni *et al.*, 2001) can yield phonon frequencies at a general wave vector in the Brillouin zone. This distinction is expected to be more important at low temperatures where the long-wavelength acoustic phonons, which cannot be well represented in the relatively small supercells amenable to AIMD, may contribute significantly to the thermodynamic functions.

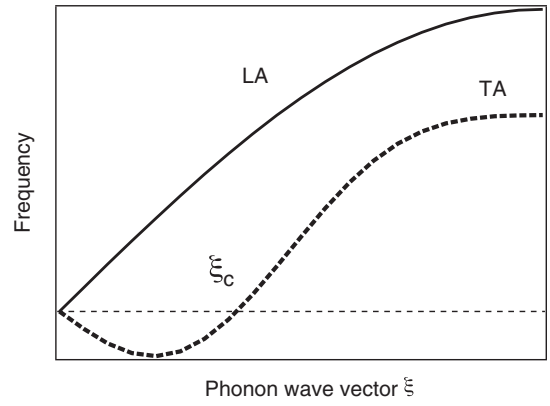

FIG. 28. Schematic dependence on the wave vector of the $[\xi\xi 0]$ phonon dispersion in fcc W at high temperatures.

D. Discussion

Since a dynamically unstable phase is not accessible to experiment, one must rely on theoretical calculations for such hypothetical structures. Temperature enters the *ab initio* calculations in three ways: explicitly through a smearing in the Fermi-Dirac factors and indirectly through thermal expansion and through changes in the effective electron band structure caused by the increased vibrational disorder (while preserving the overall lattice symmetry). Asker *et al.* (2008) and Ozoliņš (2009) found that thermal disorder dominates completely over the effect of the Fermi-Dirac factors.

Figure 29 shows the effects of vibrational disorder on the electronic density of states (eDOS) of fcc Mo. It is seen that displacements of atoms from the ideal lattice sites at 3200 K cause large changes in the eDOS around the Fermi level in both bcc and fcc phases of Mo. In particular, the sharp peak in the eDOS of fcc Mo just below the Fermi level is smeared out by positional disorder, while the pronounced valley in the eDOS of bcc Mo is filled with electronic states that have been pushed upward in energy by disorder. Asker *et al.* (2008) used this to argue that these changes in the electronic structure are responsible for dynamical stabilization of the fcc phase at high temperatures.

It is a general observation that as long as the character of the bonding (e.g., metallic) is preserved, the averaged phonon frequency $\omega_{\log}$ usually varies by less than about 5% with the lattice structure. Even in systems which are barely dynamically stable, $\omega_{\log}$ does not differ drastically when compared with other stable or metastable phases of the same substance. As an example, consider the thermodynamically stable hcp and bcc phases of Ti and Zr, where the phonon frequencies have been measured at several temperatures. From them one obtains the vibrational entropy $S_{\rm ph}(T)$; cf. Eq. (36) and the comment on anharmonicity in Sec. III.B.4. Next let Θ_S be the entropy Debye temperature which reproduces $S_{\rm ph}(T)$ when inserted in the Debye-model entropy formula. Figure 30 gives the result. In the temperature region where the hcp structure is the equilibrium phase, Θ_S has the normal gradual decrease that is largely due to thermal expansion. In the region of the

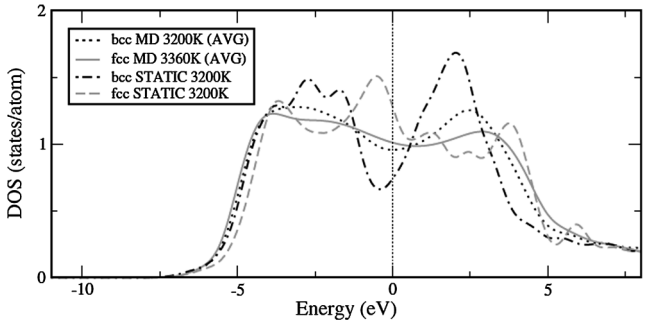

FIG. 29. The electron density of states $N(E)$ for fcc and bcc Mo, calculated at high temperatures in a static lattice and in an average thermally disordered lattice. From Asker *et al.*, 2008.

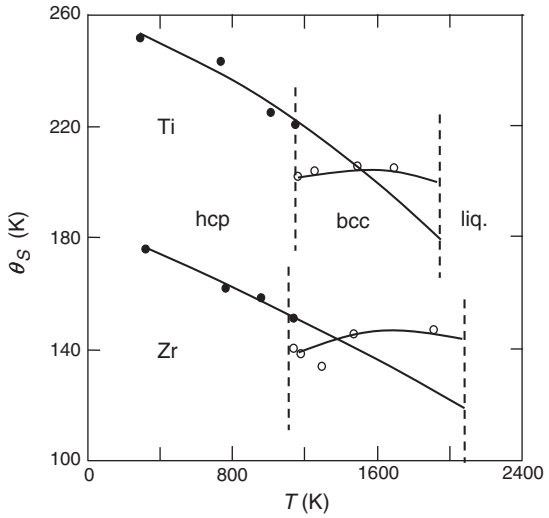

FIG. 30. The entropy Debye temperature Θ_S for hcp and bcc phases of Ti and Zr, calculated from phonon frequencies obtained in neutron scattering experiments. From Grimvall, 1999.

bcc phase, Θ_S has a maximum as a function of T. It can be understood as the combined effect of an increase due to continued stabilization of the phonons that are unstable at low T and a superimposed normal decrease with T; see also Ozoliņš (2009) for a comparison of vibrational entropies in bcc and fcc W at high temperatures, when the remaining elastic shear instability has been suppressed. An entropy Debye temperature such as that in Fig. 30 (which in fact is a one-parameter phonon model rather than the standard Debye model that is based on the long-wavelength part of the vibrations) can be viewed as a simple representation of the self-consistent phonon description without any attempt to carry out the self-consistent calculations.

The present understanding of the high-temperature vibrational properties of systems such as Mo, W, Ti, Zr, and Hf rests on computationally demanding electronic structure calculations. The results are in line with a suggestion (Grimvall, 1979) that strong electron scattering could give a unified explanation for several anomalous thermophysical properties of bcc Ti, Zr, and Hf at high temperatures: saturating electrical resistivity, self-diffusion coefficent, elastic constants, and phonon frequencies (cf. Fig. 30). It was argued that temperature-dependent force constants in an essentially harmonic model for the lattice vibrations, rather than the traditional expansion in higher-order atomic displacements, would give a simple account of the anomalies.

VII. TRENDS IN ELASTIC SHEAR CONSTANTS

A. Elements in the fifth row of the periodic table

Appendix J reviews C' and C_{44} in all the metallic elements. Here we discuss the fifth row in the periodic table because it offers the most complete set of data. Table II summarizes measured (Every and McCurdy, 1992) and theoretical C' and C_{44}. Several of the elastic constants were calculated by K. A. Persson for this review using the procedures described by Kraft *et al.* (1993). The total-energy calculations were performed with the generalized gradient approximation (GGA) in the density-functional theory as implemented in the Vienna *ab initio* simulation package (VASP) (Kresse and Furthmüller, 1996). Projected augmented wave (PAW) pseudopotentials (Kresse and Joubert, 1999) were used, and energy cutoffs were automatically chosen under the ''precision high'' scheme.

TABLE II. Elastic constants of elements in the fifth row in the periodic table.

Element	structure at 0 K	bcc C' (GPa)	bcc C_{44} (GPa)	fcc C' (GPa)	fcc C_{44} (GPa)
Cs	bcc	0.2	1.5	0.2[b]	1.9[b]
Ba	bcc	3	10	5[a]	22[a]
La	fcc	1	10	7	18
Hf	hcp	−18[a]	53[a]	28[a]	67[a]
Ta	bcc	53	83	−102[b]	19[b]
W	bcc	160	160	−180[a]	−146[a]
Re	hcp	−3[a]	174[a]	147[a]	216[a]
Os	hcp	−257[a]	253[a]	143[a]	329[a]
Ir	fcc	−383[b]	138[a]	170	263
Pt	fcc	−38[a]	158[a]	48	77
Au	fcc	−23[a]	74[a]	15	42

[a]Numbers calculated *ab initio* for this review by K. A. Persson, using VASP (GGA-PAW-Perdew-Burke-Ernzerhof functional).
[b]Numbers based on *ab initio* results cited in Appendix J. Numbers without a label refer to experiments (Every and McCurdy, 1992).

We note that while there are many examples in Table II where $C' < 0$, there is only one entry with $C_{44} < 0$ (W). This can be related to the fact that $C_{44} < 0$ implies a more severe lattice instability than $C' < 0$; cf. the discussion in Sec. II.B. Another example of $C_{44} < 0$ is V under moderate pressure as discussed in Sec. V.B, fcc Nb (but not fcc Ta), fcc Mo, fcc Cd, bcc Zn and, possibly, also fcc Zn (see Table III and Appendix J).

C' and C_{44} are plotted in Figs. 31 and 32 for fifth row elements. In most cases either the bcc or the fcc lattice is dynamically stable at 0 K. If C' is large and positive for the bcc structure, it tends to be large and negative for the fcc structure, and vice versa. The elastic constants for the third and fourth rows in the periodic table show a pattern very similar to that of the fifth row elements, but magnetism or lack of data complicate a detailed discussion. An earlier version of Figs. 31 and 32 (Grimvall, 2005) was based on less reliable elasticity data.

TABLE III. Elements with unusual stability properties. The thermodynamic equilibrium phase is denoted stable. The stability of fcc Zn is unclear. See Appendix J for references.

Element	Structure bcc	fcc	hcp
Fe	Stable	Metastable	Metastable
Cu	Unstable	Stable	Unstable
Zn	Unstable	(Unstable)	Stable
Si	Unstable	Unstable	Unstable
Po, Pr, U, Np	Unstable	Unstable	
Nb, Mo, W	Stable	C', $C_{44} < 0$	

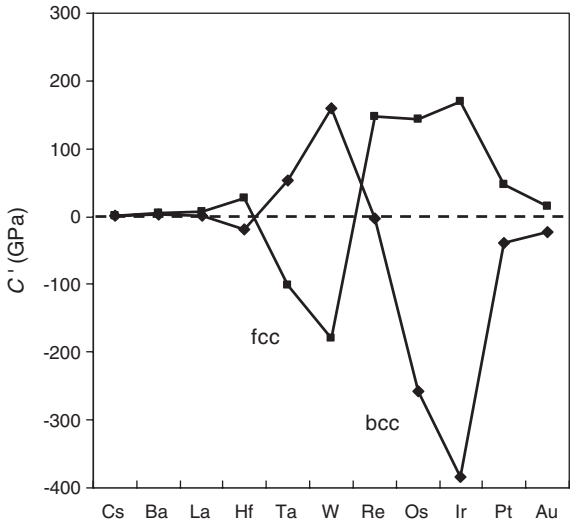

FIG. 31. The elastic shear constant C' for the fifth row elements. Data from Table II.

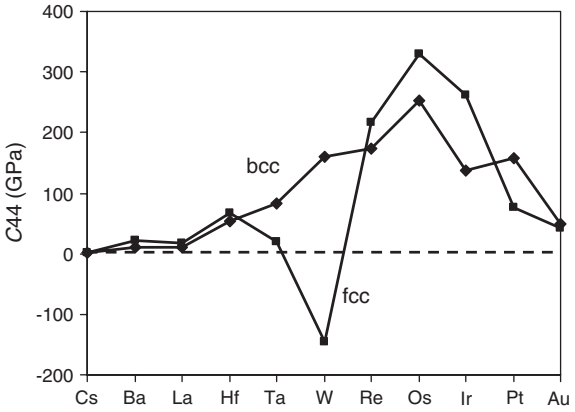

FIG. 32. The elastic shear constant C_{44} for the fifth row elements. Data from Table II.

B. Elements with unusual stability properties

Although this review does not discuss the hcp structure in detail, we note that if the hcp structure is dynamically stable at 0 K, the fcc structure is normally also dynamically stable, and vice versa (cf. Appendix J). This is natural since both structures are close packed, with identical nearest-neighbor configurations. Further, the previous section showed that when the bcc lattice is dynamically stable, the corresponding fcc lattice tends to be dynamically unstable, and vice versa. Table III gives some exceptions to these patterns, at low temperatures and ambient pressure.

The stabilities of iron phases depend on their magnetic state, as discussed in Sec. VII.D and Appendix J.

The fcc phase of Zn was found to be dynamically weakly metastable by Magyari-Köpe, Grimvall, and Vitos (2002), but weakly unstable by Müller *et al.* (1999), Marcus, Jona, and Qiu (2002), and Qiu and Marcus (2008b).

The ground states of Al and Ni are fcc, with bcc being dynamically unstable. However, stoichiometric AlNi is stable in the bcc lattice along the tetragonal Bain path but unstable in the fcc structure (Wang *et al.*, 2004). Further, AlCu is unstable in both the fcc and bcc structures along the tetragonal Bain path, although Al and Cu both have the fcc equilibrium structure (Wang *et al.*, 2004). The fcc-based Au_3Pt alloy has unstable phonon modes of intermediate wavelength at $T = 0$ K, while both Au and Pt have the fcc equilibrium structure (Li, Chang, and Peng, 2009).

Polonium is the only element that has the sc structure as the thermodynamic ground state at ambient conditions; see Appendix J. In most other cases the sc lattice is dynamically unstable. However, calcium, which is fcc at ambient conditions, becomes thermodynamically stable in the sc structure at high pressure and 300 K, although that structure has imaginary phonon frequencies when anharmonic effects are neglected (Yao, Klug *et al.*, 2009).

Niobium, molybdenum, and tungsten show the unusual behavior that both fcc shear constants are negative, implying that all transverse phonon modes are unstable in the elastic limit; cf. Sec. II.B.2.

C. Trends in the electronic structure

Friedel (1969) suggested a simple model that described the trends in the cohesion energy U_{coh} of transition metals, and their bulk modulus B, as a function of the number n_d of d electrons [see also Pettifor (1977)]. The electron density of d states $N_d(E)$ is given a rectangular shape, and the s and p electrons are ignored. In this model, $U_{coh}(n_d)$ and $B(n_d)$ get a parabolic variation with n_d. Friedel's approach represents the first term in a series expansion in the moments of $N_d(E)$ (Ducastelle, 1970). With higher moments included, one obtains approximations not only for $U_{coh}(n_d)$ and $B(n_d)$ but also for $C'(n_d)$ and $C_{44}(n_d)$ (Nastar and Willaime, 1995). The trend in the variation of C' and C_{44} across the d series that was discussed above is qualitatively reproduced when higher moments are included; cf. Figs. 31 and 32 with Fig. 33.

This discussion refers to elements, but related arguments can be applied to compounds. Under large elastic deformation FeAl fails by a shear instability, in contrast to NiAl that fails by tension. The difference in behavior of two otherwise similar compounds is explained by the filling of antibonding

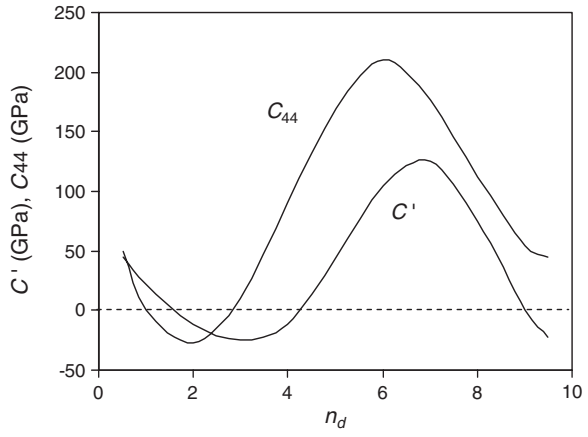

FIG. 33. The elastic constants C' and C_{44} in the fcc structure, calculated in the fifth-moment approximation, as a function of the number of electrons n_d. Adapted from Nastar and Willaime, 1995.

d states in FeAl (Li, Morris, Jr., and Chrzan, 2004; Li, Morris, Jr., and Chrzan, 2006).

Numerical electronic structure calculations provide detailed explanations of the softening or instability of phonon modes. Band structure features near the Fermi energy are then of particular importance. A Fermi surface nesting effect arises between two almost parallel flat pieces of the Fermi surface. It is responsible for phonon softening in Li under high presssure (Kasinathan *et al.*, 2006; Profeta, 2006; Rodriguez-Prieto *et al.*, 2006). Electronic topological transitions, for instance, the sudden appearance or disappearance of a neck in the Fermi surface, can also occur when the alloy composition is varied. Electron band Jahn-Teller–like effects, invoking splitting, shifting, or hybridization, can open or close energy gaps at the Fermi energy. Landa *et al.* (2006a, 2006b) discussed various such electronic structure effects in the V-Nb system.

Ab initio calculations can, in some sense, be considered as a ''brute force'' approach. There is a need also for more intuitive understanding. Rousseau *et al.* (2011) showed how Li and Na, which are free-electron-like metals with high-symmetry lattices at ambient conditions, radically change their electronic structure under high pressure and take complex structures of low symmetry. Before the era of computers, alloy stability considerations were often based on the well-known rules of Hume-Rothery and Mott and Jones that referred to the Brillouin zone concept. Such ideas have been revived, in combination with *ab initio* work, to get deeper insight into the stability of compounds under pressure (Feng *et al.*, 2008; Feng, Hoffmann, and Ashcroft, 2010).

D. Magnetic effects

Usually, the ground-state structure is the same within a column in the periodic table, but the elements Mn, Fe, and Co are exceptions (cf. Fig. 3) due to their magnetic properties. Symmetry breaking through an ordered magnetic state is coupled to a structural distortion, i.e., a lattice instability (Marsman and Hafner, 2002). In this section we focus on results for the stability of phonons (elastic constants) in Mn, Fe, Co, Cr, and Ni, and only briefly refer to their magnetic structures *per se*. References are found in Appendix J.

The ground state of Mn at ambient conditions (α-Mn) has a complex bcc-related structure with 58 atoms per unit cell, and not much is known about its vibrational properties. *Ab initio* electronic structure calculations gave two energy minima in the antiferromagnetic tetragonal structure. The state with the lowest energy and lattice parameter ratio $c/a = 0.94$ was connected with γ-Mn, while a metastable state with lower c/a was connected with δ-Mn. Antiferromagnetic Mn is dynamically unstable in the bcc structure. Nonmagnetic bcc Mn has $C' < 0$. The information on close-packed Mn in hypothetical magnetic states is incomplete and uncertain (Qiu, Marcus, and Ma, 2000a, 2000b).

Many papers are devoted to *ab initio* studies of Fe. In hypothetical nonmagnetic Fe, the fcc and hcp structures are stable under shear, with hcp Fe being lowest in energy, while the bcc lattice has $C' < 0$, in agreement with the trends in Figs. 3, 31, and 32, Also the N-point transverse phonon is unstable in nonmagnetic bcc Fe. Thus it is ferromagnetism that makes bcc Fe (α-Fe) the most stable phase at ambient conditions. On the other hand, ferromagnetism makes close-packed Fe unstable in shear. The equilibrium phase (γ-Fe) between 1173 and 1660 K has a paramagnetic fcc structure. That lattice symmetry would be broken at low temperatures where *ab initio* calculations show an antiferromagnetic state, which explains why fcc Fe cannot be retained at low temperatures by quenching. The hcp structure, which is stable at high pressures, is nonmagnetic. (Note the difference between a nonmagnetic state, i.e., complete absence of local magnetic moments, and a paramagnetic state with disordered magnetic moments.)

Ferromagnetism stabilizes the hcp structure of Co. In the absence of magnetic effects, Co takes the fcc structure that is observed also for the elements Rh and Ir in the same column in the periodic table. Nonmagnetic and ferromagnetic bcc Co are dynamically unstable.

Cr and Ni have the same crystal structures as the nonmagnetic elements in the same columns in the periodic table, i.e., bcc and fcc, respectively. The ground state of Cr has a complicated spin wave structure (Fawcett, 1988), and Ni is ferromagnetic. Hypothetical nonmagnetic Cr is dynamically unstable in the fcc structure and metastable in the fcc structure, with the opposite behavior for nonmagnetic Ni, in agreement with the trends in Figs. 31 and 32.

In *ab initio* calculations one can study the variation in the total energy and the equilibrium magnetic moment as one moves along a Bain-type path and assuming nonmagnetic, ferromagnetic, or various antiferromagnetic states. Such works illustrate the complex and important role of magnetism in stabilizing the lattice structures of some 3*d* transition elements; see, e.g., Friák (2011) on α-Fe and Zelený, Friák, and Šob (2011) on Fe, Co, and Ni along the trigonal deformation path.

E. Effect of alloying on C' and C_{44}

Consider a (dilute) solid solution of atoms in a host lattice with the fcc or bcc lattice structure. The effect of alloying on the elastic constants can be divided into two parts: a ''global'' term that is related to the volume change as expressed through the lattice parameters, and a ''local'' or ''chemical'' term that is related to the changes in the interatomic force constants. Volume changes were considered in Eqs. (33) and (34). The total change of the elastic constants with the alloy composition c can now be written as

$$\frac{dC'}{dc} = \left\{-\gamma'\left[\frac{1}{V}\left(\frac{\partial V}{\partial c}\right)\right] + \frac{1}{C'}\left(\frac{\partial C'}{\partial c}\right)_V\right\}C' \tag{37}$$

and

$$\frac{dC_{44}}{dc} = \left\{-\gamma_{44}\left[\frac{1}{V}\left(\frac{\partial V}{\partial c}\right)\right] + \frac{1}{C_{44}}\left(\frac{\partial C_{44}}{\partial c}\right)_V\right\}C_{44}. \tag{38}$$

The Grüneisen-type parameters γ' and γ_{44} were discussed in Sec. V.A. If also $\partial V/\partial c$ is known, we readily obtain the contribution from the change in the average volume per atom. Often the effect is small compared with that from the local change in the interatomic forces (Taga *et al.*, 2005). We now give three examples of the variation of elastic shear constants with composition, relying on experimental data

for bcc Zr-Nb-Mo and Fe(bcc)-Ga alloys, and *ab initio* calculations for fcc and bcc Ag-Zn alloys, respectively.

1. Zr-Nb-Mo

There are experimental elastic constant data at low temperatures in the bcc Zr-Nb-Mo binary solid solution series, from $Zr_{0.8}Nb_{0.2}$ to pure Mo (see Fig. 34). Taking into account that the experimental uncertainty in C' and C_{44} is at least as large as the height of the symbols in the graph, Fig. 34 suggests that Zr in a hypothetical bcc structure is close to being either stable or unstable under shear, $C' \approx 0$. However, there is a general decrease in the interatomic forces toward either end of the transition metal series in the periodic table, as exemplified by Figs. 31 and 32. Therefore one can get further insight if C' and C_{44} are normalized as C'/B and C_{44}/B. The resulting Fig. 35 shows that C_{44} tends to stiffen significantly as one approaches bcc Zr ($n = 4$), while the near instability related to C' prevails. Above 1138 K the thermodynamically stable structure of Zr changes from hcp to bcc, but the bcc lattice cannot be retained in Zr at room temperature by quenching from high temperatures. This has been taken as experimental evidence that the bcc phase is dynamically unstable at low temperatures. Many theoretical phonon calculations corroborate this idea. For instance, using the method described in Sec. VII.A, K. A. Persson obtained $C' = -3$ GPa and $C_{44} = 28$ GPa at $T = 0$ K, in good agreement with Fig. 34. The stabilization of the bcc phase at high temperatures was discussed in Sec. VI.

2. Fe-Ga

The bcc Fe-Ga system can form a random solid solution at room temperature, up to about 20 at. % Ga. Above that concentration, the cubic structure is more complex. The volume per atom increases almost linearly with Ga content being about 5% higher at 20 at. % Ga, compared with pure Fe (Kawamiya, Adachi, and Nakamura, 1972). Combined with the value $\gamma' = 3.9$ for Fe quoted in Sec. V.A, the uniform lattice expansion alone would account for about $\frac{1}{3}$ of the decrease in C' shown in Fig. 36. The large remaining part is related to exceptional magnetostrictive effects.

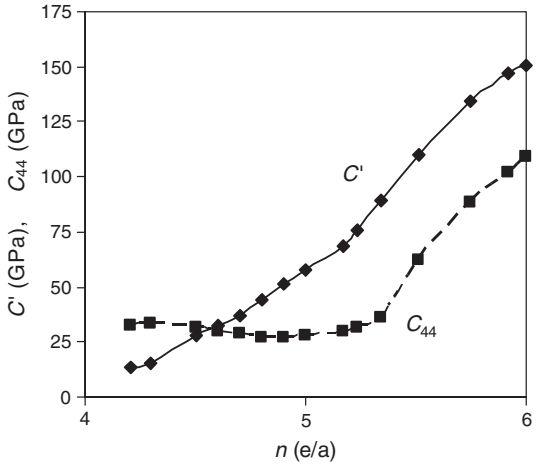

FIG. 34. The measured elastic constants C' and C_{44} of binary bcc Zr-Nb-Mo alloys at room temperature, plotted vs the number n of electrons per atom ($n = 4$, 5, and 6 for Zr, Nb, and Mo). Data from the compilation by Every and McCurdy (1992).

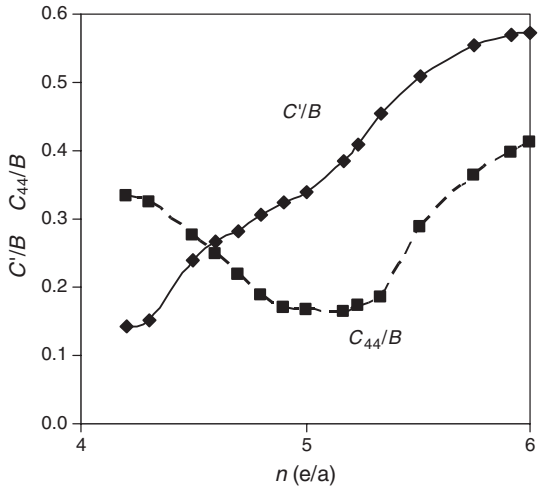

FIG. 35. Data as in Fig. 34 but now normalized as C'/B and C_{44}/B, where B is the bulk modulus.

3. Ag-Zn

In the Ag-Zn system at high temperatures there is an fcc solid solution (α phase) up to about 40 at. % Zn and a narrow region of bcc solid solution (β phase) near 50 at. % Zn. The hcp ϵ phase is stable in the range 65–85 at. % Zn, and the hcp η phase is stable close to pure Zn. *Ab initio* calculations give results for hypothetical random solid solutions in the whole concentration range of the Ag-Zn system. Figures 37 and 38 show the results for C' and C_{44} in bcc and fcc lattice structures (Magyari-Köpe, Grimvall, and Vitos, 2002). We note that if the elastic constants were calculated only for the thermodynamically stable phases, e.g., fcc (stable only below 40 at. % Zn), and then extrapolated to higher concentrations, an instability would have been predicted at about 60 at. % Zn for the fcc C'. Our *ab initio* calculations for the whole range of concentrations, from pure Ag to pure Zn, show that such an extrapolation is strongly misleading. In fact, the trend in C' is reversed as one approaches pure Zn. Similarly, the other calculated elastic constants in Figs. 37 and 38 illustrate that a trend that is well established over a wide concentration range can be broken very suddenly. We note that the fcc C'

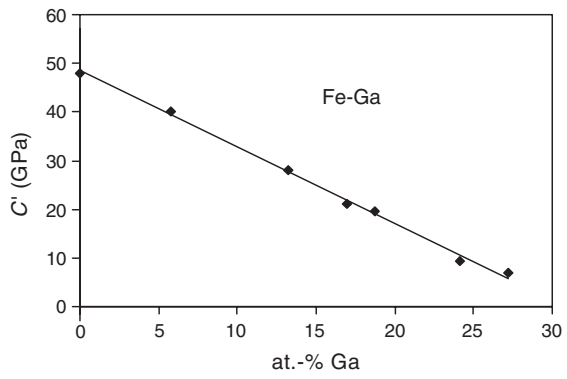

FIG. 36. The room-temperature elastic shear constant C' in solid solutions of Ga in Fe. Adapted from Clark *et al.*, 2003.

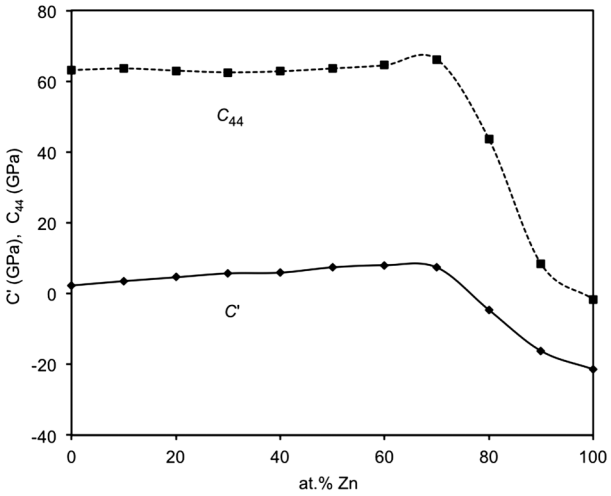

FIG. 37. The elastic constants C' and C_{44} for hypothetical random bcc solid solutions in the Ag-Zn system, obtained in *ab initio* electronic structure calculations. From Magyari-Köpe, Grimvall, and Vitos, 2002.

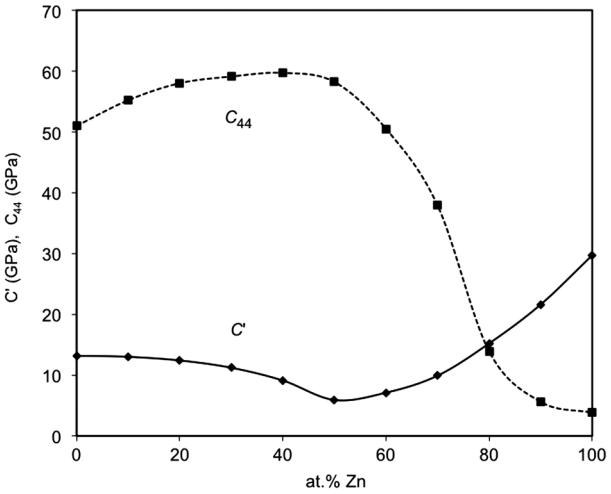

FIG. 38. Elastic constants C' and C_{44} as in Fig. 37, but for the fcc lattice structure.

and C_{44} elastic constants are positive throughout the whole range of Zn concentrations, but with a minimum in C' where the bcc phase is thermodynamically stable. Further, C' and C_{44} in the bcc structure decrease rapidly in the concentration range where the hcp phase is thermodynamically stable. Both these features are in line with the general observation that the stabilities of bcc and close-packed structures alternate.

F. Relation between lattice energy and C'

It has been noted that a large enthalpy difference $\Delta H = H_{\rm fcc} - H_{\rm bcc}$ is qualitatively correlated with large values of C' (Wills *et al.*, 1992; Söderlind, Eriksson, Wills, and Boring, 1993; Söderlind *et al.*, 1994). In a simple model for the energy variation along the tetragonal Bain path we get (Appendix F)

$$C'_{\rm fcc} = C'_{\rm bcc} - (\sqrt{2}+1)^2\left(\frac{\Delta H}{\Omega_a}\right). \tag{39}$$

Craievich *et al.* (1997) used this idea in Ni-Cr alloys; see also Eq. (7) in the work by Sliwko *et al.* (1996) for Ti and V. When C' of a thermodynamically stable phase (bcc or fcc) is known from experiment, and ΔH from *ab initio* calculations, Eq. (39) may yield a semiempirical value for the remaining unknown C'.

VIII. IDEAL STRENGTH OF MATERIALS

A. General aspects

The strength of materials, as measured by the stress which leads to failure, normally depends on lattice defects, for instance, as in the generation and motion of dislocations. Here we are instead concerned with the ideal (or theoretical, or ultimate) strength. The lattice is strained until it yields, without invoking any preexisting lattice defects. In practice, this situation may be relevant in whiskers, nanopillars, and nanoindentation experiments (Krenn *et al.*, 2002; Van Vliet *et al.*, 2003; Lee, 2009; Lowry *et al.*, 2010). Interestingly, a group of multicomponent bcc Ti alloys, called Gum metals, appear to fail close to the theoretical strength, and without conventional dislocation processes (Li *et al.*, 2007; Withey *et al.*, 2008, 2010).

The ideal strength depends on how the external load is applied. Further, the failure mode (e.g., fracture, shear instability) can vary with the type of material, even if the load condition and the crystal structure are the same. The ideal strength $\sigma_{\rm ideal}$ under tension is of the order of $E/10$, and the ideal strength $\tau_{\rm ideal}$ under shear is of the order of $G/10$, where E and G are the Young's and shear moduli, respectively. Thus the components of the strain tensor are large when failure sets in. In spite of all complications, well-defined values of the ideal strength can be associated with every type of load condition (Morris, Jr. and Krenn, 2000); see also Hill and Milstein (1977).

Early works on ideal strengths relied on simple interaction potentials, e.g., of the Morse type (Milstein, 1971, 1973b, 1980), and later on more elaborate potentials, e.g., of the embedded-atom type (Milstein and Chantasiriwan, 1998). The first *ab initio* electronic structure calculation yielding the ideal tensile strength (in Cu) probably is that by Esposito *et al.* (1980), and the first calculation of the ideal shear strength (in bcc V, Nb, Cr, Mo, W and fcc Ir, Cu, Al) is that by Paxton, Gumbsch, and Methfessel (1991). Price, Cooper, and Wills (1992) published the first *ab initio* calculation of the tensile strength (in TiC) when the lattice was allowed to be completely relaxed perpendicular to the load direction, i.e., the volume was not conserved. Subsequently, Šob and coworkers initiated systematic *ab initio* studies of the theoretical strength and lattice stability in metals and intermetallic compounds under extreme loading conditions, simulating tensile tests of defect-free materials. Thus, Šob, Wang, and Vitek (1997b) obtained the theoretical tensile strengths for [001] and [111] loading axes in tungsten, in good agreement with experiments on tungsten whiskers (Mikhailovskii, Poltinin, and Fedorova, 1981). Further, the ideal tensile strength was calculated in NiAl (Šob, Wang, and Vitek, 1998a, 1998b) and Cu (Šob, Wang, and Vitek, 1998b). These results established a basis for later *ab initio*

investigations of the ideal tensile strength and lattice stability of materials under large loading. Since then many *ab initio* calculations of the ideal strength have been performed under varying load conditions and for many solids. The early development of ideal-strength calculations has been reviewed by Milstein (1980), and later works by, e.g., Šob *et al.* (2004, 2005), Pokluda *et al.* (2004), and Ogata, Umeno, and Kohyama (2009). Our treatment emphasizes those aspects that make contact with elastic or phonon instabilities in metallic bcc and fcc elements. The following account mainly rests on results from *ab initio* calculations for pure metals such as Al, Cu, Fe, Mo, Nb, and W.

We considered the theoretical strength at four levels of complexity. At the simplest level, the lattice is deformed quasistatically (the atoms are held immobile for each configuration) and homogeneously under tension, shear, or a combination thereof (but allowing for volume relaxation), until one reaches the unstable state of an inflection point in the elastic energy versus the strain; cf. the Frenkel-Orowan model (Appendix G). However, because the elastic constants change during such a deformation, the Born elastic stability criteria may be violated and the deformation branches off into another deformation path prior to reaching the unstable configuration corresponding to the inflection point. That is the second complexity level. At the third level, the deformed lattice can reach a state where a phonon mode with a finite $\mathbf{q}$ vector becomes dynamically unstable, $\omega^2(\mathbf{q}, s) < 0$. In all these cases one usually ignores explicit temperature effects, i.e., the analysis is performed as if $T = 0$ K. The fourth level of complexity in our review allows for thermal motion of the atoms. It still starts from a perfect lattice but defects may be generated during the deformation to failure. The discussion in this section can be summarized as follows: There is a hierarchy of theoretically possible failure modes under given load conditions. The ideal strength refers to the failure mode that is first encountered when the load increases.

B. Homogeneous deformation

1. Uniaxial tension

Let a specimen of an initially cubic crystal structure be subject to pure tension in the [001] direction and under volume conservation. The amount of deformation is measured by the engineering tensile strain ϵ_{eng} (also called the Cauchy strain), defined as $\epsilon_{\text{eng}} = (L - L_0)/L_0$ for a line element (fiber) axially loaded so that its length changes from L_0 to L. The energy $U(\epsilon_{\text{eng}})$ has the same variation as in the tetragonal volume-conserving Bain path, in which we identify the engineering strain through

$$1 + \epsilon_{\text{eng}} = \left(\frac{c}{a}\right)^{2/3}. \tag{40}$$

With the bcc structure corresponding to $c/a = 1$ and the fcc structure to $c/a = \sqrt{2}$, we get the engineering strain $\epsilon_{\text{eng}} = 2^{1/3} - 1 = \epsilon_{\max} \approx 0.26$ at the fcc structure. The tension σ_{001} is obtained as

$$\sigma_{001} = \frac{1}{V}\frac{\partial U}{\partial \epsilon_{\text{eng}}}. \tag{41}$$

If $U(\epsilon_{\text{eng}})$ is fitted to a sinusoidal shape near the bcc structure, where $\epsilon_{\text{eng}} = 0$, we get

$$\sigma_{001} = E_{001}\frac{\epsilon_{\max}}{\pi}\sin\left(\frac{\epsilon_{\text{eng}}}{\epsilon_{\max}}\pi\right) \tag{42}$$

with $E_{001} = (C_{11} - C_{12})(C_{11} + 2C_{12})/(C_{11} + C_{12})$ (Morris, Jr. and Krenn, 2000; Krenn *et al.*, 2001a; Roundy *et al.*, 2001). The ideal strength σ_{ideal} is given by the location of the inflection point in $U(\epsilon_{\text{eng}})$, i.e., when $\epsilon_{\text{eng}} = \epsilon_{\max}/2 \approx 0.13$. Then $\sigma_{\text{ideal}} \approx 0.08E_{001}$. Note that this is a model calculation that not only assumes a simple sinusoidal shape but, more importantly, ignores bifurcation as discussed in Sec. VIII.B.4.

Figure 39 shows $U(\epsilon_{\text{eng}})$ per atom in bcc W during a tensile test, i.e., under uniaxial tension in the [001] and [111] directions, when the perpendicular dimensions of the crystal are relaxed, so that the defomation follows the non-volume-conserving uniaxial tetragonal and trigonal Bain paths, respectively. The elastic properties of the unstrained bcc W lattice are almost isotropic, $C_{11} - C_{12} \approx 2C_{44}$. Therefore the curvature of $U(\epsilon_{\text{eng}})$ at small ϵ_{eng} is the same for the two deformation paths. In spite of this, the inflection point of $U(\epsilon_{\text{eng}})$ corresponds to a higher theoretical strength σ_{ideal} and a higher strain ϵ_{eng} for [111], compared with [001] tension. Hence elastic isotropy does not imply that the theoretical strength is isotropic.

The ideal strength under tension has been studied with various uniaxial loadings by Milstein and Chantasiriwan (1998) in 12 cubic metals, Milstein, Zhao, and Maroudas (2004), Milstein *et al.* (2005), and Djohari, Milstein, and Maroudas (2006) in fcc crystals, Li and Wang (1998) and Yashiro, Oho, and Tomita (2004) in Al, Šob, Wang, and Vitek (1998b), Černý *et al.* (2004) and Zhang *et al.* (2008a) in Cu, and Yashiro *et al.* (2006) in nonmagnetic Ni, to mention only a few papers, which sometimes treat also pure shear. Magnetism adds to the complexity, and one must take into account how the magnetic state varies along the Bain path at

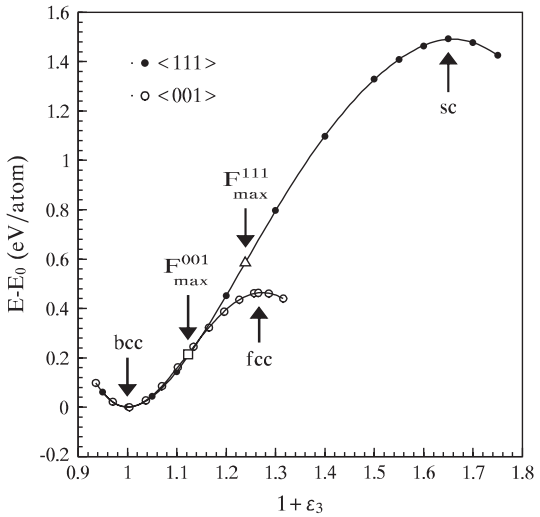

FIG. 39. The total energy per atom, as a function of the engineering strain, for uniaxial loading of tungsten along the [001] and [111] directions (perpendicular dimensions of the lattice are relaxed). The arrows show the inflection points, corresponding to the maximum theoretical strength. From Šob, Wang, and Vitek, 1997b.

large strains; see, e.g., Krasko and Olson (1990), Peng and Jansen (1991), Herper, Hoffmann, and Entel (1999), Qiu and Marcus (1999), Qiu, Marcus, and Ma (2000a), Friák, Šob, and Vitek (2001, 2003), Šob *et al.* (2002, 2004), Clatterbuck, Chrzan, and Morris, Jr. (2002, 2003b), Tsetseris (2005), Liu *et al.* (2008), Okatov *et al.* (2009), Friák (2011), and Leonov *et al.* (2011). Other examples of works dealing with uniaxial loading are Zelený, Legut, and Šob (2008) and Zelený and Šob (2008) on epitaxy, and Friák and Šob (2008) and Djohari, Milstein, and Maroudas (2009) on bcc-hcp structures.

As pointed out by Milstein and Farber (1980) it is important to distinguish between, e.g., a cubic crystal subject to [001] loading (with transverse stresses being zero), and one subject to [001] deformation (transverse stretches being zero). In the first case the loading path goes through unstressed fcc, bcc, and bct states. We also note the equivalence of uniaxial tension and biaxial compression in the epitaxial Bain path.

2. Pure shear

The engineering shear strain γ_{eng} is defined as the change in the angle between two material line elements that are perpendicular to each other in the undeformed or initial configuration. For shear along [111], a relation analogous to Eq. (42) yields $\gamma_{\mathrm{ideal}} \approx 0.11 G_{111}$, where $G_{111} = 3C_{44}(C_{11} - C_{12})/(4C_{44} + C_{11} - C_{12})$ (Krenn *et al.*, 2001a).

Figure 40 shows the stress under shear for bcc W. Krenn *et al.* (2001b) and Ogata, Li, and Yip (2002) obtained similar results for shear in fcc Al and Cu.

The work by Söderlind and Moriarty (1998) on Ta and Roundy *et al.* (1999) on Al and Cu represented the state of the art in *ab initio* calculations at that time. The progress achieved during the following decade is exemplified by the works of Jahnátek, Hafner, and Krajčí (2009), who calculated the ideal strength in Al and Cu under shear, and Nagasako *et al.* (2010) who considered V, Nb, and Ta. Ogata *et al.* (2004) formulated a "master curve" that approximately describes the shear strength of metals and ceramics, and Černý and Pokluda (2009) predicted the tensile strength of fcc crystals from shear strength calculations.

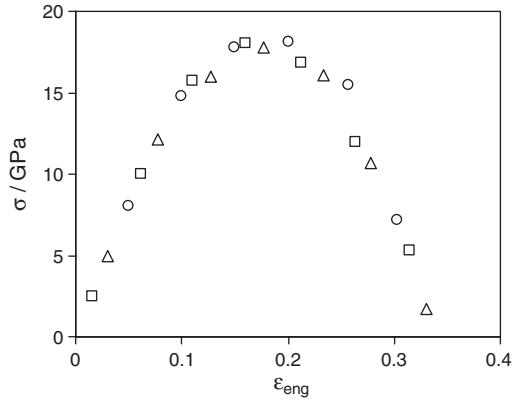

FIG. 40. The stress σ as a function of the engineering shear strain ϵ_{eng} in bcc W for ⟨111⟩ shear in the {110} (circles), {112} (squares), and {123} (triangles) planes. Adapted from Krenn *et al.*, 2001a.

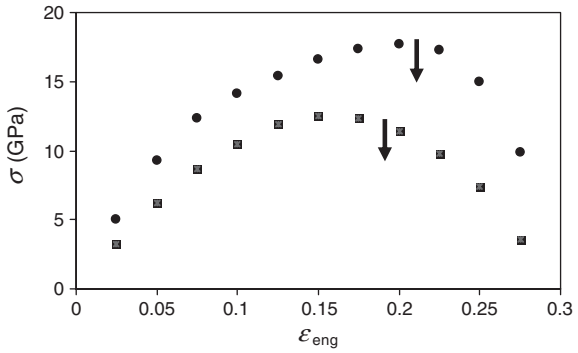

FIG. 41. The stress σ as a function of the engineering shear strain ϵ_{eng} calculated in ferromagnetic bcc iron for uniaxial tension (squares) and uniaxial tension plus a biaxial tension (circles), with the largest tensile stress in the [001] direction. Arrows indicate the location of the tetragonal-to-orthorhombic bifurcation instability. From Clatterbuck, Chrzan, and Morris, Jr., 2003a.

3. Triaxial stress

Hydrostatic pressure P is a special case of triaxial stress (Šandera *et al.*, 1997; Song *et al.*, 1999). Under tension ($\sigma = -P$) the stability condition in Eq. (12) for the bulk modulus,

$$B + P/3 = B - \sigma/3 > 0, \tag{43}$$

can be violated. Černý (2007) calculated that this spinodal instability occurs for Fe, Ni, and Cr at volume increases by factors of 1.58, 1.46, and 1.46, respectively, relative to the equilibrium volume of a stress-free crystal. In similar work, Černý *et al.* (2003) considered Fe, Co, Ni, and Cr in various magnetic states.

Clatterbuck, Chrzan, and Morris, Jr. (2003a) investigated multiaxial loads in ferromagnetic iron. Figure 41 shows the stress as a function of the engineering strain for two load configurations. Many other works discuss the ideal strength under complex loading, e.g., Krenn *et al.* (2002) on modeling nanoindentation, Černý and Pokluda (2007, 2008a, 2008b, 2008c, 2010a, 2010b), and Černý, Šesták, and Pokluda (2010) on fcc metals, and Umeno and Černý (2008) on covalent crystals. See also a review by Pokluda *et al.* (2004) and references to the pressure dependence of lattice instabilities in Appendix J.

4. Bifurcation

We identified the ideal strength with the stress where $dU(\epsilon)/d\epsilon$ has its largest value, but one must also check for other failure modes under the same kind of load, in particular, the violation of Born-type stability criteria. This possibility was pointed out already by Born (1940) and Born and Fürth (1940). For instance, let the deformation initially follow a tetragonal strain. Before one has reached the critical $\epsilon_{\mathrm{ideal}}$ along this primary path, failure can occur through an instability leading into a secondary, orthorhombic path. Such a branching off, or bifurcation, is found in Nb but not in Mo (Luo *et al.*, 2002). The elements Nb and Mo are neighbors in adjacent columns in the periodic table; they both have metallic bonding and are very stable in the bcc lattice structure. In spite of these similarities they show different failure

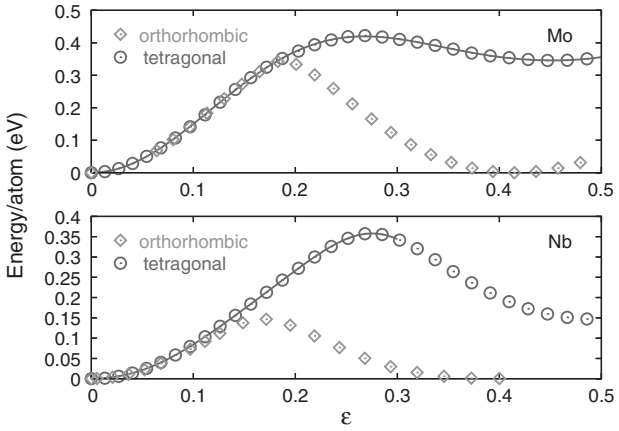

FIG. 42. The energy $U(\epsilon)$ per atom as a function of the relaxed [001] tensile strain ϵ, calculated for Mo and Nb along the tetragonal Bain deformation path (circles) and along an orthorhombic path that is branching off. The maximum of the orthorhombic path has the same energy as the local minimum of the tetragonal path, since they correspond to the same tetragonal saddle-point structure. From Luo *et al.*, 2002.

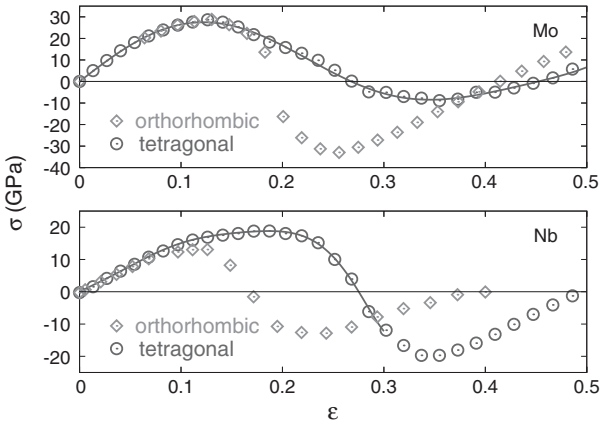

FIG. 43. The stress-strain relation for the same loads as in Fig. 42. From Luo *et al.*, 2002.

modes under uniaxial tension in the [001] direction (see Figs. 42 and 43). Bifurcation was observed in several other bcc or fcc metals; e.g., by Milstein, Marschall, and Fang (1995), Milstein and Rasky (1996), and Milstein *et al.* (1996) in alkali metals; Wang *et al.* (1993) in Cu; Milstein and Farber (1980) and Milstein *et al.* (2005) in Cu and Ni; Li and Wang (1998) and Yashiro, Oho, and Tomita (2004) in Al; Yashiro *et al.* (2006) in Ni; Zhang *et al.* (2008a) in Cu; Wang and Li (2009) in Au; and Nagasako *et al.* (2010) in V, Nb, and Ta. These are only examples illustrating the complexity of the concept of ideal strength, even in straightforward model calculations for simple load geometries.

5. Phonon instabilities

The failure modes discussed above correspond to homogeneous deformations in a quasistatic lattice. However, failure can also be initiated by a particular phonon mode becoming unstable [i.e., $\omega^2(\mathbf{q}, s) < 0$] before one reaches a critical

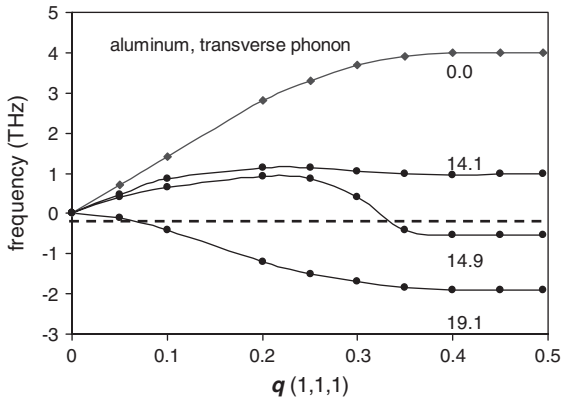

FIG. 44. Transverse phonon dispersion curve in the [111] direction of aluminum, for $[11\bar{2}](111)$ shear at four different amounts of shear strain ϵ (given in %). The onset of the shear instabilities appears very suddenly above $\epsilon = 0.14$. Adapted from Clatterbuck *et al.*, 2003.

condition in the stress-strain relations referring to homogeneous deformations. This fact makes a complete analysis of the ideal strength a formidable task. In principle, the stability of all phonon modes and all loading conditions should be investigated. Figure 44 shows, as an example, failure in Al when a [111] transverse mode becomes unstable under $[11\bar{2}](111)$ shear (Clatterbuck *et al.*, 2003). Note how rapid is the onset of the phonon instability for $\epsilon > 0.14$.

C. Defect formation

Our discussion so far assumed that the material is initially free of defects and is subject to a uniform deformation. Real materials contain dislocations and other imperfections which can multiply during the deformation, but to make contact with the ideal strength we restrict the analysis to homogeneous defect nucleation, leading ultimately to, e.g., plastic flow, crack formation, and fracture. (This is in analogy to homogeneous melting in superheated systems; see Sec. X.A). We then need a theoretical framework to formulate instability criteria describing local properties of atoms or groups of atoms, which can replace the macroscopic quantities of stress, strain, and elastic constants. A general condition, that may be referred to as the Wallace criterion (Wallace, 1972; Delph *et al.*, 2009), is that a given atomic equilibrium configuration is stable if all admissible infinitesimal virtual displacements of an atom, or a group of atoms, result in an increase in the energy of the system. For sufficiently large systems, this criterion is equivalent to Eq. (1) that all phonon frequencies are real (Wallace, 1972). Other stability criteria that can handle nonuniform deformation fields have been formulated by Alber *et al.* (1992) involving atomic-scale elastic constants, by Van Vliet *et al.* (2003) in an extension of work by Hill (1962) to a local-energy based, local elastic constant relation called the Λ criterion, and by Kitamura, Umeno, and Fushino (2004), Lu and Zhang (2006), and Miller and Rodney (2008) using the positive definiteness of an atomic-scale acoustic tensor.

Molecular-dynamics simulations offer a realistic, but computationally demanding, approach to the application of

stability criteria in real systems. With a given interaction between the atoms, one monitors the position of each atom during a large number of computation steps and for a large number of atoms. A molecular-dynamics simulation by Li, Ngan, and Gumbsch (2003), using a Morse-type interaction, illustrates how an unstable continuum wave can evolve into a local defect. Four stages were identified. The unstable elastic wave first grows in amplitude. The wave form is then distorted into a steep front that is still wide compared with the lattice spacing. Next an atomistically sharp front is developed, and finally the wave front is arrested and forms a low-dimensional defect. Kimminau *et al.* (2010) used molecular-dynamics simulations to study how a phonon instability in uniaxially compressed fcc Cu develops into a stacking fault. Other examples of simulations starting from a defect-free lattice involve hydrostatic tension in Au (Wang *et al.*, 1995); shear in Au (Pacheco and Batra, 2008); nanoindentation in Al and Cu (Wang *et al.*, 1995) and Al, Cu, and Fe (Li, Ngan, and Gumbsch, 2003); high-rate tension in Fe (Norman, Stegailov, and Yanilkin, 2007); and cavitation, crack growth, and nanoindentation in an fcc lattice (Delph *et al.*, 2009; Delph and Zimmerman, 2010). The field of atomistic simulations is rapidly developing, mainly as a consequence of improved computer performance. Various hybrid techniques, regarding both the interaction (potentials, *ab initio* energy calculations) and size (e.g., local atomistic modeling embedded in a continuum model), and explicit temperature and time dependence, will give a deeper understanding of real materials subject to plastic deformation.

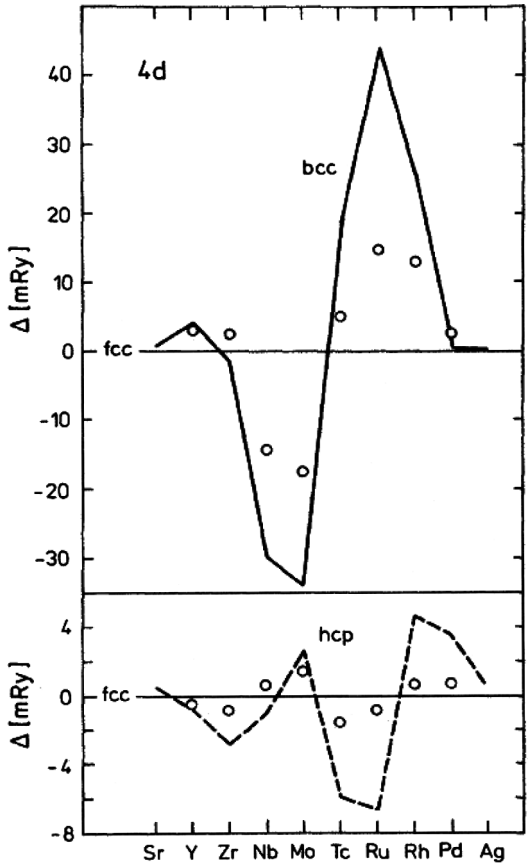

FIG. 45. The energy difference $\Delta H_{\text{bcc-fcc}}$ between the bcc and fcc structures for 4*d* metals, as calculated *ab initio* (lines) and as obtained at that time by CALPHAD methods (circles). Corresponding results for the hcp structure are also shown. From Skriver, 1985.

IX. CALPHAD APPROACH TO PHASE DIAGRAMS

A. General aspects

The CALPHAD method (computer coupling of phase diagrams and thermochemistry) is a well-established procedure to analyze and predict phase diagrams, in particular, as a function of composition c and temperature T in multicomponent systems. A phase diagram is determined, for each (c, T), by that combination of phases which minimizes the total Gibbs free energy G. One therefore needs information on $G(c, T)$ of all competing phases $(\alpha, \beta, \ldots)$. Even for such a simple case as a binary system with atoms A and B, this can be a very demanding task. $G(c, T)$ must be known not only for solid solutions of B in A, and vice versa, as well as for the stable crystal structures of pure A and B, but also for all other conceivable crystal structures of pure A and B. Moreover, $G(c, T)$ should be known for all stoichiometric compounds A_mB_n and for deviations from their exact stoichiometric compositions. The existence of short-range order in solid solutions, the presence of a liquid phase, and perhaps external pressure, exemplify further complications. However, it often suffices to consider only a few phases and to make many simplifying assumptions. Then the CALPHAD method was very successful in accounting for experimental phase diagram information and predicting new phase diagrams for systems where the experimental information is meager or absent. It was therefore a matter of great concern when, in the late 1980s, there was a striking disagreement between cohesive-energy predictions obtained by the CALPHAD method (there called lattice stability values) and by *ab initio* electronic structure calculations for bcc and fcc lattices of elemental transition metals; see Fig. 45 from Skriver (1985), a historical account by Grimvall (1998), and discussions by Wang *et al.* (2004) and Kissavos *et al.* (2005). The discrepancy is pronounced only when the enthalpy difference $\Delta H_{\text{fcc-bcc}}$ is large. The correlation of $\Delta H_{\text{fcc-bcc}}$ and lattice instabilities (see Sec. VII.E) points to dynamical lattice instabilities as the reason for the discrepancy between CALPHAD and *ab initio* enthalpy data.

B. A model example

Before we discuss the CALPHAD method in some detail, the effect of lattice instability in a binary phase diagram is illustrated through a simple example. A and B are two elements, which in their pure forms have structures α and β, respectively. Let $P = 0$, and consider $G = H - TS$ for random solid solutions of B in A, and vice versa. When there is no significant difference $S_\alpha - S_\beta$ in the vibrational entropy, our model gives $G_\alpha(c)$ and $G_\beta(c)$ as in Fig. 46, with end points c_1 and c_2 of the two-phase field in the phase diagram obtained from the common-tangent construction. We next compare this result with what we would get if phase α is dynamically unstable beyond $c_{\text{crit}} = 0.8$. That gives rise

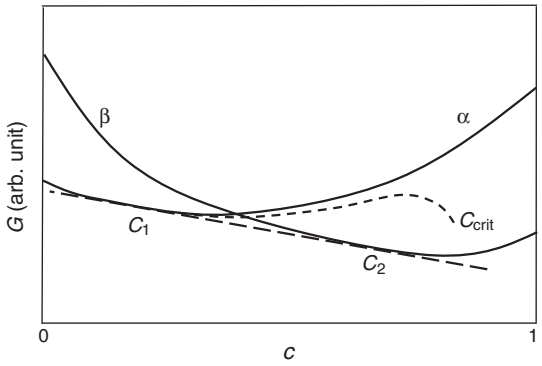

FIG. 46. The Gibbs free energy G_α and G_β for two phases that are dynamically stable at all concentrations c (solid curves) and also for the case that phase α becomes dynamically unstable at c_{crit} (short-dashed curve). G_α is not a thermodynamically defined quantity when $c > c_{crit}$. The common-tangent construction (long-dashed curve) gives the concentrations c_1 and c_2 of the end points of the two-phase field in the phase diagram. Model assumptions: $H(T = 0)$ varies with c as $H_\alpha = H_{A,\alpha} + cH'_\alpha$ and $H_\beta = H_{A,\beta} + cH'_\beta$. The temperature-dependent part of H is described by the classical result $3k_BT$ per atom, and cancels in $G_\alpha - G_\beta$. There is a random disorder entropy (per mole) $S = R[c\ln(c) + (1 - c)\ln(1 - c)]$. The vibrational entropy difference $S_\alpha - S_\beta = 0$. At the considered T, $H_{A,\alpha}/(RT) = 0$; $H_{B,\beta}/(RT) = 0.75$; $H'_\alpha/(RT) = 0.5$; and $H'_\beta/(RT) = 1.5$.

to an increase in S_α, and hence a decrease in G_α, as c_{crit} is approached; cf. the entropy variation in Fig. 6. The dashed curve in Fig. 46 shows a possible result for G_α. Obviously, the common-tangent construction based on the dashed line for G_α (instead of the solid line) does not give any significant changes in the phase-field boundaries c_1 and c_2. From this example we expect that incipient lattice instabilities often go unnoticed in the experimentally determined phase diagram.

C. CALPHAD versus *ab initio* approaches

We now relate the discrepancy between the CALPHAD and the *ab initio* calculated lattice energies to the existence of dynamical instabilities. In the CALPHAD method, the Gibbs free energy G is described by simple mathematical functions of temperature and composition (usually low-order polynomials in T and in the concentrations c_j of the components j), so that $G = H - TS$ gives a good account of the equilibrium part of the phase diagram. This expression for G is then extrapolated into regions that are assumed to represent metastable phases. It is the total function $H - TS$ that fits the phase diagram. In order to extract quantities such as $\Delta H_{\alpha-\beta}$ for an element in two crystal structures α and β, one must have additional information on the entropy difference $\Delta S_{\alpha-\beta}$. The CALPHAD approach assumes that the vibrational $\Delta S_{\alpha-\beta}$ is small (or even zero). This is often a reasonable approximation (cf. Fig. 30), but it obviously fails when the entropy is not a thermodynamically well-defined quantity. Then $\Delta H_{\alpha-\beta}$ cannot be extracted from the extrapolated G as $\Delta H = \Delta G + T\Delta S$.

Conversely, one may attempt to derive $\Delta S_{\alpha-\beta}$ from G fitted to a phase diagram, combined with $\Delta H_{\alpha-\beta}$ from an *ab initio* calculation. If $\Delta H_{\alpha-\beta}$ is calculated for rigid structures (perhaps disordered to represent thermal motion), it has a well-defined value. However, that does not allow us take G from an extrapolation of a fit to a phase diagram, and obtain $S = (H - G)/T$ for a phase that is dynamically unstable.

In Sec. VII.E we saw that the difference in enthalpy between two phases at $T = 0$ is correlated with differences in the vibrational properties, which would lead to a partial cancellation in $\Delta G = \Delta H - T\Delta S$. Further, anomalous temperature-dependent contributions to H_α and S_α are connected through the corresponding effect in the heat capacity and therefore also tend to cancel in $\Delta G = \Delta H - T\Delta S$. (We compare with the melting process, where there is a latent heat, but the Gibbs free energy remains unchanged.) The almost linear relationship between ΔH and $T\Delta S$ is well demonstrated by Guillermet *et al.* (1995).

What is then the possible role of *ab initio* calculations as a source of information in CALPHAD-type analyses? When a phase is dynamically stable, *ab initio* results for the enthalpy and vibrational entropy can be used as input data without any problem (Liu, 2009; Šob *et al.*, 2009; Dubiel *et al.*, 2010; Pavlů, Vřeštál, and Šob, 2010). From a practical point of view, one can often assume that the Gibbs free energy is a well-defined quantity even in the region of a dynamically unstable phase, as long as G is not given a physical interpretation in terms of extracted quantities H and S that are thought to represent truly metastable states. On the other hand, *ab initio* enthalpy data calculated for stabilized binary alloys can be extrapolated to the pure unstable element, thus giving an enthalpy in satisfactory agreement with CALPHAD enthalpies; see Wang *et al.* (2004). This is because the extrapolated CALPHAD enthalpy refers to a fictitious metastable state that has a rigid lattice. We also recall that a phase, which is dynamically unstable at $T = 0$ K, may be stabilized at high T. In fact, work by Ozoliņš (2009) suggests that the enthalpy difference between fcc and bcc W obtained *ab initio* at high temperatures (where short-wavelength phonons are stabilized) may be relevant as an input parameter for this quantity in CALPHAD modeling of multicomponent phase diagrams. However, detailed work on fcc and hcp Ru-Mo alloys (Kissavos *et al.*, 2005) shows that there are still some problems in reconciling *ab initio* results and the thermodynamic quantities obtained in a CALPHAD-type fitting of phase diagrams. We also recall that the vibrational properties in an alloy, and hence the corresponding entropy, can show a very slow variation over a large concentration interval, followed by the onset of a rapid change; see the Ag-Zn system in Sec. VII.E.

X. LOSS OF LATTICE PERIODICITY

A. Melting

The thermodynamic melting temperature T_m of a solid is the temperature at which the Gibbs free energies of the solid and the liquid phases are equal. Melting normally starts from the surface of a specimen, where the energy barrier for the nucleation of the liquid phase is low. In the absence of a free surface, as in a theoretical simulation of crystalline systems with periodic boundary conditions, that melting mechanism is

suppressed and the solid can remain in a superheated state at temperatures well above T_m. Ultimately the crystal must transform to a liquid state, and a hierarchy of several kinds of stability criteria that limit the amount of superheating was suggested (Tallon, 1989). Of interest in this review is the possibility that the lattice becomes dynamically unstable under shear. Brillouin (1938) and Born (1939) studied data on the temperature dependence of shear elastic constants and suggested that T_m be connected with a vanishing shear resistance. It is now known that the elastic shear constants are finite at T_m (cf. Fig. 47), but the question remains if instability under shear puts a limit to superheating. More precisely, is the shear instability the first instability condition reached, as the temperature is increased? The knowledge is incomplete, but a partial answer was obtained by Forsblom and Grimvall (2005a, 2005b) in a molecular-dynamics simulation relevant for aluminum. They found that the generation of vacancy-interstitial pairs leads to melting at $T > 1.3T_m$, where C' and C_{44} are still finite, i.e., prior to any shear instability. The role of vacancy-interstitial pairs was also discussed by Delogu (2005). Bai and Li (2008) obtained a different initial defect configuration in their work on melting in a superheated fcc solid, but still with no evidence of a shear-related melting mechanism.

The well-known (Lindemann, 1910) melting criterion, which was actually introduced much later by Gilvarry (1956) on the basis of Lindemann's work, says that melting takes place when the root mean square of the atomic thermal displacement is a certain fraction (typically $\sim$12%) of the distance between nearest-neighbor atoms. It is an erroneous but widespread belief that a lattice then becomes unstable and "shakes apart." In fact, the Lindemann rule holds only for a restricted class of systems and then can be viewed as a simple consequence of scaling through dimensional analysis; see Appendix H.

A different kind of instability can arise in some systems under intense photon radiation. For instance, in a covalently bonded crystal such as InSb, the character of the chemical bonding is changed. That results in new interatomic forces, for which the original lattice structure may be dynamically unstable; see Lindenberg (2005).

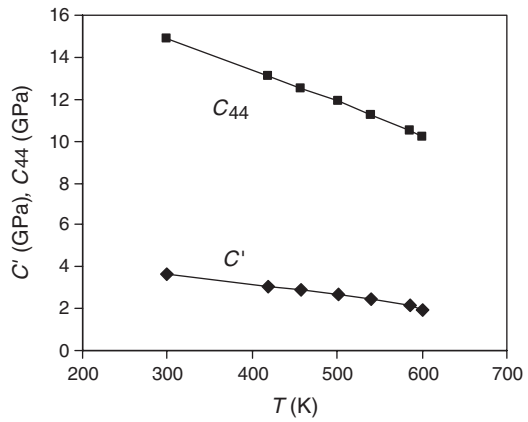

FIG. 47. The elastic constants C' and C_{44} in fcc Pb (Every and McCurdy, 1992) do not extrapolate to zero as T approaches $T_m = 601$ K.

In the reverse of melting, i.e., nucleation of a solid phase from the liquid, the bcc structure takes a special place (Alexander and McTague, 1978; Groh and Mulder, 1999). However, molecular-dynamics simulations of aluminum give the correct fcc structure on solidification (Desgranges and Delhommelle, 2007).

B. Amorphization

The apparent similarity of a liquid and an amorphous structure, and the incorrect assumption that the melting mechanism of crystals is caused by a vanishing shear modulus, has led to the idea that amorphization is related to an elastic instability. Such an instability could then be due to high pressure or to the volume changes of the lattice, e.g., on alloying with atoms differing in size from those of the host lattice [see Delogu (2004a, 2004b), and references therein]. Much work has been done on pressure-induced amorphization in covalently bonded solids, in particular, α-SiO_2. In that compound there is evidence for an elastic instability (Binggeli, Keskar, and Chelikowsky, 1994) but also for vanishing phonon frequencies at the Brillouin zone boundary (Chaplot and Sikka, 1993) or at other wave vectors (Watson and Parker, 1995). Although these lattice instabilities have similarities with instabilities in the metallic elements discussed in this review, there seems to be no example of a pressure-induced amorphization in bcc or fcc structures. Zhang, Lai, and Liu (2000) performed molecular-dynamics simulations in the Ni-Ta system. They related amorphization to a pronounced vibrational softening, but not to direct dynamical instability. Through molecular-dynamics studies, Yip *et al.* (2001) compared the tendency to amorphization or to polymorphic transition under pressure. Burakovsky, Greeff, and Preston (2006) refuted a claim by Kechin (2004) that the shear modulus of metals should vanish and transform a crystalline substance to a liquid at high pressure and $T = 0$ K. Delogu (2004b) studied shear instability and amorphization caused by atomic-size differences in fcc Ni-Cr and hcp Zr-Ni. Alexander (1998) gave a broad general review of the structure, lattice dynamics, and elasticity of amorphous solids.

C. Nanostructures

In nanocrystalline materials, the disordered grain boundaries can be almost dynamically unstable. Even if no instability is reached, the grain boundary atoms make up such a large fraction of the atoms that they can affect the crystal structure of the entire grain. Ball milling, in which the material is subject to mechanical attrition, may produce nanocrystalline materials with a lattice structure different from that of bulk material. As an example, nanocrystalline Nb undergoes a bcc-to-fcc phase transformation when the grain size is reduced below 10 nm (Chattopadhyay *et al.*, 2001). See also Manna *et al.* (2002, 2003) for work on Ti and Zr. Sheng *et al.* (1997) obtained amorphous $Fe_{1-x}Al_x$ through ball milling and attributed it to a dynamical lattice instability. Finally, surface stress can play a significant role in structural changes in nanowires. For instance, in the absence of surface reconstruction, fcc ⟨100⟩ Au and Pt nanowires

spontaneously relax to the bct structure when the wire diameter is less than 2 nm [see Haftel and Gall (2006) and also Ma and Xu (2007)]. In a molecular-dynamics study of Fe and Mo, Kotrechko, Filatov, and Ovsjannikov (2006) concluded that bcc nanocrystals develop shear instability under uniaxial and hydrostatic tension. Metallic nanowires and their mechanical and elastic properties is a field of intense research; see Ogata, Umeno, and Kohyama (2009). Finally it should be mentioned that nanometer-scale precipitates of Cu in bcc Fe form a coherent bcc lattice (Liu *et al.*, 2005), and precipitates of Fe in fcc Cu form an fcc lattice (Haneda *et al.*, 1992).

XI. CONCLUSIONS

The condition for a lattice structure to be dynamically stable is trivial; all phonon frequencies must be positive. However, a thorough understanding of dynamical lattice instabilities was not reached until recently, and then from advanced *ab initio* electronic structure calculations. Before that, most work was limited to studies of elastic constants, often based on Lennard-Jones or similar analytic forms of atomic interactions. The gradual development of the field, spanning more than seven decades, has clarified many technical details. Of more general interest are qualitative results, which often seem surprising or contradict widespread beliefs. We conclude this review with several such statements.

Instabilities may seem counterintuitive.—The fcc and hcp monatomic lattices represent the densest possible packing of spheres. Each atom is surrounded by 12 nearest-neighbor atoms, forming a symmetric "cage." One might assume that this is a very stable configuration. Nevertheless, there are at least nine metallic transition elements in the periodic table for which the fcc lattice is known to be unstable under elastic shear. In contrast, the bcc lattice is referred to as an open structure. When formed by hard spheres, it is unstable under $(110)[\bar{1}10]$ shear. However, tungsten in the bcc structure is exceptionally stable, while the fcc tungsten lattice is unstable at $T = 0$ K. We conclude that stability arguments relying on a representation of atoms by (hard) spheres can be strongly misleading.

Elastic stability does not guarantee overall stability.—The common, more or less sinusoidal, shape of the acoustic phonon dispersion curves suggests that if a structure is dynamically stable in the long-wavelength limit, it is also stable for phonons with short wavelengths (Born, 1940; Born and Fürth, 1940; Power, 1942). There are now many counterexamples showing that this is not a universal rule.

The stability of fcc or hcp and bcc lattice alternates.—Among the transition metals in the periodic table there is a strong trend that an element with a close-packed (fcc or hcp) equilibrium structure is dynamically unstable in the bcc structure, and vice versa (see Figs. 31 and 32). This behavior can be understood from the energy variation along the Bain path that connects the fcc and bcc structures (see Fig. 9).

Magnetism is very important.—For instance, both ferromagnetic and paramagnetic bcc iron are dynamically stable, while nonmagnetic bcc iron is unstable, which gives a counterexample to the trend of alternating fcc or hcp and bcc structures. There can be significant changes in the magnetic state, with accompanying changes in the vibrational properties, along a deformation path.

Phonon instabilities may arise abruptly.—Usually the elastic constants and the corresponding phonon spectrum vary slowly with chemical composition or pressure, as long as the crystal structure is not changed. However, there are also examples showing a sudden onset of rapid variation as a function of alloy composition (see Figs. 37 and 38) or pressure (see Fig. 44). Such behavior is hard to predict without accurate electronic band structure calculations, and it is a warning against the uncritical extrapolation of experimental data.

Precursor effects of instabilities may go unnoticed in phase diagrams.—Consider a phase diagram with an equilibrium phase that is dynamically unstable in other parts of the diagram. The boundaries in such a diagram are not located where a phase becomes dynamically unstable, but are determined by a comparison of the total Gibbs free energy of (meta)stable structures. Therefore, such a phase diagram may show only weak precursor effects of an instability (see Figs. 23 and 46).

Phonon instabilities can limit the theoretical strength.—In the classical Frenkel-Orowan description of the theoretical strength of a solid, the energy U increases with the strain ϵ until one reaches an inflection point in $U(\epsilon)$. But the strain also imposes changes in the elastic constants and in the rest of the phonon spectrum. It can then happen that an instability arises before the inflection point of the classical model is reached. Of particular interest is the phenomenon of bifurcation, where an initial deformation path branches off into another path. Thus there can be a hierarchy of various types of instabilities along the deformation path. The theoretical strength is determined by the instability that is first encountered.

Melting is not caused by lattice instability.—It has been thought that ordinary melting arises when the elastic shear resistance has decreased to zero, but it is now well established that the elastic constants remain finite as the melting temperature is approached. Further, the Lindemann melting rule is an empirical observation for monatomic solids that can be understood with reference to dimensional analysis. It is not related to an instability induced by increasing vibrational displacements.

The Debye model is inadequate to describe a dynamical lattice instability.—The standard Debye model, with a phonon spectrum represented by a single parameter θ_D, cannot describe a solid phase when it is close to becoming dynamically unstable. In that model the vibrational entropy S diverges as $\ln(T/\theta_D)$ when $\theta_D \to 0$ and incorrectly implies that the phase is stabilized due to the low value of the Gibbs energy $H - TS$. However, a generalized Debye model that allows for elastic anisotropy does not show this shortcoming.

Lattice instabilities are common.—This review focused on instabilities in bcc and fcc structures but illustrates a very common phenomenon that was not getting broader attention until the 1990s. According to the traditional understanding of structure and bonding in $A_N B_{8-N}$ octet semiconductors one expects that they show the structural sequence ZB (zinc blende, diamond) $\to$ NaCl $\to$ β-Sn, as pressure is increased. However, the β-Sn structure is systematically absent, and the

NaCl structure is obtained in only some of these compounds, a fact that can be understood with reference to lattice instabilities (Ozoliņš and Zunger, 1999). The CsCl structure shows similar behavior (Kim, Ozoliņš, and Zunger, 1999). Under ambient conditions, AgCl and AgBr crystallize in the rock salt structure characteristic of ionic compounds but show phonon instabilities under pressure (Y. Li *et al.*, 2006). Attempts to form stoichiometric MoC in the NaCl structure failed because although MoC has positive elastic shear constants, the X-point phonon in the Brillouin zone is unstable (Hart and Klein, 2000). FeAl and NiAl are in many respects similar, but when subject to elastic deformation FeAl develops a shear instability while NiAl fails by tension (Li, Morris, Jr., and Chrzan, 2006). These are just a few examples showing the importance of lattice instabilities in compounds.

Prospects for the future.—We envisage two main lines in the future development, both relying on continued progress in computing power. One of them deals with more or less exotic systems. The number of combinations of atoms that can define a new material is enormous, and it would be impractical to limit a study to those materials that have been synthesized. Instead one assumes a certain composition in a static structure, finds its properties through *ab initio* calculations, and then continues with experiments only in those cases that seem most promising. As this review showed, an assumed static structure may in fact turn out to be dynamically unstable. Just as *ab initio* calculations of the cohesive energy and the bulk modulus of stoichiometric compounds are now routinely performed, investigations of the dynamical stability properties will soon be a simple task also in complex structures. Another main line of progress deals with traditional materials subject to large strains, which ultimately lead to plastic deformation and perhaps complete failure. This is a more demanding challenge than just looking for phonon instabilities in a given crystal structure, since both temperature and deformation rate are of great practical importance. Magnetism adds to the complications in many technologically important systems. A number of hybrid techniques may be developed, where small regions that are treated *ab initio* lie embedded in regions of larger length scales where a more approximate description suffices. There are many obstacles on the route to the goal in which relatively cheap and fast computations and simulations can completely replace costly and time consuming experiments, but this is no doubt where many areas of materials science are heading.

ACKNOWLEDGMENTS

This work was performed at KTH, Stockholm, and was supported by the Swedish Foundation for Strategic Research. B. M.-K. was supported by the National Nanotechnology Infrastructure Network funded by the National Science Foundation and by the Initiative for Nanoscale Materials and Processes and Nonvolatile Memory Technology Research Initiative Centers at Stanford University. V. O. was supported by the National Science Foundation under Grant No. DMR-1106024 and by the U.S. Department of Energy, Office of Science, Basic Energy Sciences under Grants No. DE-FG02-05ER46253 and No. DE-FG02-07ER46433. Work at the Lawrence Berkeley National Laboratory by K. A. P. was supported by the Assistant Secretary for Energy Efficiency and Renewable Energy, Office of Vehicle Technologies of the U.S. Department of Energy, under Contract No. DE-AC02-05CH11231. We thank I. Abrikosov, R. Jeanloz, M. J. Mehl, F. Milstein, P. Söderlind, and P. Souvatzis for information and helpful comments. We are particularly grateful to M. Šob who read the entire manuscript and suggested many improvements.

APPENDIX A: SPINODAL DECOMPOSITION

Spinodal decomposition refers to a mechanism by which a uniform system decomposes into two phases with different compositions, thus creating a miscibility gap in the temperature-composition phase diagram. Let the Gibbs free energy of mixing $G_{\mathrm{mix}}(c)$, as a function of composition c, have a shape as in Fig. 48. Consider a uniform system in the region where $\partial^2 G_{\mathrm{mix}}/\partial c^2 < 0$. Then a small spatial fluctuation in the composition, with the overall composition maintained, lowers the total G_{mix}. The classic alloy system to study spinodal decomposition is fcc Al-Zn. From *ab initio* calculations in fcc Al-Zn and Al-Cu, Müller *et al.* (1999) concluded that the phonon instability in fcc Zn plays a significant role in the formation of the miscibility gap, showing features that are not present in the Al-Cu system; see also Smirnova *et al.* (2001) on Al-Zn.

There is an analogy between the curvature of the Gibbs free energy just discussed and the bulk modulus expressed as

$$B = V\left(\frac{\partial^2 U}{\partial V^2}\right). \tag{A1}$$

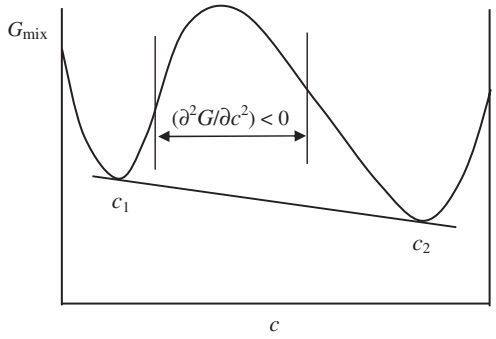

FIG. 48. The mixing Gibbs free energy G_{mix} as a function of composition c for a system that shows spinodal decomposition.

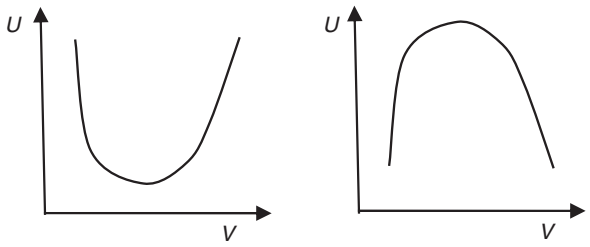

FIG. 49. The energy U as a function of volume V for two systems, where the right graph implies a spinodal instability.

The derivative in Eq. (A1) is taken where $\partial U/\partial V = 0$. Figure 49 shows two shapes of $U(V)$, corresponding to positive or negative bulk modulus. In the latter case, the Gibbs free energy is lowered if the system changes its volume, thus implying an instability. It is usually referred to as spinodal instability since it is related to the curvature of the energy, in analogy with the classical spinodal decomposition.

APPENDIX B: CENTRAL PAIRWISE INTERACTIONS

Prior to the progress in *ab initio* electronic structure calculations, many works on lattice stabilities were based on interactions between atoms expressed through central pairwise potentials. One example is the generalized Lennard-Jones potential, written in the form

$$\phi(r) = \frac{a}{r^m} - \frac{b}{r^n}. \tag{B1}$$

With this interaction, the fcc lattice is always dynamically stable, while the bcc lattice is stable for certain values of m and n (Misra, 1940; Power, 1942; Born and Huang, 1954).

There are many papers investigating the stability of lattices for various types of pairwise interactions, and we mention only a few of them as typical examples. Wallace and Patrick (1965) studied Lennard-Jones and Rydberg forms. The fcc lattice was found to be dynamically stable for all investigated parameter ranges. The bcc structure was generally unstable for short-range central forces, but stable for long-range forces. Milstein (1973a) considered the stability of fcc and bcc lattices with a generalized Morse function interaction. The fcc lattice was stable, while the bcc lattice was unstable for certain parameter values. Machlin and Shao (1983) discussed the C' instability in a bcc lattice for a Mie-type potential. Girifalco and Weizer (1959) found that a Morse potential always gave elastic stability for cubic crystals. Wolf and Jeanloz (1985) studied Lennard-Jones and Buckingham-type potentials, under compression and expansion, and found that the stability of the bcc lattice depends critically on how hard the repulsive part of the interaction is. An extreme case of hard repulsive forces is that of rigid spheres. The low value of C' in many bcc metals was attributed by Zener (1947, 1948) to the fact that the $(110)[\bar{1}10]$ shear leaves the distance between nearest-neighbor atoms unchanged, to a first approximation. Thus there is no resistance to this shear, if the atoms are represented by hard spheres. Finally we note that interaction through central pairwise interactions implies the Cauchy condition $C_{12} = C_{44}$. The Born stability criteria then become $C_{11} > C_{44} > 0$.

APPENDIX C: A THEOREM FOR PHONON FREQUENCIES

The phonon frequencies $\omega(\mathbf{q}, s)$ are obtained from the dynamical matrix $\mathbf{D}(\mathbf{q})$. According to a well-known mathematical theorem about roots to a secular equation,

$$\prod_{s=1}^{3r} \omega^2(\mathbf{q}, s) = |\mathbf{D}(\mathbf{q})|. \tag{C1}$$

The logarithm of a product becomes a sum of logarithms. Thus we can write the logarithmically averaged phonon frequency $\omega_{\log}$ as (Grimvall and Rosén, 1983)

$$\ln\omega_{\log} = \frac{1}{6N}\sum_{\mathbf{q}} \ln[|\mathbf{D}_0(\mathbf{q})|] - \frac{1}{2}\ln M_{\text{eff}}. \tag{C2}$$

M_{eff} is an effective mass, defined as the logarithmic average of all the atomic masses in the system. $\mathbf{D}_0(\mathbf{q})$ gives the forces between the atoms. It depends on the electronic structure but does not contain atomic masses. We note that Eq. (C2) is valid for any number of different atoms in the solid and for any crystal structure. Thus it holds also for alloys.

APPENDIX D: LONG-WAVELENGTH PHONONS

In the long-wavelength limit, the phonon frequencies are linear in the wave number q:

$$\omega(\theta, \phi, s) = C_{\text{sound}}(\theta, \phi, s)q. \tag{D1}$$

The sound velocities $C_{\text{sound}}(\theta, \phi, s)$ for the longitudinal branch ($s = L$) and the two transverse branches ($s = T_1, T_2$) in a certain direction (θ, ϕ) in a cubic lattice structure are determined by the elastic constants C_{11}, C_{12}, and C_{44}, the mass density ρ and the orientation of $\mathbf{q}$ as specified by its direction cosines (q_1, q_2, q_3). The result for C_{sound} in the directions [100], [110], and [111] is given in Table IV. Corresponding relations in a solid under isotropic pressure are found in Wallace (1967).

$\mathbf{D}(\mathbf{q})$ is well known in the elastic limit, see, e.g., Grimvall (1999). Then, from Eq. (C1) and in the limit that $C' \to 0$ while C_{44} remains finite,

$$\begin{aligned}(\rho/q^2)^3\omega_1^2(\mathbf{q})\omega_2^2(\mathbf{q})\omega_3^2(\mathbf{q}) &= C_{11}C_{44}^2[8q_1^2q_2^2q_3^2 - 4(q_1^2q_2^2 + q_1^2q_3^3 + q_2^2q_3^2) + 1] \\ &\quad + 4(C_{11} + C_{44})C_{44}^2q_1^2q_2^2q_3^2.\end{aligned} \tag{D2}$$

When $C_{11} > 0$ this expression is positive, except for $\mathbf{q}$ in the directions $\langle 110\rangle$ where it is zero. The instability associated with $C' \to 0$ thus arises only for the lower transverse $\langle 110\rangle$ branch of the elastic waves.

Next we let C' remain finite and consider $C_{44} \to 0$. Then

$$\begin{aligned}(\rho/q^2)^3\omega_1^2(\mathbf{q})\omega_2^2(\mathbf{q})\omega_3^2(\mathbf{q}) &= (C_{11} - C_{12})^2(C_{11} + 2C_{12})q_1^2q_2^2q_3^2.\end{aligned} \tag{D3}$$

In this case, transverse modes simultaneously become unstable for all $\mathbf{q}$ lying in (001) and equivalent planes. Therefore, $C_{44} \to 0$ gives a more severe instability than $C' \to 0$. The former case means that Zener's anisotropy index $C_{44}/C' < 1$. It is unusual, but holds in the equilibrium bcc phase of vanadium before it becomes dynamically unstable at high pressures (see Sec. V.B), in simple cubic polonium and in many compounds with the NaCl structure (Legut, Friák, and Šob, 2007, 2010). See also fcc Zn and Cd in Appendix J and the Zr-Nb-Mo alloys in Fig. 34.

TABLE IV. ρC_{sound}^2 in symmetry directions in a cubic lattice.

Mode	[100]	[110]	[111]
L	C_{11}	$(C_{11} + C_{12} + 2C_{44})/2$	$(C_{11} + 2C_{12} + 4C_{44})/3$
T_1	C_{44}	C_{44}	$(C_{11} - C_{12} + C_{44})/3$
T_2	C_{44}	$(C_{11} - C_{12})/2$	$(C_{11} - C_{12} + C_{44})/3$

In a cubic lattice that is elastically isotropic ($C' = C_{44}$), but with the longitudinal and transverse waves treated separately, the frequency $\omega_{\log}$ becomes

$$\omega_{\log} = \left[\frac{C_{11}(C_{11} - C_{12})^2}{4e^2\rho^3}\right]^{1/6} q_D. \tag{D4}$$

With this value for $\omega_{\log}$ inserted into Eq. (20), the high-temperature vibrational entropy diverges if $C_{11} - C_{12} \to 0$, which contradicts the result in Sec. III.B.1 that the entropy has a finite limit value. Thus even this model is too unrealistic, and it is necessary to include elastic anisotropy, i.e., to let C_{11}, C_{12}, and C_{44} be independent variables.

In the limit that $C_{44} \to 0$ while C' is finite (i.e., the most severe elastic instability in a cubic lattice), one obtains from Eq. (D3)

$$\omega_{\log} = \left[\frac{(C_{11} + 2C_{12})(C_{11} - C_{12})^2}{4e^2\rho^3}\right]^{1/6} q_D, \tag{D5}$$

thus giving $S_{\text{vib}}(T)$ a finite value.

APPENDIX E: A MODEL *P-T* PHASE DIAGRAM WITH A LATTICE INSTABILITY

Let the enthalpy difference between the two phases α and β vary linearly with P, so that the β phase becomes the thermodynamically stable phase at pressures $P > P_0$ when T is low:

$$H_\alpha - H_\beta = -H_0 + H'P = H'(P - P_0), \tag{E1}$$

where $H' > 0$. The instability of the β phase is assumed to cause an excess vibrational entropy

$$S_{\text{excess}} = \frac{S_{\text{crit}}}{1 + k(P - P_{\text{crit}})/P_0}. \tag{E2}$$

S_{crit} is the finite entropy limit as the instability is approached for pressures P above P_{crit} (see Sec. III.B) and k is a positive constant. With these assumptions the difference in the Gibbs free energy of the two phases is $G_\alpha(T, P) - G_\beta(T, P) = H'(P - P_0) + TS_{\text{excess}}$. The phase boundary between the α and β phases in the P-T diagram lies at the temperatures T_{eq} where $G_\alpha(T, P) = G_\beta(T, P)$:

$$T_{\text{eq}} = (H'/S_{\text{crit}})(P_0 - P)[1 + k(P - P_{\text{crit}})/P_0]. \tag{E3}$$

The vibrational entropy of the β phase (and hence also G_β) is not physically meaningful at pressures $P < P_{\text{crit}}$, but the α phase is thermodynamically well defined at all temperatures and pressures in our model. As a numerical example, take $k = 2$, $P_0/P_{\text{crit}} = 5$, and ignore the liquid phase. We get the phase diagram in Fig. 24.

The volume is related to G through $V = (\partial G/\partial P)_T$. Let V of the β phase be divided into a regular part and an excess part as

$$V = V_0 + V_{\text{excess}} = V_0 + \frac{bT}{[1 + k(P - P_{\text{crit}})/P_0]^2}, \tag{E4}$$

where b is a positive constant. The thermal expansion at constant pressure $\beta_{\text{expan}} = (1/V)(\partial V/\partial T)_P$ thus increases toward a finite limit value $\beta_0 + b$ as $P \to P_{\text{crit}}$, in analogy with the increase in vibrational entropy.

APPENDIX F: A BAIN PATH MODEL

As noted in Sec. IV, the energy $U(p)$ along a tetragonal Bain path has $\partial U(p)/\partial p = 0$ when $p = c/a = 1$ (bcc) and $p = \sqrt{2}$ (fcc), respectively, and becomes large and positive for very small or large p. The simplest polynomial in p that can reproduce this character of $U(p)$ is of fourth order. We therefore make the ansatz

$$U(p) = \alpha(p - 1)^2 + \beta(p - 1)^3 + \gamma(p - 1)^4. \tag{F1}$$

Further, $\partial^2 U/\partial p^2 = 2\alpha$ when evaluated at $p = 1$. With $U(1) = 0$, the coefficients α, β, and γ can be uniquely expressed in $\partial^2 U/\partial p^2$ and the energy difference $U(\sqrt{2}) - U(1) = \Delta H$. We get

$$\left(\frac{\partial^2 U}{\partial p^2}\right)_{p=\sqrt{2}} = \left(\frac{\partial^2 U}{\partial p^2}\right)_{p=1} - 12(\sqrt{2} + 1)^2 \Delta H, \tag{F2}$$

from which Eq. (39) follows.

APPENDIX G: FRENKEL-OROWAN MODEL

The classical Frenkel-Orowan model (Frenkel, 1926; Orowan, 1949) assumes a sinusoidal variation of the strain energy $U(\epsilon)$, so that the shear stress $\tau = dU/d\epsilon$ becomes

$$\tau = \frac{Gb}{2\pi a} \sin\left(\frac{2\pi x}{b}\right). \tag{G1}$$

G is the shear modulus, a and b are lattice distances as shown in Fig. 50 (b may be identified with a Burgers vector), and x is a displacement along the sheared planes, thus expressing the amount of strain. The ideal shear strength

$$\tau_{\text{ideal}} = \frac{Gb}{2\pi a} \tag{G2}$$

is reached at the inflection point $x = b/4$, i.e., where $dU(x)/dx$ has its largest value.

The ideas of Frenkel and Orowan were applied in a study of the ideal strength of 12 bcc metals in common bcc slip systems (Krenn *et al.*, 2001a). Ogata *et al.* (2004) also built on the Frenkel-Orowan description and formulated it as a two-parameter relation, which gives a good account of the deformation behavior (the so-called shearability) of a large number of metals and ceramics.

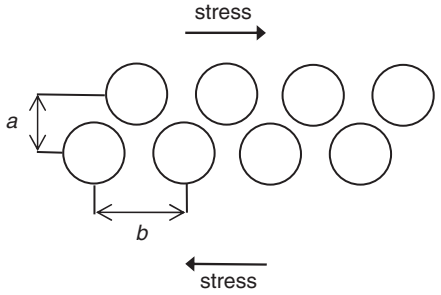

FIG. 50. Simple model geometry, with two planes sliding over each other.

APPENDIX H: LINDEMANN MELTING RULE

Consider the ratio $\xi = u_{\rm rms}/d$ where $u_{\rm rms}$ is the root mean square of the vibrational atomic displacements and d is a characteristic distance between neighboring atoms. It is striking that ξ has an almost constant value at the melting temperature T_m: $\xi = 0.13$ (Na, bcc), 0.11 (Cu, fcc), 0.10 (Pb, fcc), 0.10 (Al, fcc), 0.11 (Mg, hcp), and 0.12 (Tl, hcp) (Grimvall, 1999). This result might suggest that a lattice cannot remain stable above $u_{\rm rms}/d \approx 0.12$. However, the regularity rather reflects that interatomic forces in these substances can be approximately modeled by a common simple potential function $V(r)$. We write

$$V(r) = V_0\phi(\mathbf{r}/r_0). \tag{H1}$$

V_0 gives the strength of the interaction, r_0 is a length parameter that can be thought of as representing the size of an atom, and ϕ is a shape function for the interaction (a simple case being the Lennard-Jones potential). For a given shape ϕ, there are only two parameters in the model: V_0 with the dimension of energy and r_0 with the dimension of length. All physical properties (with quantum effects ignored) therefore scale with these two parameters. For instance, d must scale as r_0. Further, $k_{\rm B}T_m$ being an energy must scale as V_0, so that $k_{\rm B}T_m/V_0$ has a definite value given by the function ϕ. We seek a ratio $\xi = u_{\rm rms}/d$ at $T = T_m$. Buckingham's Π theorem (Buckingham, 1914), which uses dimensional analysis, implies that for any temperature T we can write

$$u_{\rm rms}/r_0 = \Phi(k_{\rm B}T/V_0). \tag{H2}$$

Φ is a function that depends on the mathematical form (shape) of the interaction $\phi(\mathbf{r}/r_0)$. It follows that $\Phi(k_{\rm B}T_m/V_0)$ is a dimensionless number, which is determined uniquely by ϕ. If a group of elements are well described by a certain common ϕ but differ in the strength V_0 and the size parameter r_0, they will all have the same value of $u_{\rm rms}/d$ at the melting point T_m, thus obeying the Lindemann melting rule. This result, which was further developed by Grimvall (1999, 2008), follows from dimensional analysis and is not related to a lattice instability.

APPENDIX I: PESUDOMORPHIC EPITAXY

Pseudomorphism refers to the case when the epitaxial film assumes the same in-plane lattice parameters as the substrate, leading to a crystalline form different from that which a substance normally has. There are numerous examples of pseudomorphism when an ultrathin layer of one material is grown epitaxially on a specified crystallographic surface of another material. In addition to the works cited in Sec. IV.A.2, we let the following examples illustrate various aspects of this important and rapidly expanding field of research. Films of bcc Cu and Pd were formed on W(100) (Wormeester, Hüger, and Bauer, 1996). Epitaxial thin films of Cu are stabilized in the bcc structure on bcc Fe (Wang *et al.*, 1987) and on fcc Ag (100) (Li *et al.*, 1991). Marcus and Jona (1997) discussed the stability of fcc Ti on Al(100). See also Alippi, Marcus, and Scheffler (1997) on V, Co, and Cu films, Ozoliņš, Wolverton, and Zunger (1998) on strains and phase stabilities in epitaxial noble metal films, Ji and Jona (2002) on fcc Mg on W(100), Friák, Šob, and Vitek (2001) and Spišák and Hafner (2002) on tetragonally strained layers of fcc Fe in various magnetic states on Cu(100), Lai and Zhao (2004) on vanishing shear resistance in an ultrathin fcc Fe film, Kolluri, Gungor, and Maroudas (2008) on fcc-hcp transformations in strained ultrathin Cu films, Zelený, Legut, and Šob (2008) and Zelený and Šob (2008) on Co and Ni under loading in epitaxial layers, Buschbeck *et al.* (2009) on the $Fe_{0.7}Pd_{0.3}$ magnetic shape memory alloy along most of the fcc-bcc Bain path, and Tsetseris (2005) and Shimada, Ishii, and Kitamura (2010) on magnetism in Fe.

APPENDIX J: C' AND C_{44} IN bcc AND fcc STRUCTURES OF METALLIC ELEMENTS

For each of the elements discussed below we first give the thermodynamically stable crystal structure at ambient pressure, as determined experimentally (Donohue, 1974; Young, 1991). Every and McCurdy (1992) gave data for the measured elastic constants of many of these equilibrium phases, usually at room temperature. References to experimentally determined phonon dispersion curves are given in only a few cases. An analysis by Ledbetter *et al.* (2004) for bcc Ti at 1000 K illustrates the uncertainty in C_{ij} when derived from phonon dispersion curves rather than from ultrasound measurements. There are numerous papers dealing with the relative energies of simple structures for elements under zero or finite pressure when $T = 0$ K, but without addressing lattice instabilities *per se*; see, e.g., Cazorla, Alfè, and Gillan (2008a) on 4*d* transition metals and Burakovsky *et al.* (2010) for the complicated case of Ta. The exotic high-pressure behavior of Li and Na also falls outside the scope of this review (Rousseau *et al.*, 2011). Further, we will not cover works on the equation of state, e.g., as discussed by Karbasi, Saxena, and Hrubiak (2011) for several stable metallic elements.

The emphasis in this Appendix is on metastable or dynamically unstable fcc and bcc structures. Unless otherwise stated, the results are obtained through *ab initio* electron structure calculations of some kind. Most of them are for $T = 0$ K and ambient pressure ($P = 0$). There is no attempt to be complete in these references. In particular, early or less accurate calculations were ignored, and we may give just a single recent reference to high-pressure works. Magnetic states are specified as FM, AFM, and NM. In many cases there is more than one source of data. The spread in the numerical values illustrates their uncertainty. The data in Table II are usually not repeated. All values for C' and C_{44} in this Appendix are expressed in GPa.

1. Lithium, sodium, potassium, rubidium, and cesium

Li, Na, K, Rb, and Cs have bcc structure at ambient conditions. The fcc structure of all alkali metals has $C' > 0$ and $C_{44} > 0$ at ambient conditions (Xie *et al.*, 2008), in agreement with results obtained by Sliwko *et al.* (1996) and Marcus, Jona, and Qiu (2002) for Li, K, and Rb, and Xie *et al.* (2000) for Cs. Vaks *et al.* (1991), Milstein and Rasky (1996), Milstein *et al.* (1996), and Xie *et al.* (2007, 2008)

considered alkali metals under pressure at low temperatures. All alkali metals in the bcc structure have $C' < 0$ at high pressure, and in Li (Rodriguez-Prieto *et al.*, 2006) and Na (Xie *et al.*, 2008) the instability is present also for the N-point phonon. Shear instabilities in bcc and fcc Na and K at ultrahigh pressures are considered by Katsnelson *et al.* (2000). In fcc Li there is an unstable transverse phonon mode near the K point above about 33 GPa (Kasinathan *et al.*, 2006; Profeta, 2006; Yao, Tse *et al.*, 2009). Kong and Jepsen (2000) found a corresponding result in Cs. The phonon changes in Li at high P are examples of Fermi surface nesting effects (Kasinathan *et al.*, 2006; Profeta, 2006; Rodriguez-Prieto *et al.*, 2006).

2. Beryllium, magnesium, calcium, strontium, barium, and radium

Be transforms from an hcp to a bcc structure at 1530 K and melts at 1560 K. Mg has hcp structure up to the melting point. Ca and Sr have fcc structures, which transform to bcc at 721 and 830 K, respectively, while Ba is bcc at all temperatures. In Be, Lam, Chou, and Cohen (1984) calculated $C_{44} = 186$ (fcc) and 170 (bcc), $C' = 78$ (fcc) and 5 (bcc). Sin'ko and Smirnov (2005) found that bcc and fcc Be are elastically stable up to high pressures. In bcc Be, C' becomes negative on expansion to $1.17V_0$, where V_0 is the volume at 0 K (Kádas *et al.*, 2007), but stiffens to 3.7 on compression to $0.3V_0$ (Lam, Chou, and Cohen, 1984). The fcc phase of Mg is dynamically stable, with $C' = 6$, $C_{44} = 24$ (Jona and Marcus, 2002b), and $C' = 6.3$, $C_{44} = 31.5$, while bcc Mg has $C' < 0$ at low pressure and $T = 0$ (Sin'ko and Smirnov, 2009). The behavior of Mg under pressure is treated in Sec. V.C, but see also Sin'ko and Smirnov (2009). There are neutron scattering data for phonons in the bcc and fcc structures of Ca (Heiroth *et al.*, 1986), and fcc Sr and bcc Ba (Buchenau *et al.*, 1984). Jona and Marcus (2006) reviewed experimental and *ab initio* work and performed calculations for Ca, Sr, and Ba. Their $T = 0$ K results for metastable bcc Ca and Sr are in fair agreement with those of Sliwko *et al.* (1996). Calculations of the shear elastic constants in Ca, Sr, and Ba can have large uncertainties and give the wrong sign; see Mehl and Papaconstantopoulos (1996) and Pollack *et al.* (1997). Ca and Sr transform from fcc to bcc, and Ba from bcc to hcp, under pressure (Chen, Ho, and Harmon, 1988; Jona and Marcus, 2006; Qiu and Marcus, 2009). C' and C_{44} in Ca, Sr, and Ba show sudden elastic variations and instabilities as a function of pressure (Vaks *et al.*, 1991). Pollack *et al.* (1997) found that the $T = 0$ K low transverse [110] phonon branch becomes stabilized in bcc Be, Mg, Ca, Sr, and Ba under pressure. Teweldeberhan and Bonev (2008) and Yao, Klug *et al.* (2009) considered the stabilization of the simple cubic structure of Ca under pressure. Ra transforms from bcc to fcc under pressure (Khojandi and Papaconstantopoulos, 2010).

3. Scandium, yttrium, and lanthanum

Sc and Y have hcp structure, followed by bcc above 1608 and 1752 K, respectively. La transforms from hcp to fcc at 550 K and to bcc at 1134 K. The bcc structure of Sc and La is unstable at $T = 0$ K; $C' = -10$ (Sc) and -25 (La), $C_{44} = 30$ (Sc) and 10 (La) (Persson, Ekman, and Ozoliņš, 2000). Nixon, Papaconstantopoulos, and Mehl (2008) reported $C' = -38$ (-35) and the very low values $C_{44} = 0.4$ (0.8) in the local density and GGA approximations, respectively, for bcc La. See also Wills *et al.* (1992) for La and Craievich *et al.* (1997) for Sc. The fcc phases of La (Wills *et al.*, 1992), Sc, and Y are elastically stable (Papaconstantopoulos, Lach-hab, and Mehl, 2001), with $C' = 12.6$, and $C_{44} = 31.1$ in fcc Y (Marcus and Jona, 2005).

4. Titanium, zirconium, and hafnium

Ti, Zr, and Hf have hcp structure, followed by bcc above 1155, 1136, and 2030 K, respectively. Theoretical phonon dispersion curves show signs of instabilities in bcc Ti (Sanati *et al.*, 2001; Hennig *et al.*, 2008) and bcc Zr (Chen *et al.*, 1985; Sanati *et al.*, 2001), in agreement with high-T experiments. The experimental fact that the high-temperature bcc phase cannot be retained under quenching to low temperatures is consistent with qualitative results from early *ab initio* calculations at $T = 0$ K, which gave $C' < 0$ for Ti (Craievich *et al.*, 1994; Sliwko *et al.*, 1996; Marcus and Jona, 1997) and Hf (Wills *et al.*, 1992). Other calculations for the bcc structure gave $C' = -10$ (Ti) and -20 (Hf), $C_{44} = 20$ (Ti) and 40 (Hf) (Persson, Ekman, and Ozoliņš, 2000), $C' = -15$ (Ti), $C_{44} = 39$ (Ti) (Wang, Šob, and Zhang, 2003), $C' = -8$ (Ti), $C_{44} = 53$ (Ti) (Hennig *et al.*, 2008), $C' = -12.2$ (Ti) and -3.6 (Zr), $C_{44} = 39.8$ (Ti) and 32.3 (Zr) (Ikehata *et al.*, 2004). Porta and Castán (2001) calculated the phonon spectrum of bcc Zr at $T = 0$, with $C' = -5.8$ and $C_{44} = 36$. The fcc phases of Ti, Zr, and Hf are elastically stable (Marcus and Jona, 1997; Papaconstantopoulos, Lach-hab, and Mehl, 2001), with $C' = 22$, 21, 28 and $C_{44} = 61$, 53, 67, respectively (Aguayo, Murrieta, and de Coss, 2002), and $C' = 20$ (Ti), $C_{44} = 50$ (Ti) (Wang, Šob, and Zhang, 2003). Several papers discussed the bcc stabilization at high T. In a Monte Carlo simulation by Porta and Castán (2001), C' was stabilized above about 1500 K. Masuda-Jindo, Nishitani, and Hung (2004) used an embedded-atom potential and allowed for anharmonicity in bcc Ti, thus stabilizing C' at about 800 K. See also Trubitsin (2006a, 2006b), Ye *et al.* (1987), and the discussion in Sec. VI.B on bcc Zr, and the high-T *ab initio* calculations by Souvatzis *et al.* (2008, 2009) for Ti, Zr, and Hf. Ahuja *et al.* (1993) found bcc Ti, Zr, and Hf stabilized at high pressure and $T = 0$ K; see also Hu, Lu, and Yang (2008), and Hu *et al.* (2010), and references therein. Hsueh *et al.* (2002) noted that the phonon structure in bcc Zr could be stabilized if a magnetic moment was imposed.

5. Vanadium, niobium, and tantalum

V, Nb, and Ta have bcc structure up to the melting temperature, and $C' < 0$ in the fcc structure at $T = 0$ K (Craievich *et al.*, 1994; Papaconstantopoulos, Lach-hab, and Mehl, 2001; Nnolim, Tyson, and Axe, 2003). $C' < 0$ was also obtained by Wills *et al.* (1992) for Ta, Mehl *et al.* (2004) for V and Nb, Sliwko *et al.* (1996) and Alippi, Marcus, and Scheffler (1997) for V, and Söderlind and Moriarty (1998) for Ta. Wang, Šob, and Zhang (2003) calculated $C' = -152$, $C_{44} = -57$ in fcc Nb, and

$C' = -102$, $C_{44} = 19$ in fcc Ta. C_{44} in V shows an unusual variation with pressure; see Qiu and Marcus (2008a) and Sec. V.B. Both bcc and fcc Ta are elastically stable above $P =$ 1000 GPa (Söderlind and Moriarty, 1998). Craievich *et al.* (1997) found hcp Nb unstable.

6. Chromium, molybdenum, and tungsten

Cr, Mo, and W have bcc structure up to the melting temperature. It is well established that $C' < 0$ in the fcc structure at $T = 0$ K; see Wills *et al.* (1992) and Šob, Wang, and Vitek (1997a) for W, Craievich *et al.* (1994) and Nnolim, Tyson, and Axe (2003) for Cr(NM), Mo, and W, Mehl and Papaconstantopoulos (1996) for Mo, and Papaconstantopoulos, Lach-hab, and Mehl (2001), Wang, Šob, and Zhang (2003), and Mehl *et al.* (2004) for Mo and W. Einarsdotter *et al.* (1997) calculated the full phonon spectrum for fcc W at different pressures, with the $P = 0$ results $C' = -159$ and $C_{44} = -128$. Guo and Wang (2000a) obtained $C' = 169$, $C_{44} = 127$ in bcc Cr(NM), $C' = 174$, $C_{44} = 119$ in bcc Cr(AF), $C' = -141$, $C_{44} = -76$ in fcc Cr(NM), and $C' = -117$ in hcp Cr(NM). Wang, Šob, and Zhang (2003) calculated $C' = -88$, $C_{44} = -7$ in fcc Mo and $C' = -142$, $C_{44} = -60$ in fcc W. The stabilization of fcc W at high pressures (Einarsdotter *et al.*, 1997) is in agreement with $C' > 0$ and $C_{44} > 0$ at high P (Ruoff, Rodriguez, and Christensen, 1998), and work by Zeng *et al.* (2010) on Mo. Belonoshko *et al.* (2008) found both bcc and fcc Mo dynamically stable from 350 GPa up to at least 850 GPa; see also Jona and Marcus (2005) and Cazorla, Alfè, and Gillan (2008b). The possible stabilization of the fcc structure at high T was treated by Asker *et al.* (2008) for Mo and by Ozoliņš (2009) for W. The hcp phase of Mo is elastically unstable (Craievich *et al.*, 1997; Cazorla, Alfè, and Gillan, 2008b).

7. Manganese, technetium, and rhenium

Mn has bcc structure (complex, 58 atoms/unit cell) up to about 1000 K, followed by two disputed structures and then again the bcc structure. Tc and Re have hcp structure up to the melting temperatures. Craievich *et al.* (1994) obtained $C' > 0$ for the fcc structure and $C' < 0$ for the bcc structure of Mn (NM), Tc, and Re. This is consistent with C' (Wills *et al.*, 1992) and phonon spectrum (Persson, Ekman, and Grimvall, 1999) calculations for Re at $P = 0$, and under pressure (Verma *et al.*, 2003). Further, $C' < 0$ in bcc Mn (AF) (Qiu and Marcus, 1999; Qiu, Marcus, and Ma (2000a, 2000b). Papaconstantopoulos, Lach-hab, and Mehl (2001) found fcc Tc and Re elastically stable.

8. Iron, ruthenium, and osmium

Fe has bcc structure up to 1173 K, followed by fcc and then a return to bcc at 1660 K. Ru and Os have hcp structure up to the melting temperature. In Fe, the experimental values of C_{11}, C_{12}, and C_{44} do not change much on the transition from bcc-to-fcc structure (Every and McCurdy, 1992). Craievich *et al.* (1994) obtained $C' < 0$ (bcc), $C' > 0$ (fcc) in Fe (NM), Ru, and Os, as confirmed by Wang *et al.* (2004) for Ru and Os. Wills *et al.* (1992) obtained $C' < 0$ in bcc Os, and Papaconstantopoulos, Lach-hab, and Mehl (2001) found fcc Ru and Os elastically stable. Much work has been done on the stability of Fe lattices in different magnetic states, and the following account is not complete. The N-point transverse phonon mode is unstable in bcc Fe (NM) (Ekman *et al.*, 1998), and fcc Fe (FM) and bcc Fe (NM) are unstable under shear (Krasko and Olson, 1990). Friák, Šob, and Vitek (2001) considered bcc and fcc Fe at different volumes and magnetic configurations, and found bcc Fe (NM) unstable. A quantum Monte Carlo bcc-fcc Bain path calculation by Leonov *et al.* (2011) showed that paramagnetic bcc Fe is dynamically unstable well above the Curie temperature. Peng and Jansen (1991), Marcus, Moruzzi, and Qiu (1999), Qiu, Marcus, and Ma (2001) and Spišák and Hafner (2002) considered tetragonal Fe. Friák and Šob (2008) and Johnson and Carter (2008) investigated the Fe bcc-hcp transformation path in various magnetic states. Guo and Wang (2000b) calculated $C' = -110$, $C_{44} = 141$ in bcc Fe (NM), $C' = -77$, $C_{44} = 23$ in fcc Fe (FM), $C' = 125$, $C_{44} = 287$ in fcc Fe (NM), $C' = -15$ in hcp Fe (FM), and $C' = 193$ in hcp Fe (NM). See also work on the role of magnetism in bcc Fe (Hsueh *et al.*, 2002) and in Bain path calculations (Herper, Hoffmann, and Entel, 1999; Qiu and Marcus, 1999; Qiu, Marcus, and Ma, 2000a; Friák, Šob, and Vitek, 2001; Tsetseris, 2005; Qiu, Apostol, and Marcus, 2008; Okatov *et al.*, 2009). Zelený, Friák, and Šob (2011) compared the energetics of the NM, FM, and AFM states in Fe along the trigonal deformation path. The magnetic structure in γ-Fe was discussed by Marsman and Hafner (2002). High-pressure effects in Fe have been investigated by several groups. It is well known (Stixrude, Cohen, and Singh, 1994; Stixrude and Cohen, 1995; Söderlind, Moriarty, and Wills, 1996; Ekman *et al.*, 1998; Ma, Qiu, and Marcus, 2002; Mathon *et al.*, 2004) that bcc Fe becomes dynamically unstable at high pressures, and that the emerging instability can be attributed to magnetic effects. However, bcc Fe may be stabilized at the conditions of the Earth's inner core (Belonoshko, Ahuja, and Johansson, 2003). For other works on Fe under pressure, see Vočadlo *et al.* (2008) and references therein. An overview of *ab initio* calculations of elastic properties from the electronic ground state to the stability limit, with an application to bcc Fe, is given by Friák (2011). Work by Körmann *et al.* (2008, 2010) showed how the magnetic, vibrational, and electronic contributions to the thermodynamic properties of bcc Fe can be simultaneously calculated *ab initio*.

9. Cobalt, rhodium, and iridium

Co (FM) has hcp structure up to 661 K, where it transforms to fcc structure. Rh and Ir have fcc structure up to the melting temperature. Guo and Wang (2000b) found fcc Co (NM), fcc Co (FM), and hcp Co (NM) elastically stable at $T = 0$ K. In bcc Co (FM) and bcc Co (NM) their calculations gave $C' = -24$, $C_{44} = 131$, and $C' = -270$, $C_{44} = 368$, respectively, in agreement with the bcc instability obtained by Craievich *et al.* (1994), and bcc Co (FM) being unstable with $C' = -36.5$, $C_{44} = 152$ (Liu and Singh, 1993), $C' = -29$, $C_{44} = 131$ (Söderlind *et al.*, 1994); see also Fox and Jansen (1999) Hsueh *et al.* (2002), Zelený and Šob (2008), Zelený, Legut, and Šob (2008), and

Laenens *et al.* (2009). Zelený, Friák, and Šob (2011) compared the energetics of NM, FM, and AFM states in Co along the trigonal deformation path. Further, $C' < 0$ in bcc Ir (Mehl and Boyer, 1991; Wills *et al.*, 1992; Craievich *et al.*, 1994), and in bcc Rh (NM) (Craievich *et al.*, 1994), while Rh in a bcc lattice is ferromagnetically ordered (Hüger and Osuch, 2004; Cui *et al.*, 2010). Šob, Wang, and Vitek (1997a) obtained $C' = -383$ and $C_{44} = 217$ in bcc Ir.

10. Nickel, palladium, and platinum

Ni (FM), Pd, and Pt have fcc structure. Also fcc Ni (NM) is elastically stable (Guo and Wang, 2000b; Zelený, Legut, and Šob, 2008). Calculations on bcc Ni (FM) and bcc Ni (NM) gave $C' = -33$, $C_{44} = 156$, and $C' = -96$, $C_{44} = 395$, respectively (Guo and Wang, 2000b), in agreement with the bcc instability obtained by Craievich *et al.* (1994), Mishin *et al.* (1999), Zhang, Li, and Xu (2007), Zelený, Legut, and Šob (2008), and Zelený and Šob (2008). Zelený, Friák, and Šob (2011) compared the energetics of NM, FM, and AFM states in Ni along the trigonal deformation path. Further, $C' < 0$ in bcc Pd (Jona and Marcus, 2002a), and bcc Pt (Mehl *et al.*, 2004). Yashiro *et al.* (2006) studied Ni under pressure. Both hcp Ni (FM) and hcp Ni (NM) are elastically stable (Guo and Wang, 2000b).

11. Copper, silver, and gold

Cu, Ag, and Au have fcc structure up to the melting temperature. While hcp Cu is unstable (Jona, Ji, and Marcus, 2003), hcp Ag and Au are elastically stable (Jona and Marcus, 2004). The bcc structure of Cu is unstable, with $C' = -6$, $C_{44} = 112$ (Wang and Šob, 1999; Wang, Šob, and Zhang, 2003), $C' = -14.5$, $C_{44} = 95.9$ (Liu *et al.*, 2005); see also Kraft *et al.* (1993), Alippi, Marcus, and Scheffler (1997), Jona and Marcus (2001), Mishin *et al.* (2001) and Černý *et al.* (2004). Magyari-Köpe, Grimvall, and Vitos (2002) calculated $C' = 3$ and $C_{44} = 65$ in bcc Ag. Wills *et al.* (1992) found $C' \approx 0$ for bcc Au, and Papaconstantopoulos and Mehl (2003) obtained $C' < 0$ in bcc Cu and Au; see also Zhang *et al.* (2008a, 2008b). In bcc Cu-Fe alloys, the elastic instability extends up to about 50 at. % Fe (Liu *et al.*, 2005).

12. Zinc, cadmium, and mercury

Zn and Cd have hcp structures with c/a significantly higher than the ideal value of 1.63. Hg has a low-temperature tetragonal structure followed by a rhombohedral structure. While bcc Zn is strongly unstable, the stability of the fcc phase has been more uncertain. Müller *et al.* (1999) and Marcus, Jona, and Qiu (2002) found C_{44} to be slightly negative in fcc Zn, and Magyari-Köpe, Grimvall, and Vitos (2002) obtained $C' = -21$ (bcc), 30 (fcc) and $C_{44} = -2$ (bcc), 5 (fcc). Qiu and Marcus (2008b) studied several Zn phases under pressure and found fcc Zn to be very stable above 32 GPa. Marcus and Jona (2005) obtained $C' = 16.4$, $C_{44} = -1.9$ in fcc Cd. The high-pressure hcp phase of Hg was studied by Jona and Marcus (2007).

13. Aluminum, gallium, indium, and thallium

Al has fcc structure up to the melting temperature, Ga has orthorhombic, and In has tetragonal structure. Tl has hcp structure, followed by bcc at high temperatures. Al is unstable in the bcc structure; $C' < 0$ (Mehl and Boyer, 1991; Craievich *et al.*, 1997; Mishin *et al.*, 1999; Tambe, Bonini, and Marzari, 2008), $C' = -24.5$, $C_{44} = 26.7$ (Li and Wang, 1998), $C' = -17$, $C_{44} = 44$ (Sin'ko and Smirnov, 2002), $C' = -16$, $C_{44} = 46$ (Wang, Šob, and Zhang, 2003), with C' being stabilized at high pressure, while C' in fcc Al becomes unstable (Sin'ko and Smirnov, 2002; Marcus and Qiu, 2009b). Above 725 GPa, fcc Al becomes elastically unstable (Tambe, Bonini, and Marzari, 2008). In fcc Ga, $C' < 0$ at ambient pressure (Kenichi, Kazuaki, and Masao, 1998; Baskes, Chen, and Cherne, 2002) but all $\omega^2(\mathbf{q}) > 0$ at high pressure (Li and Tse, 2000). The thermodynamically stable bcc Tl has a pronounced dip in $\omega(\mathbf{q})$ for $\mathbf{q} = (2/3) \times [111]$, and very low C' (Iizumi, 1983). Pseudopotential calculations by Pollack *et al.* (1997) gave $C' < 0$ for bcc and $C' > 0$ for fcc Al, Ga, In, and Tl.

14. Carbon, silicon, germanium, tin, and lead

C, Si, and Ge have diamond-type structure, Sn a low-temperature diamond-type structure followed by tetragonal structure, and Pb a fcc structure. Cohen, Stixrude, and Wasserman (1997) found elastic instability in fcc and hcp Si. Ekman, Persson, and Grimvall (2000) found bcc and fcc Si to be metallic, with $C' < 0$ at $T = 0$ K. Pseudopotential calculations by Pollack *et al.* (1997) gave $C' < 0$ for bcc and $C' > 0$ for fcc Sn and Pb. Katzke and Tolédano (2007) reviewed the structural transformations in Si, Ge, Sn, and Pb at high pressure, but without discussion of instabilities. Sun, Klug, and Martoňák (2009) considered structures of C in the TPa pressure range and found evidence for a simple cubic phase.

15. Tellurium and polonium

Te is a semiconductor at ambient conditions but transforms to metallic phases at high pressure. The calculated bcc phonon dispersion curve develops an instability near [0.2, 0, 0] below about 20 GPa (Mauri *et al.*, 1996). Po is the only element that has the sc structure in the thermodynamic ground state at ambient conditions. The calculated elastic constants depend strongly on volume and on *ab initio* model approximations, with the bcc and fcc structures being elastically unstable (Kraig, Roundy, and Cohen, 2004; Legut, Friák, and Šob, 2007, 2010); see also Šob, Legut, and Friák (2009) and Kim, Choi, and Min (2009).

16. Arsenic, antimony, and bismuth

As, Sb, and Bi have rhombohedral layered structures at ambient conditions and a high-pressure bcc phase (Iwasaki and Kikegawa, 1997). Gutiérrez, Menéndez-Proupin, and Singh (2006) calculated the elastic constants of bcc Bi at high P.

17. Lanthanides

La was discussed above. Söderlind, Eriksson, Wills, and Johansson *et al.* (1993) showed how the dynamical stability of bcc and fcc Sm at ultrahigh pressure depends critically on assumptions about the magnetic structure. Pr is dynamically unstable in both bcc and fcc structure (Söderlind, 2002).

18. Actinides

Söderlind (1998) reviewed the light actinides Th, Pa, U, Np, and Pu. At ambient conditions both bcc and fcc U and Np have $C' < 0$. The high-temperature phase δ-Pu has a magnetically disordered fcc structure. Nonmagnetic fcc Pu is unstable, with $C' = -69$, $C_{44} = 15$ (Söderlind *et al.*, 2004); see also Söderlind (1998). Pu melts in the bcc structure (ϵ-Pu), which, however, is unstable at $T = 0$ K (Söderlind, 1998; Dai *et al.*, 2003; Söderlind *et al.*, 2010). $C' < 0$ in fcc Th above $P = 80$ GPa (Bouchet and Albers, 2011).

REFERENCES

Aguayo, A., G. Murrieta, and R. de Coss, 2002, Phys. Rev. B **65**, 092106.

Ahuja, R., J. M. Wills, B. Johansson, and O. Eriksson, 1993, Phys. Rev. B **48**, 16 269.

Alber, I., J. L. Bassani, M. Khantha, V. Vitek, and G. J. Wang, 1992, Phil. Trans. R. Soc. A **339**, 555.

Alexander, S., 1998, Phys. Rep. **296**, 65.

Alexander, S., and J. McTague, 1978, Phys. Rev. Lett. **41**, 702.

Alippi, P., P. M. Marcus, and M. Scheffler, 1997, Phys. Rev. Lett. **78**, 3892.

Asker, C., A. B. Belonoshko, A. S. Mikhaylushkin, and I. A. Abrikosov, 2008, Phys. Rev. B **77**, 220102(R).

Bai, X.-M., and M. Li, 2008, Phys. Rev. B **77**, 134109.

Bain, E. C., 1924, Trans. Am. Inst. Min., Metall. Engrs. **70**, 25.

Baroni, S., S. de Gironcoli, A. dal Corso, and P. Giannozzi, 2001, Rev. Mod. Phys. **73**, 515.

Barron, T. H. K., 1965, in *Lattice Dynamics*, edited by R. F. Wallis (Pergamon Press, Oxford), p. 247.

Barron, T. H. K., and M. L. Klein, 1965, Proc. Phys. Soc. London **85**, 523.

Baskes, M. I., S. P. Chen, and F. J. Cherne, 2002, Phys. Rev. B **66**, 104107.

Belonoshko, A. B., R. Ahuja, and B. Johansson, 2003, Nature (London) **424**, 1032.

Belonoshko, A. B., L. Burakovsky, S. P. Chen, B. Johansson, A. S. Mikhaylushkin, D. L. Preston, S. I. Simak, and D. C. Swift, 2008, Phys. Rev. Lett. **100**, 135701.

Binggeli, N., N. R. Keskar, and J. R. Chelikowsky, 1994, Phys. Rev. B **49**, 3075.

Boppart, H., A. Treindl, P. Wachter, and S. Roth, 1980, Solid State Commun. **35**, 483.

Born, M., 1939, J. Chem. Phys. **7**, 591.

Born, M., 1940, Proc. Cambridge Philos. Soc. **36**, 160.

Born, M., 1951, *Festschrift zur Feier des zweihundertjährigen Bestehens der Akademie der Wissenschaften in Göttingen I* (Springer-Verlag, Berlin), p. 1.

Born, M., and R. Fürth, 1940, Proc. Cambridge Philos. Soc. **36**, 454.

Born, M., and K. Huang, 1954, *Dynamical Theory of Crystal Lattices* (Oxford University Press, London).

Bouchet, J., and R. C. Albers, 2011, J. Phys. Condens. Matter **23**, 215402.

Brillouin, L., 1938, Phys. Rev. **54**, 916.

Buchenau, U., M. Heiroth, H. R. Schober, J. Evers, and G. Oehlinger, 1984, Phys. Rev. B **30**, 3502.

Buckingham, E., 1914, Phys. Rev. **4**, 345.

Burakovsky, L., S. P. Chen, D. L. Preston, A. B. Belonoshko, A. Rosengren, A. S. Mikhaylushkin, S. I. Simak, and J. A. Moriarty, 2010, Phys. Rev. Lett. **104**, 255702.

Burakovsky, L., C. W. Greeff, and D. L. Preston, 2006, Solid State Commun. **137**, 436.

Burgers, W. G., 1934, Physica (Utrecht) **1**, 561.

Buschbeck, J., I. Opahle, M. Richter, U. K. Rössler, P. Klaer, M. Kallmayer, E. J. Elmers, G. Jakob, L. Schultz, and S. Fähler, 2009, Phys. Rev. Lett. **103**, 216101.

Cazorla, C., D. Alfè, and M. J. Gillan, 2008a, Phys. Rev. B **77**, 224103.

Cazorla, C., D. Alfè, and M. J. Gillan, 2008b, Phys. Rev. Lett. **101**, 049601.

Černý, M., 2007, Mater. Sci. Eng. A **462**, 432.

Černý, M., R. Boyer, M. Šob, and S. Yip, 2005, J. Computer-Aided Mater. Design **12**, 161.

Černý, M., and J. Pokluda, 2007, Phys. Rev. B **76**, 024115.

Černý, M., and J. Pokluda, 2008a, Mater. Sci. Eng. A **483–484**, 692.

Černý, M., and J. Pokluda, 2008b, Mater. Sci. Forum **567–568**, 73.

Černý, M., and J. Pokluda, 2008c, Comput. Mater. Sci. **44**, 127.

Černý, M., and J. Pokluda, 2009, J. Phys. Condens. Matter **21**, 145406.

Černý, M., and J. Pokluda, 2010a, Acta Mater. **58**, 3117.

Černý, M., and J. Pokluda, 2010b, Phys. Rev. B **82**, 174106.

Černý, M., J. Pokluda, M. Šob, M. Friák, and P. Šandera, 2003, Phys. Rev. B **67**, 035116.

Černý, M., P. Šesták, and J. Pokluda, 2010, Comput. Mater. Sci. **47**, 907.

Černý, M., M. Šob, J. Pokluda, and P. Šandera, 2004, J. Phys. Condens. Matter **16**, 1045.

Chaplot, S. L., and S. K. Sikka, 1993, Phys. Rev. Lett. **71**, 2674.

Chattopadhyay, P. P., P. M. G. Nambissan, S. K. Pabi, and I. Manna, 2001, Phys. Rev. B **63**, 054107.

Chen, Y., C. Fu, K. Ho, and B. N. Harmon, 1985, Phys. Rev. B **31**, 6775.

Chen, Y., K. M. Ho, and B. N. Harmon, 1988, Phys. Rev. B **37**, 283.

Clark, A. E., K. B. Hathaway, M. Wun-Fogle, J. B. Restorff, T. A. Lograsso, V. M. Keppens, G. Petculescu, and R. A. Taylor, 2003, J. Appl. Phys. **93**, 8621.

Clatterbuck, D. M., D. C. Chrzan, and J. W. Morris, Jr., 2002, Philos. Mag. Lett. **82**, 141.

Clatterbuck, D. M., D. C. Chrzan, and J. W. Morris, Jr., 2003a, Scr. Mater. **49**, 1007.

Clatterbuck, D. M., D. C. Chrzan, and J. W. Morris, Jr., 2003b, Acta Mater. **51**, 2271.

Clatterbuck, D. M., C. R. Krenn, M. L. Cohen, and J. W. Morris, Jr., 2003, Phys. Rev. Lett. **91**, 135501.

Cleri, F., J. Wang, and S. Yip, 1995, J. Appl. Phys. **77**, 1449.

Cohen, R. E., L. Stixrude, and E. Wasserman, 1997, Phys. Rev. B **56**, 8575.

Cowley, E. R., and R. A. Cowley, 1966, Proc. R. Soc. A **292**, 209.

Craievich, P. J., J. M. Sanchez, R. E. Watson, and M. Weinert, 1997, Phys. Rev. B **55**, 787.

Craievich, P. J., M. Weinert, J. M. Sanchez, and R. E. Watson, 1994, Phys. Rev. Lett. **72**, 3076.

Cui, X., J.-T. Wang, X.-X. Liang, and G.-Z. Zhao, 2010, Chin. Phys. Lett. **27**, 027101.

Dai, X., S. Y. Savrasov, G. Kotliar, A. Migliori, H. Ledbetter, and E. Abrahams, 2003, Science **300**, 953.
Delogu, F., 2004a, Mater. Sci. Eng. A **367**, 162.
Delogu, F., 2004b, Mater. Sci. Eng. A **375–377**, 675.
Delogu, F., 2005, Mater. Sci. Eng. A **403**, 48.
Delph, T. J., and J. A. Zimmerman, 2010, Model. Simul. Mater. Sci. Eng. **18**, 045008.
Delph, T. J., J. A. Zimmerman, J. M. Rickman, and J. M. Kunz, 2009, J. Mech. Phys. Solids **57**, 67.
Desgranges, C., and J. Delhommelle, 2007, J. Chem. Phys. **127**, 144509.
Djohari, H., F. Milstein, and D. Maroudas, 2006, Appl. Phys. Lett. **89**, 181907.
Djohari, H., F. Milstein, and D. Maroudas, 2009, Phys. Rev. B **79**, 174109.
Donohue, J., 1974, *The Structures of The Elements* (Wiley, New York).
Drummond, N. D., and G. J. Ackland, 2002, Phys. Rev. B **65**, 184104.
Dubiel, S. M., J. Cieslak, W. Sturham, M. Sternik, P. Piekarz, S. Stankov, and K. Parlinski, 2010, Phys. Rev. Lett. **104**, 155503.
Ducastelle, F., 1970, J. Phys. (Paris) **31**, 1055.
Einarsdotter, K., B. Sadigh, G. Grimvall, and V. Ozoliņš, 1997, Phys. Rev. Lett. **79**, 2073.
Ekman, M., K. Persson, and G. Grimvall, 2000, Phys. Rev. B **62**, 14 784.
Ekman, M., B. Sadigh, K. Einarsdotter, and P. Blaha, 1998, Phys. Rev. B **58**, 5296.
Errandonea, D., Y. Meng, D. Häusermann, and T. Uchida, 2003, J. Phys. Condens. Matter **15**, 1277.
Esposito, E., A. E. Carlson, D. D. Ling, H. Ehrenreich, and C. D. Gelatt, Jr., 1980, Philos. Mag. A **41**, 251.
Every, A. G., and A. K. McCurdy, 1992, in *Landolt-Börnstein Tables: New Series*, edited by D. F. Nelson (Springer-Verlag, Berlin), p. 1, Vol. III/29a.
Fast, L., J. M. Mill, B. Johansson, and O. Eriksson, 1995, Phys. Rev. B **51**, 17 431.
Fawcett, E., 1988, Rev. Mod. Phys. **60**, 209.
Feng, J., R. G. Hennig, N. W. Ashcroft, and R. Hoffmann, 2008, Nature (London) **451**, 445.
Feng, J., R. Hoffmann, and N. W. Ashcroft, 2010, J. Chem. Phys. **132**, 114106.
Feynman, R. P., 1972, *Statistical Mechanics* (Benjamin, New York).
Folkins, I., and M. B. Walker, 1990, Phys. Rev. Lett. **65**, 127.
Forsblom, M., and G. Grimvall, 2005a, Nature Mater. **4**, 388.
Forsblom, M., and G. Grimvall, 2005b, Phys. Rev. B **72**, 054107.
Forsblom, M., N. Sandberg, and G. Grimvall, 2004, Phys. Rev. B **69**, 165106.
Fox, S., and H. J. F. Jansen, 1999, Phys. Rev. B **60**, 4397.
Frenkel, J., 1926, Z. Phys. **37**, 572.
Friák, M., 2011, Steel Research Int. **82**, 86.
Friák, M., and M. Šob, 2008, Phys. Rev. B **77**, 174117.
Friák, M., M. Šob, and V. Vitek, 2001, Phys. Rev. B **63**, 052405.
Friák, M., M. Šob, and V. Vitek, 2003, Philos. Mag. **83**, 3529.
Friedel, J., 1969, in *The Physics of Metals I. Electrons*, edited by J. M. Ziman (Cambridge University Press, Cambridge, England), p. 340.
Gilvarry, J. J., 1956, Phys. Rev. **102**, 308.
Girifalco, L. A., and V. G. Weizer, 1959, Phys. Rev. **114**, 687.
Grabowski, B., T. Hickel, and J. Neugebauer, 2007, Phys. Rev. B **76**, 024309.
Grabowski, B., L. Ismer, T. Hickel, and J. Neugebauer, 2009, Phys. Rev. B **79**, 134106.
Grimvall, G., 1979, Rev. Int. Hautes Tempér. Réfract. (France) **16**, 411.
Grimvall, G., 1998, Ber. Bunsenges. Phys. Chem. **102**, 1083.
Grimvall, G., 1999, *Thermophysical Properties of Materials*, enlarged and revised edition (North-Holland, Amsterdam).
Grimvall, G., 2005, in *Complex Inorganic Solids. Structural, Stability, and Magnetic Properties of Alloys*, edited by P. E. A. Turchi, A. Gonis, K. Rajan, and A. Meike (Springer, New York), p. 295.
Grimvall, G., 2008, Sci. Model Simul. **15**, 21.
Grimvall, G., and J. Rosén, 1983, Int. J. Thermophys. **4**, 139.
Groh, B., and B. Mulder, 1999, Phys. Rev. E **59**, 5613.
Grüneisen, E., and E. Goens, 1924, Z. Phys. **29**, 141.
Guillermet, A. F., V. Ozoliņš, G. Grimvall, and M. Körling, 1995, Phys. Rev. B **51**, 10 364.
Guo, G. Y., and H. H. Wang, 2000a, Phys. Rev. B **62**, 5136.
Guo, G. Y., and H. H. Wang, 2000b, Chin. J. Phys. **38**, 949.
Gutiérrez, G., E. Menéndez-Proupin, and A. K. Singh, 2006, J. Appl. Phys. **99**, 103504.
Haftel, M. I., and K. Gall, 2006, Phys. Rev. B **74**, 035420.
Haneda, K., Z. X. Zhou, A. H. Morrish, T. Majima, and T. Miyahara, 1992, Phys. Rev. B **46**, 13 832.
Hart, G. L. W., and B. M. Klein, 2000, Phys. Rev. B **61**, 3151.
Hatcher, N., O. Y. Kontsevoi, and A. J. Freeman, 2009, Phys. Rev. B **80**, 144203.
Heiming, A., W. Petry, J. Trampenau, M. Alba, C. Herzig, H. R. Schober, and G. Vogl, 1991, Phys. Rev. B **43**, 10 948.
Heinrich, B., A. S. Arrott, J. F. Cochran, S. T. Purcell, K. B. Urquhart, and K. Myrtle, 1987, J. Cryst. Growth **81**, 562.
Heiroth, M., U. Buchenau, H. R. Schober, and J. Evers, 1986, Phys. Rev. B **34**, 6681.
Hennig, R. G., T. J. Lenosky, D. R. Trinkle, S. P. Rudin, and J. W. Wilkins, 2008, Phys. Rev. B **78**, 054121.
Herper, H. C., E. Hoffmann, and P. Entel, 1999, Phys. Rev. B **60**, 3839.
Hill, R., 1962, J. Mech. Phys. Solids **10**, 1.
Hill, R., 1975, Math. Proc. Cambridge Philos. Soc. **77**, 225.
Hill, R., and F. Milstein, 1977, Phys. Rev. B **15**, 3087.
Ho, K.-M., C.-L. Fu, and B. N. Harmon, 1983, Phys. Rev. B **28**, 6687.
Hooton, D. J., 1958, Philos. Mag. **3**, 49.
Hsueh, H. C., J. Crain, G. Y. Guo, H. Y. Chen, C. C. Lee, K. P. Chang, and H. L. Shih, 2002, Phys. Rev. B **66**, 052420.
Hu, C.-E., Z.-Y. Zeng, L. Zhang, X.-R. Chen, L.-C. Cai, and D. Alfè, 2010, J. Appl. Phys. **107**, 093509.
Hu, Q.-M., S. Lu, and R. Yang, 2008, Phys. Rev. B **78**, 052102.
Hüger, E., and K. Osuch, 2004, Solid State Commun. **131**, 175.
Iizumi, M., 1983, J. Phys. Soc. Jpn. **52**, 549.
Ikehata, H., N. Nagasako, T. Foruta, A. Fukumoto, K. Miwa, and T. Saito, 2004, Phys. Rev. B **70**, 174113.
Iwasaki, H., and T. Kikegawa, 1997, Acta Crystallogr. Sect. B **53**, 353.
Jahnátek, M., J. Hafner, and M. Krajčí, 2009, Phys, Rev. B **79**, 224103.
Ji, X. Z., and F. Jona, 2002, J. Phys. Condens. Matter **14**, 12 451.
Johnson, D. F., and E. A. Carter, 2008, J. Chem. Phys. **128**, 104703.
Jona, F., and P. M. Marcus, 2001, Phys. Rev. B **63**, 094113.
Jona, F., X. Z. Ji, and P. M. Marcus, 2003, Phys. Rev. B **68**, 172101.
Jona, F., and P. M. Marcus, 2002a, Phys. Rev. B **65**, 155403.
Jona, F., and P. M. Marcus, 2002b, Phys. Rev. B **66**, 094104.
Jona, F., and P. M. Marcus, 2004, J. Phys. Condens. Matter **16**, 5199.
Jona, F., and P. M. Marcus, 2005, J. Phys. Condens. Matter **17**, 1049.
Jona, F., and P. M. Marcus, 2006, J. Phys. Condens. Matter **18**, 4623.

Jona, F., and P. M. Marcus, 2007, J. Phys. Condens. Matter **19**, 036103.
Kádas, K., L. Vitos, B. Johansson, and J. Kollár, 2007, Phys. Rev. B **75**, 035132.
Karbasi, A., S. K. Saxena, and R. Hrubiak, 2011, CALPHAD: Comput. Coupling Phase Diagrams Thermochem. **35**, 72.
Karki, R. M., B. B. Wentzcovitch, S. Karato, and C. R. S. D. Silva, 1998, Earth Planet. Sci. Lett. **164**, 371.
Kasinathan, D., J. Kuneš, A. Lazicki, H. Rosner, C. S. Yoo, R. T. Scalettar, and W. E. Pickett, 2006, Phys. Rev. Lett. **96**, 047004.
Katsnelson, M. I., G. V. Sinko, N. A. Smirnov, A. V. Trefilov, and K. Y. Khromov, 2000, Phys. Rev. B **61**, 14420.
Katzke, H., and P. Tolédano, 2007, J. Phys. Condens. Matter **19**, 275204.
Kawamiya, N., K. Adachi, and Y. Nakamura, 1972, J. Phys. Soc. Jpn. **33**, 1318.
Kechin, V. V., 2004, J. Phys. Condens. Matter **16**, L125.
Kenichi, T., K. Kazuaki, and A. Masao, 1998, Phys. Rev. B **58**, 2482.
Khojandi, A. I., and D. A. Papaconstantopoulos, 2010, Phys. Rev. B **82**, 155121.
Kim, K., H. C. Choi, and B. I. Min, 2009, Phys. Rev. Lett. **102**, 079701.
Kim, K., V. Ozoliņš, and A. Zunger, 1999, Phys. Rev. B **60**, R8449.
Kimminau, G., P. Erhart, E. M. Bringa, B. Reminton, and J. S. Wark, 2010, Phys. Rev. B **81**, 092102.
Kissavos, A. E., S. Shallcross, V. Meded, L. Kaufman, and I. A. Abrikosov, 2005, CALPHAD: Computer Coupling Phase Diagrams Thermochem. **29**, 17.
Kitamura, T., Y. Umeno, and R. Fushino, 2004, Mater. Sci. Eng. A **379**, 229.
Koehler, T. R., 1968, Phys. Rev. **165**, 942.
Kolluri, K., M. R. Gungor, and D. Maroudas, 2008, Phys. Rev. B **78**, 195408.
Kong, Y., and O. Jepsen, 2000, J. Phys. Condens. Matter **12**, 8973.
Körmann, F., A. Dick, B. Grabowski, B. Hallstedt, T. Hickel, and J. Neugebauer, 2008, Phys. Rev. B **78**, 033102.
Körmann, F., A. Dick, T. Hickel, and J. Neugebauer, 2010, Phys. Rev. B **81**, 134425.
Kotrechko, S. A., A. V. Filatov, and A. V. Ovsjannikov, 2006, Theor. Appl. Fract. Mech. **45**, 92.
Kraft, T., P. M. Marcus, M. Methfessel, and M. Scheffler, 1993, Phys. Rev. B **48**, 5886.
Kraig, R. E., D. Roundy, and M. L. Cohen, 2004, Solid State Commun. **129**, 411.
Krasko, G. L., and G. B. Olson, 1990, J. Appl. Phys. **67**, 4570.
Krenn, C. R., D. Roundy, M. L. Cohen, D. C. Chrzan, and J. W. Morris, Jr., 2002, Phys. Rev. B **65**, 134111.
Krenn, C. R., D. Roundy, J. W. Morris, Jr., and M. L. Cohen, 2001a, Mater. Sci. Eng. A **319–321**, 111.
Krenn, C. R., D. Roundy, J. W. Morris, Jr., and M. L. Cohen, 2001b, Mater. Sci. Eng. A **317**, 44.
Kresse, G., and J. Furthmüller, 1996, Phys. Rev. B **54**, 11 169.
Kresse, G., and D. Joubert, 1999, Phys. Rev. B **59**, 1758.
Krumhansl, J. A., 1992, Solid State Commun. **84**, 251.
Krumhansl, J. A., and R. J. Gooding, 1989, Phys. Rev. B **39**, 3047.
Laenens, B., N. Planckaert, M. Sternik, P. T. Jochym, K. Parliński, A. Vantomme, and J. Meersschaut, 2009, Phys. Rev. B **79**, 224303.
Lai, W. S., and X. S. Zhao, 2004, Appl. Phys. Lett. **85**, 4340.
Lam, P. K., M. Y. Chou, and M. L. Cohen, 1984, J. Phys. C **17**, 2065.
Landa, A., J. Klepeis, P. Söderlind, I. Naumov, O. Velikokhatnyi, L. Vitos, and A. Ruban, 2006a, J. Phys. Condens. Matter **18**, 5079.
Landa, A., J. Klepeis, P. Söderlind, I. Naumov, O. Velikokhatnyi, L. Vitos, and A. Ruban, 2006b, J. Phys. Chem. Solids **67**, 2056.
Ledbetter, H., H. Ogi, S. Kai, S. Kim, and M. Hirao, 2004, J. Appl. Phys. **95**, 4642.
Lee, B., R. E. Rudd, J. E. Klepeis, P. Söderlind, and A. Landa, 2007, Phys. Rev. B **75**, 180101.
Lee, G., 2010, Acta Mater. **58**, 1361.
Legut, D., M. Friák, and M. Šob, 2007, Phys. Rev. Lett. **99**, 016402.
Legut, D., M. Friák, and M. Šob, 2010, Phys. Rev. B **81**, 214118.
Leonov, I., A. I. Poteryaev, V. I. Anisimov, and D. Vollhardt, 2011, Phys. Rev. Lett. **106**, 106405.
Le Page, Y., and P. Saxe, 2002, Phys. Rev. B **65**, 104104.
Le Page, Y., P. W. Saxe, and J. R. Rogers, 2002, Acta Crystallogr. Sect. B **58**, 349.
Li, H., D. Tian, J. Quinn, Y. S. Li, F. Jona, and P. M. Marcus, 1991, Phys. Rev. B **43**, 6342.
Li, J., A. H. W. Ngan, and P. Gumbsch, 2003, Acta Mater. **51**, 5711.
Li, T., J. W. Morris, Jr., and D. C. Chrzan, 2004, Phys. Rev. B **70**, 054107.
Li, T., J. W. Morris, Jr., and D. C. Chrzan, 2006, Phys. Rev. B **73**, 024105.
Li, T., J. W. Morris, Jr., N. Nagasako, S. Kuramoto, and D. C. Chrzan, 2007, Phys. Rev. Lett. **98**, 105503.
Li, W., and T. Wang, 1998, J. Phys. Condens. Matter **10**, 9889.
Li, Y., L. Zhang, T. Cui, Y. Ma, G. Zou, and D. D. Klug, 2006, Phys. Rev. B **74**, 054102.
Li, Z., Y. Chang, and C. Peng, 2009, Solid State Commun. **149**, 952.
Li, Z. Q., and J. S. Tse, 2000, Phys. Rev. B **62**, 9900.
Lindemann, F. A., 1910, Zeitschr. Physik **11**, 609.
Lindenberg, A. M., 2005, Science **308**, 392.
Liu, A. Y., and D. J. Singh, 1993, Phys. Rev. B **47**, 8515.
Liu, J. Z., A. van de Walle, G. Ghosh, and M. Asta, 2005, Phys. Rev. B **72**, 144109.
Liu, Y.-L., Y. Zhang, H.-B. Zhou, G.-H. Lu, and M. Kohyama, 2008, J. Phys. Condens. Matter **20**, 335216.
Liu, Z. K., 2009, J. Phase Equilibria and Diffusion **30**, 517.
Lowry, M. B., D. Kiener, M. M. LeBlanc, C. Chisholm, J. N. Florando, J. W. Morris, Jr., and A. M. Minor, 2010, Acta Mater. **58**, 5160.
Lu, J., and L. Zhang, 2006, J. Mech. Mater. Struct. **1**, 633.
Luo, W., D. Roundy, M. L. Cohen, and J. W. Morris, Jr., 2002, Phys. Rev. B **66**, 094110.
Ma, F., and K. W. Xu, 2007, J. Mater. Res. **22**, 1299.
Ma, H., S. L. Qiu, and P. M. Marcus, 2002, Phys. Rev. B **66**, 024113.
Machlin, E. S., and J. Shao, 1983, J. Phys. Chem. Solids **44**, 435.
Magyari-Köpe, B., G. Grimvall, and L. Vitos, 2002, Phys. Rev. B **66**, 064210.
Manna, I., P. P. Chattopadhyay, F. Banhart, and H.-J. Fecht, 2002, Appl. Phys. Lett. **81**, 4136.
Manna, I., P. P. Chattopadhyay, P. Nandi, F. Banhart, and H.-J. Fecht, 2003, J. Appl. Phys. **93**, 1520.
Marcus, P. M., and F. Jona, 1997, J. Phys. Condens. Matter **9**, 6241.
Marcus, P. M., and F. Jona, 2005, Eur. Phys. J. B **45**, 39.
Marcus, P. M., F. Jona, and S. L. Qiu, 2002, Phys. Rev. B **66**, 064111.
Marcus, P. M., H. Ma, and S. L. Qiu, 2002, J. Phys. Condens. Matter **14**, L525.
Marcus, P. M., V. L. Moruzzi, and S. L. Qiu, 1999, Phys. Rev. B **60**, 369.
Marcus, P. M., and S. L. Qiu, 2004, J. Phys. Condens. Matter **16**, 8787.
Marcus, P. M., and S. L. Qiu, 2009a, J. Phys. Condens. Matter **21**, 115401.

Marcus, P. M., and S. L. Qiu, 2009b, J. Phys. Condens. Matter **21**, 125404.
Marsman, M., and J. Hafner, 2002, Phys. Rev. B **66**, 224409.
Masuda-Jindo, K., S. R. Nishitani, and V. V. Hung, 2004, Phys. Rev. B **70**, 184122.
Mathon, O., F. Baudelet, J. P. Itié, A. Polian, M. d'Astuto, J. C. Chervin, and S. Pascarelli, 2004, Phys. Rev. Lett. **93**, 255503.
Mauri, F., O. Zakharov, S. de Gironcoli, S. G. Louie, and M. L. Cohen, 1996, Phys. Rev. Lett. **77**, 1151.
Mehl, M. J., A. Aguayo, L. L. Boyer, and R. de Coss, 2004, Phys. Rev. B **70**, 014105.
Mehl, M. J., and L. L. Boyer, 1991, Phys. Rev. B **43**, 9498.
Mehl, M. J., and D. Finkenstadt, 2008, Phys. Rev. B **77**, 052102.
Mehl, M. J., and D. Papaconstantopoulos, 1996, Phys. Rev. B **54**, 4519.
Metoki, N., W. Donner, and H. Zabel, 1994, Phys. Rev. B **49**, 17 351.
Mikhailovskii, I. M., P. Y. Poltinin, and L. I. Fedorova, 1981, Sov. Phys. Solid State **23**, 757.
Miller, R. E., and D. Rodney, 2008, J. Mech. Phys. Solids **56**, 1203.
Milstein, F., 1971, Phys. Rev. B **3**, 1130.
Milstein, F., 1973a, J. Appl. Phys. **44**, 3825.
Milstein, F., 1973b, J. Appl. Phys. **44**, 3833.
Milstein, F., 1980, J. Mater. Sci. **15**, 1071.
Milstein, F., and S. Chantasiriwan, 1998, Phys. Rev. B **58**, 6006.
Milstein, F., H. E. Fang, X.-Y. Gong, and D. J. Rasky, 1996, Solid State Commun. **99**, 807.
Milstein, F., H. E. Fang, and J. Marschall, 1994, Philos. Mag. A **70**, 621.
Milstein, F., and B. Farber, 1980, Philos. Mag. A **42**, 19.
Milstein, F., and R. Hill, 1979a, Phys. Rev. Lett. **43**, 1411.
Milstein, F., and R. Hill, 1979b, J. Mech. Phys. Solids **27**, 255.
Milstein, F., and K. Huang, 1978, Phys. Rev. B **18**, 2529.
Milstein, F., J. Marschall, and H. E. Fang, 1995, Phys. Rev. Lett. **74**, 2977.
Milstein, F., and D. J. Rasky, 1996, Phys. Rev. B **54**, 7016.
Milstein, F., J. Zhao, S. Chantasiriwan, and D. Maroudas, 2005, Appl. Phys. Lett. **87**, 251919.
Milstein, F., J. Zhao, and D. Maroudas, 2004, Phys. Rev. B **70**, 184102.
Mishin, Y., D. Farkas, M. J. Mehl, and D. A. Papaconstantopoulos, 1999, Phys. Rev. B **59**, 3393.
Mishin, Y., M. J. Mehl, D. A. Papaconstantopoulos, A. F. Voter, and J. D. Kress, 2001, Phys. Rev. B **63**, 224106.
Misra, R. D., 1940, Proc. Cambridge Philos. Soc. **36**, 173.
Mizushima, K., S. Yip, and E. Kaxiras, 1994, Phys. Rev. B **50**, 14 952.
Moriarty, J. A., and J. D. Althoff, 1995, Phys. Rev. B **51**, 5609.
Morris, J. R., and K. M. Ho, 2001, Phys. Rev. B **63**, 224116.
Morris, Jr., J. W., and C. R. Krenn, 2000, Philos. Mag. A **80**, 2827.
Müller, S., L.-W. Wang, A. Zunger, and C. Wolverton, 1999, Phys. Rev. B **60**, 16 448.
Nagasako, N., M. Jahnátek, R. Asahi, and J. Hafner, 2010, Phys. Rev. B **81**, 094108.
Nastar, M., and F. Willaime, 1995, Phys. Rev. B **51**, 6896.
Nishitani, S. R., H. Kawabe, and M. Aoki, 2001, Mater. Sci. Eng. A **312**, 77.
Nixon, L. W., D. A. Papaconstantopoulos, and M. J. Mehl, 2008, Phys. Rev. B **78**, 214510.
Nnolim, N. O., T. A. Tyson, and L. Axe, 2003, J. Appl. Phys. **93**, 4543.
Norman, G. E., V. V. Stegailov, and A. V. Yanilkin, 2007, High Temp. **45**, 164.
Ogata, S., J. Li, N. Hirosaki, Y. Shibutani, and S. Yip, 2004, Phys. Rev. B **70**, 104104.
Ogata, S., J. Li, and S. Yip, 2002, Science **298**, 807.
Ogata, S., Y. Umeno, and M. Kohyama, 2009, Modelling Simul. Mater. Sci. Eng. **17**, 013001.
Okatov, S. V., A. R. Kuznetsov, Y. N. Gornostyrev, V. N. Urtsev, and M. I. Katsnelson, 2009, Phys. Rev. B **79**, 094111.
Orowan, E., 1949, Rep. Prog. Phys. **12**, 185.
Ozoliņš, V., 2009, Phys. Rev. Lett. **102**, 065702.
Ozoliņš, V., C. Wolverton, and A. Zunger, 1998, Phys. Rev. B **57**, 4816.
Ozoliņš, V., and A. Zunger, 1999, Phys. Rev. Lett. **82**, 767.
Pacheco, A. A., and R. C. Batra, 2008, J. Mech. Phys. Solids **56**, 3116.
Papaconstantopoulos, D. A., M. Lach-hab, and M. J. Mehl, 2001, Physica (Amsterdam) **296B**, 129.
Papaconstantopoulos, D. A., and M. J. Mehl, 2003, J. Phys. Condens. Matter **15**, R413.
Paszkiewicz, T., M. Pruchnik, and P. Zieliński, 2001, Eur. Phys. J. B **24**, 327.
Paszkiewicz, T., and S. Wolski, 2007, Phys. Status Solidi B **244**, 966.
Paszkiewicz, T., and S. Wolski, 2008, J. Phys. Conf. Ser. **104**, 012038.
Pavlů, J., J. Vřeštál, and M. Šob, 2010, CALPHAD: Comput. Coupling Phase Diagrams Thermochem. **34**, 215.
Paxton, A. T., P. Gumbsch, and M. Methfessel, 1991, Philos. Mag. Lett. **63**, 267.
Peng, S. S., and H. J. F. Jansen, 1991, J. Appl. Phys. **69**, 6132.
Persson, K., 2001, "Thermodynamical and dynamical instabilities from Ab initio electronic-structure calculations, Ph.D. thesis (Royal Institute of Technology).
Persson, K., M. Ekman, and G. Grimvall, 1999, Phys. Rev. B **60**, 9999.
Persson, K., M. Ekman, and V. Ozoliņš, 2000, Phys. Rev. B **61**, 11 221.
Petry, W., A. Heiming, J. Trampenau, M. Alba, C. Herzig, H. R. Schober, and G. Vogl, 1991, Phys. Rev. B **43**, 10 933.
Pettifor, D. G., 1977, CALPHAD: Comput. Coupling Phase Diagrams Thermochem. **1**, 305.
Pfeifer, M. A., O. Robach, B. M. Ocko, and I. K. Robinson, 2005, Physica B (Amsterdam) **357**, 152.
Pinsook, U., and G. J. Ackland, 1998, Phys. Rev. B **58**, 11 252.
Pinsook, U., and G. J. Ackland, 2000, Phys. Rev. B **62**, 5427.
Pokluda, J., M. Černý, P. Šandera, and M. Šob, 2004, J. Comput.-Aided Mater. Des. **11**, 1.
Pollack, L., J. P. Perdew, J. He, M. Marques, F. Nogueira, and C. Fiolhais, 1997, Phys. Rev. B **55**, 15 544.
Porta, M., and T. Castán, 2001, Phys. Rev. B **63**, 134104.
Power, S. C., 1942, Proc. Cambridge Philos. Soc. **38**, 61.
Price, D. L., B. R. Cooper, and J. M. Wills, 1992, Phys. Rev. B **46**, 11 368.
Prinz, G. A., 1985, Phys. Rev. Lett. **54**, 1051.
Profeta, G., 2006, Phys. Rev. Lett. **96**, 047003.
Qiu, S. L., F. Apostol, and P. M. Marcus, 2008, J. Phys. Condens. Matter **20**, 345233.
Qiu, S. L., and P. M. Marcus, 1999, Phys. Rev. B **60**, 14 533.
Qiu, S. L., and P. M. Marcus, 2008a, J. Phys. Condens. Matter **20**, 275218.
Qiu, S. L., and P. M. Marcus, 2008b, Eur. Phys. J. B **66**, 1.
Qiu, S. L., and P. M. Marcus, 2009, J. Phys. Condens. Matter **21**, 435403.
Qiu, S. L., P. M. Marcus, and H. Ma, 2000a, J. Appl. Phys. **87**, 5932.

Qiu, S. L., P. M. Marcus, and H. Ma, 2000b, Phys. Rev. B **62**, 3292.
Qiu, S. L., P. M. Marcus, and H. Ma, 2001, Phys. Rev. B **64**, 104431.
Rodriguez-Prieto, A., A. Bergara, V. M. Silkin, and P. M. Echenique, 2006, Phys. Rev. B **74**, 172104.
Rosén, J., and G. Grimvall, 1983, Phys. Rev. B **27**, 7199.
Roundy, D., C. R. Krenn, M. L. Cohen, and J. W. Morris, Jr, 1999, Phys. Rev. Lett. **82**, 2713.
Roundy, D., C. R. Krenn, M. L. Cohen, and J. W. Morris, Jr, 2001, Philos. Mag. A **81**, 1725.
Rousseau, B., Y. Xie, Y. Ma, and A. Bergara, 2011, Eur. Phys. J. B **81**, 1.
Ruoff, A. L., C. O. Rodriguez, and N. E. Christensen, 1998, Phys. Rev. B **58**, 2998.
Sanati, M., A. Saxena, T. Lookman, and R. C. Albers, 2001, Phys. Rev. B **63**, 224114.
Šandera, P., J. Pokluda, L. G. Wang, and M. Šob, 1997, Mater. Sci. Eng. A **234–236**, 370.
Schärer, U., and P. Wachter, 1995, Solid State Commun. **96**, 497.
Sheng, H. W., Y. H. Zhao, Z. Q. Hu, and K. Lu, 1997, Phys. Rev. B **56**, 2302.
Shimada, T., Y. Ishii, and T. Kitamura, 2010, Phys. Rev. B **81**, 134420.
Sin'ko, G. V., and N. A. Smirnov, 2002, J. Phys. Condens. Matter **14**, 6989.
Sin'ko, G. V., and N. A. Smirnov, 2004, J. Phys. Condens. Matter **16**, 8101.
Sin'ko, G. V., and N. A. Smirnov, 2005, Phys. Rev. B **71**, 214108.
Sin'ko, G. V., and N. A. Smirnov, 2009, Phys. Rev. B **80**, 104113.
Skriver, H. L., 1985, Phys. Rev. B **31**, 1909.
Sliwko, V. L., P. Mohn, K. Schwarz, and P. Blaha, 1996, J. Phys. Condens. Matter **8**, 799.
Smirnova, E. A., P. A. Korzhavyi, Y. K. Vekilov, B. Johansson, and I. A. Abrikosov, 2001, Phys. Rev. B **64**, 020101(R).
Šob, M., M. Friák, D. Legut, J. Fiala, and V. Vitek, 2004, Mater. Sci. Eng. A **387–389**, 148.
Šob, M., M. Friák, D. Legut, and V. Vitek, 2005, in *Complex Inorganic Solids. Structural, Stability, and Magnetic Properties of Alloys*, edited by P. E. A. Turchi, A. Gonis, K. Rajan, and A. Meike (Springer, New York), p. 307.
Šob, M., M. Friák, L. G. Wang, and V. Vitek, 2002, Key Eng. Mater. **227**, 261.
Šob, M., A. Kroupa, J. Pavlů, and J. Vřešt'ál, 2009, Diffus. Defect Data, Solid State Phenomena, Pt. B **150**, 1.
Šob, M., D. Legut, and M. Friák, 2009, Phys. Rev. Lett. **102**, 079702.
Šob, M., L. G. Wang, and V. Vitek, 1997a, Comput. Mater. Sci. **8**, 100.
Šob, M., L. G. Wang, and V. Vitek, 1997b, Mater. Sci. Eng. A **234–236**, 1075.
Šob, M., L. G. Wang, and V. Vitek, 1998a, Philos. Mag. B **78**, 653.
Šob, M., L. G. Wang, and V. Vitek, 1998b, Kovore Materialy Metallic Materials **36**, 145.
Söderlind, P., 1998, Adv. Phys. **47**, 959.
Söderlind, P., 2002, Phys. Rev. B **65**, 115105.
Söderlind, P., R. Ahuja, O. Eriksson, M. Wills, and B. Johansson, 1994, Phys. Rev. B **50**, 5918.
Söderlind, P., O. Eriksson, J. M. Wills, and A. M. Boring, 1993, Phys. Rev. B **48**, 5844.
Söderlind, P., O. Eriksson, J. M. Wills, and B. Johansson, 1993, Phys. Rev. B **48**, 9212.
Söderlind, P., A. Landa, J. E. Klepeis, Y. Suzuki, and A. Migliori, 2010, Phys. Rev. B **81**, 224110.
Söderlind, P., A. Landa, B. Sadigh, L. Vitos, and A. Ruban, 2004, Phys. Rev. B **70**, 144103.
Söderlind, P., and J. A. Moriarty, 1998, Phys. Rev. B **57**, 10 340.
Söderlind, P., J. A. Moriarty, and J. M. Wills, 1996, Phys. Rev. B **53**, 14 063.
Song, Y., R. Yang, D. Li, W. T. Wu, and Z. X. Guo, 1999, Phys. Rev. B **59**, 14 220.
Souvatzis, P., O. Eriksson, M. Katsnelson, and S. P. Rudin, 2008, Phys. Rev. Lett. **100**, 095901.
Souvatzis, P., O. Eriksson, M. I. Katsnelson, and S. P. Rudin, 2009, Comput. Mater. Sci. **44**, 888.
Spišák, D., and J. Hafner, 2002, Phys. Rev. Lett. **88**, 056101.
Steinle-Neumann, G., and R. E. Cohen, 2004, J. Phys. Condens. Matter **16**, 8783.
Steinle-Neumann, G., L. Stixrude, and R. E. Cohen, 1999, Phys. Rev. B **60**, 791.
Stixrude, L., and R. E. Cohen, 1995, Science **267**, 1972.
Stixrude, L., R. E. Cohen, and D. J. Singh, 1994, Phys. Rev. B **50**, 6442.
Sun, J., D. Klug, and R. Martoňák, 2009, J. Chem. Phys. **130**, 194512.
Suzuki, N., and M. Otani, 2002, J. Phys. Condens. Matter **14**, 10 869.
Taga, A., L. Vitos, B. Johansson, and G. Grimvall, 2005, Phys. Rev. B **71**, 014201.
Tallon, J. L., 1989, Nature (London) **342**, 658.
Tambe, M. J., N. Bonini, and N. Marzari, 2008, Phys. Rev. B **77**, 172102.
Teweldeberhan, A. M., and S. A. Bonev, 2008, Phys. Rev. B **78**, 140101(R).
Thompson, G. B., R. Banerjee, S. A. Dregia, M. K. Miller, and H. L. Fraser, 2004, J. Mater. Res. **19**, 707.
Trampenau, J., A. Heiming, W. Petry, M. Alba, C. Herzig, W. Miekeley, and H. R. Schober, 1991, Phys. Rev. B **43**, 10 963.
Trubitsin, V. Y., 2006a, Phys. Rev. B **73**, 214302.
Trubitsin, V. Y., 2006b, Phys. Rev. B **73**, 214303.
Tsetseris, L., 2005, Phys. Rev. B **72**, 012411.
Umeno, Y., and M. Černý, 2008, Phys. Rev. B **77**, 100101.
Umeno, Y., T. Kitamura, and M. Tagawa, 2007, Mater. Sci. Eng. A **462**, 450.
Vaks, V. G., M. I. Katsnelson, A. I. Likhtenstein, G. V. Peschanskikh, and A. V. Trefilov, 1991, J. Phys. Condens. Matter **3**, 1409.
Van Vliet, K. J., J. Li, T. Zhu, S. Yip, and S. Suresh, 2003, Phys. Rev. B **67**, 104105.
Verma, A. K., and P. Modak, 2008, Europhys. Lett. **81**, 37 003.
Verma, A. K., P. Ravindran, R. S. Rao, B. K. Godwal, and R. Jeanloz, 2003, Bull. Mater. Sci. **26**, 183.
Vočadlo, L., I. G. Wood, M. J. Gillan, J. P. Brodholt, D. P. Dobson, G. D. Price, and D. Alfè, 2008, Phys. Earth Planet. Inter. **170**, 52.
Wallace, D. C., 1967, Phys. Rev. **162**, 776.
Wallace, D. C., 1972, *Thermodynamics of Crystals* (Wiley, New York).
Wallace, D. C., and J. L. Patrick, 1965, Phys. Rev. **137**, A152.
Wang, H., and M. Li, 2009, J. Phys. Condens. Matter **21**, 455401.
Wang, J., S. Yip, S. R. Phillpot, and D. Wolf, 1993, Phys. Rev. Lett. **71**, 4182.
Wang, J. H., J. Li, S. Yip, S. Phillpot, and D. Wolf, 1995, Phys. Rev. B **52**, 12 627.
Wang, L. G., and M. Šob, 1999, Phys. Rev. B **60**, 844.
Wang, L. G., M. Šob, and Z. Zhang, 2003, J. Phys. Chem. Solids **64**, 863.
Wang, Y., R. Ahuja, M. C. Qian, and B. Johansson, 2002, J. Phys. Condens. Matter **14**, L695.
Wang, Y., S. Curtarolo, C. Jiang, R. Arroyave, T. Wang, G. Ceder, L.-Q. Chen, and Z.-K. Liu, 2004, CALPHAD: Computer Coupling of Phase Diagrams and Thermochemistry **28**, 79.

Wang, Z. Q., S. H. Lu, Y. S. Li, F. Jona, and P. M. Marcus, 1987, Phys. Rev. B **35**, 9322.
Warren, B. E., 1969, *X-ray Diffraction* (Addison-Wesley, Reading, MA).
Watson, G. W., and S. C. Parker, 1995, Phys. Rev. B **52**, 13 306.
Wei, Q. M., X.-Y. Liu, and A. Misra, 2011, Appl. Phys. Lett. **98**, 111907.
Wentzcovitch, R. M., and M. L. Cohen, 1988, Phys. Rev. B **37**, 5571.
Willaime, F., and C. Massobrio, 1991, Phys. Rev. B **43**, 11 653.
Wills, J. M., O. Eriksson, P. Söderlind, and A. M. Boring, 1992, Phys. Rev. Lett. **68**, 2802.
Withey, E., M. Jin, A. Minor, S. Kuramoto, D. C. Chrzan, and J. W. Morris, Jr., 2008, Mater. Sci. Eng. A **493**, 26.
Withey, E. A., J. Ye, A. Minor, S. Kuramoto, D. C. Chrzan, and J. W. Morris, Jr., 2010, Exp. Mech. **50**, 37.
Wolf, G. H., and R. Jeanloz, 1985, Phys. Rev. B **32**, 7798.
Wormeester, H., E. Hüger, and E. Bauer, 1996, Phys. Rev. Lett. **77**, 1540.
Xie, J. J., S. P. Chen, J. S. Tse, D. D. Klug, Z. Q. Li, K. Uehara, and L. G. Wang, 2000, Phys. Rev. B **62**, 3624.
Xie, Y., Y. M. Ma, T. Cui, Y. Li, J. Qui, and G. T. Zou, 2008, New J. Phys. **10**, 063022.
Xie, Y., J. S. Tse, T. Cui, A. R. Oganov, Z. He, Y. Ma, and G. Zou, 2007, Phys. Rev. B **75**, 064102.
Yao, Y., D. D. Klug, J. Sun, and R. Martoňák, 2009, Phys. Rev. Lett. **103**, 055503.
Yao, Y., J. S. Tse, K. Tanaka, F. Marsiglio, and Y. Ma, 2009, Phys. Rev. B **79**, 054524.
Yashiro, K., M. Oho, and Y. Tomita, 2004, Comput. Mater. Sci. **29**, 397.
Yashiro, K., K. Yamagami, K. Kubo, and Y. Tomita, 2006, JSME Int. J., Ser. A **49**, 100.
Ye, Y.-Y., Y. Chen, K.-M. Ho, B. N. Harmon, and P.-A. Lindgård, 1987, Phys. Rev. Lett. **58**, 1769.
Yin, M. T., and M. L. Cohen, 1982, Phys. Rev. B **26**, 5668.
Yip, S., J. Li, M. Tang, and J. Wang, 2001, Mater. Sci. Eng. A **317**, 236.
Young, D. A., 1991, *Phase Diagrams of the Elements* (University California Press Berkeley, Berkeley).
Zelený, M., M. Friák, and M. Šob, 2011, Phys. Rev. B **83**, 184424.
Zelený, M., D. Legut, and M. Šob, 2008, Phys. Rev. B **78**, 224105.
Zelený, M., and M. Šob, 2008, Phys. Rev. B **77**, 155435.
Zener, C., 1947, Phys. Rev. B **71**, 846.
Zener, C., 1948, *Elasticity and Anelasticity of Metals* (University of Chicago Press, Chicago).
Zeng, Z.-Y., C.-E. Hu, L.-C. Cai, X.-R. Chen, and F.-Q. Jing, 2010, J. Phys. Chem. B **114**, 298.
Zhang, B., C. Wang, K. Ho, D. Turner, and Y. Ye, 1995, Phys. Rev. Lett. **74**, 1375.
Zhang, J.-M., H.-T. Li, and K.-W. Xu, 2007, Solid State Commun. **141**, 535.
Zhang, J.-M., Y. Yang, K.-W. Xu, and V. Ji, 2008a, Comput. Mater. Sci. **43**, 917.
Zhang, J.-M., Y. Yang, K.-W. Xu, and V. Ji, 2008b, Can. J. Phys. **86**, 935.
Zhang, Q., W. S. Lai, and B. X. Liu, 2000, Phys. Rev. B **61**, 9345.
Zhao, J., D. Maroudas, and F. Milstein, 2000, Phys. Rev. B **62**, 13 799.
Zhou, Z., and B. Joós, 1996, Phys. Rev. B **54**, 3841.